Universidad de Oviedo
*Universidá d'Uviéu*
*University of Oviedo*

Departamento de Morfología y Biología Celular

Programa de Doctorado de Ciencias de la Salud

# Afectación de la hipertrofia condrocítica del cartílago de crecimiento en un modelo experimental de uremia. Efecto de la hormona de crecimiento.

# Disturbance of the growth cartilage chondrocyte hypertrophy in an animal model of uremia. Effect of growth hormone

Autora/Author
**Ángela Fernández Iglesias**

Universidad de Oviedo
*Universidá d'Uviéu*
*University of Oviedo*

Departamento de Morfología y Biología Celular

Programa de Doctorado de Ciencias de la Salud

# Afectación de la hipertrofia condrocítica del cartílago de crecimiento en un modelo experimental de uremia. Efecto de la hormona de crecimiento.

# Disturbance of the growth cartilage chondrocyte hypertrophy in an animal model of uremia. Effect of growth hormone

Autora/Author
**Ángela Fernández Iglesias**

Universidad de Oviedo
*Universidá d'Uviéu*
*University of Oviedo*

# RESUMEN DEL CONTENIDO DE TESIS DOCTORAL

| **1.- Título de la Tesis Doctoral** | |
|---|---|
| Español/Otro Idioma:<br>Afectación de la hipertrofia condrocítica del cartílago de crecimiento en un modelo experimental de uremia. Efecto de la hormona de crecimiento | Inglés:<br>Disturbance of the growth cartilage chondrocytic hypertrophy in an animal model of uremia. Effect of growth hormone. |

| **2.- Autor** | |
|---|---|
| Nombre: Ángela Fernández Iglesias | DNI/Pasaporte/NIE: |
| Programa de Doctorado: CIENCIAS DE LA SALUD<br><br>Línea de Investigación: Investigación en Pediatría | |
| Órgano responsable: COMISION ACADÉMICA DEL PROGRAMA DE CIENCIAS DE LA SALUD | |



## RESUMEN (en español)

El retraso del crecimiento sigue siendo una complicación importante en los pacientes pediátricos con enfermedad renal crónica (ERC) ya que solo el 30% de los adultos con ERC de inicio en la infancia alcanza una altura final normal. La ERC modifica la morfología y función de la placa de crecimiento (GP) de los huesos largos al alterar el proceso de maduración de los condrocitos.

El objetivo general de esta tesis fue contribuir a esclarecer el mecanismo de retraso del crecimiento secundario a la ERC, así como el efecto que la hormona de crecimiento (GH) ejerce sobre la placa de crecimiento para revertir este retraso. Además, los objetivos específicos: (1) desarrollar un nuevo procedimiento que permitiera el uso de la microscopía confocal para investigar el proceso de hipertrofia de condrocitos; (2) estudiar el mecanismo de retraso del crecimiento en la enfermedad renal crónica experimental; (3) analizar la expresión de marcadores de hipertrofia, (4) conocer el efecto de la administración de GH en las fases mencionadas y (5) analizar la formación y función de la placa de hueso epifisaria.

En una primera fase del estudio, desarrollamos una nueva técnica basada en la microscopía confocal que permitió la discriminación objetiva de distintos grupos de poblaciones de condrocitos en la placa de crecimiento. Al aplicar esta metodología a ratas en crecimiento normal, clasificamos los condrocitos en siete clústeres diferentes, con cuatro subfases en la zona prehipertrófica y tres en la zona hipertrófica. Para obtener nuevos conocimientos sobre el proceso de diferenciación de condrocitos en la ERC y, por tanto, cumplir con los objetivos restantes, se aplicó la metodología a un modelo de rata con hipocrecimiento inducido por ERC. Se analizaron los condrocitos en ratas jóvenes con retraso del crecimiento con ERC inducida por adenina (AD), con restricción de alimentación, pareada con el grupo AD (PF) y ratas con ERC tratadas con hormona del crecimiento (ADGH). Los resultados obtenidos mostraron que: (1) El volumen celular que los condrocitos alcanzaron al final de la hipertrofia se redujo en el grupo AD, pero el tratamiento con GH pudo normalizarlo; (2) La uremia produjo en los condrocitos una alteración del patrón de variación en la densidad del citoplasma celular que implica un retraso en el comienzo del proceso de hipertrofia; (3) La uremia produjo una disminución de la expresión de las proteínas Igf1 y Aqp1; (4) El tratamiento con hormona de crecimiento fue eficaz para revertir la alteración de la maduración de los condrocitos en la ERC mediante la restitución del comienzo normal

del proceso de hipertrofia; (5) El efecto de la GH está parcialmente mediado por su acción sobre la expresión del cotransportador de membrana Nkcc1, que juega un papel importante en el incremento de volumen de los condrocitos durante la hipertrofia. Además, para estudiar la formación de la placa ósea epifisaria, realizamos un análisis del curso temporal de las tibias de ratas en diferentes etapas de crecimiento y encontramos que la formación de la placa ósea epifisaria se produce de una manera que puede considerarse como una osificación intramembranosa.
En conclusión, el nuevo método desarrollado en esta tesis ha permitido obtener información adicional a las mediciones comunes de condrocitos y ha mejorado la comprensión de la secuencia de eventos que tienen lugar durante el proceso de diferenciación de estas células. Al aplicar por primera vez este enfoque tridimensional para estudiar las anomalías en la maduración de los condrocitos urémicos, hemos visto que los condrocitos urémicos experimentan una entrada retardada en la hipertrofia, impidiendo que alcancen un tamaño normal al final del proceso de diferenciación. El tratamiento con GH compensó esto al desencadenar un agrandamiento temprano de los condrocitos mediante un mecanismo no totalmente establecido, pero en el que el cotransportador de membrana Nkcc1 podría tener un papel importante.

**RESUMEN (en Inglés)**

Growth impairment remains a major complication in pediatric patients with chronic kidney disease (CKD) as only 30% of adults with childhood onset CKD reach a normal final height. CKD alters the morphology and function of the growth plate (GP) of long bones by disturbing the maturation process of chondrocytes.
The general objective of this thesis was to contribute to clarify the mechanism of growth retardation secondary to CKD as well as the effect that growth hormone (GH) exerts on the GP to reverse this delay. Moreover, the specific objectives were: (1) to develop a new procedure that would allow the use of confocal microscopy to investigate the process of chondrocyte hypertrophy; (2) to study the mechanism of growth retardation in experimental chronic kidney disease; (3) to analyze the expression of hypertrophy markers, (4) to know the effect of GH administration on the above-mentioned phases and (5) to analyze the formation and function of the epiphyseal bone plate.
In a first phase of the study, we developed a new procedure based on confocal microscopy that allowed the objective discrimination of different groups of chondrocyte populations on the GP. When applying this methodology to normal growing rats, we classified the chondrocytes in seven different clusters, with four subphases in the pre-hypertrophic zone and three in the hypertrophic zone.
In order to obtain new knowledge about the process of differentiation of chondrocytes in CKD and, therefore, meet the following objectives, the methodology was applied to a CKD induced growth retardation rat model. Chondrocytes were analyzed in growth-retarded young rats with CKD induced by adenine (AD), pair-fed with the AD group (PF) and CKD rats treated with growth hormone (ADGH). The results obtained showed that: (1) The cell volume that chondrocytes reach at the end of hypertrophy was reduced in AD rats, but treatment with GH was able to normalize it; (2) Uremia produced in chondrocytes an alteration of the pattern of variation in the density of the cell cytoplasm that implied a delay in the beginning of the hypertrophy process; (3) Uremia produced a decrease in the expression of the Igf1 and Aqp1 proteins; (4) GH treatment was effective in reversing the impaired maturation of chondrocytes in CKD by restoring the normal onset of the hypertrophy process; (5) The effect of GH was partially mediated by its action on the expression of the membrane cotransporter

Nkcc1, which plays an important role in the increase in volume of chondrocytes during hypertrophy. Additionally, to study the formation of the epiphyseal bone plate we performed a time course analysis of tibias of rats at different stages of growth and found that formation of the epiphyseal bone plate occurs in a manner that may be considered as intramembranous-like ossification.
In conclusion, the new method developed in this thesis allowed to obtain additional information to the common measurements of chondrocytes and improved the understanding of the sequence of events that take place during the differentiation process of these cells. When applying this three-dimensional approach for the first time to study abnormalities in uremic chondrocyte maturation, we have seen that uremic chondrocytes experience a delayed entry into hypertrophy, preventing them from reaching a normal size at the end of the differentiation process. Growth hormone treatment improves growth impairment and reverts the effects of uremia on the final chondrocyte volume, likely by triggering an early chondrocyte enlargement that could be mediated by Nkcc1.

**SR. PRESIDENTE DE LA COMISIÓN ACADÉMICA DEL PROGRAMA DE DOCTORADO EN CIENCIAS DE LA SALUD**

# ACKNOWLEDGMENTS/ AGRADECIMIENTOS

*The world is full of wonders, but they become more wonderful, not less, when science looks at them.*

*Sir David Attenborough*

# TABLE OF CONTENTS

# ABBREVIATIONS

| | |
|---|---|
| **ALS** | acid labile subunit |
| **AQP1** | aquaporin 1 |
| **BrdU** | Bromo-5-deoxyuridine |
| **BUN** | Blood urea nitrogen |
| **CKD** | Chronic kidney disease |
| **CP** | Cytoplasm conservation |
| **Col2a1** | Collagen 2 alpha chain 1 |
| **Col10a1** | Collagen 10 alpha chain 1 |
| **DAPI** | 4,6-diamidino-2-phenylindole |
| **GH** | Growth hormone |
| **GP** | Growth plate |
| **IGF** | Insulin growth factor |
| **IGFBP** | Insulin growth factor binding protein |
| **IGF1R** | IGF-1 receptor |
| **IHH** | Indian hedgehog |
| **IOD** | Integrated optical density |
| **NKCC1** | Na-K-Cl cotransporter 1 |
| **MAPK** | Mitogen-activated protein kinase |
| **MMA** | Methyl-methacrylate |
| **PFA** | Paraformaldehyde |
| **PI3K** | Phosphatinositide-3 kinase |
| **POC** | Primary ossification centre |
| **PTHrP** | Parathyroid hormone related protein |
| **OFA** | Osseous front advance |
| **rhGH** | Recombinant human growth hormone |
| **rpm** | Revolutions per minute |
| **SI** | Structural integrity |

| | |
|---|---|
| **SOC** | Secondary ossification centre |
| **SOCS2** | Suppressor of cytokine signaling 2 |
| **SOX9** | SRY-Box Transcription Factor 9 |
| **STAT** | Signal transducer and activator of transcription |

# SUMMARY/ RESUMEN

# | SUMMARY

Growth impairment remains a major complication in pediatric patients with chronic kidney disease (CKD) as only 30% of adults with childhood onset CKD reach a normal final height. CKD alters the morphology and function of the growth plate (GP) of long bones by disturbing the maturation process of chondrocytes.

The general objective of this thesis was to contribute to clarify the mechanism of growth retardation secondary to CKD as well as the effect that growth hormone (GH) exerts on the GP to reverse this delay. Moreover, the specific objectives were: (1) to develop a new procedure that would allow the use of confocal microscopy to investigate the process of chondrocyte hypertrophy; (2) to study the mechanism of growth retardation in experimental chronic kidney disease; (3) to analyze the expression of hypertrophy markers, (4) to know the effect of GH administration on the above-mentioned phases and (5) to analyze the formation and function of the epiphyseal bone plate.

In a first phase of the study, we developed a new procedure based on confocal microscopy that allowed the objective discrimination of different groups of chondrocyte populations on the GP. When applying this methodology to normal growing rats, we classified the chondrocytes in seven different clusters, with four subphases in the pre-hypertrophic zone and three in the hypertrophic zone.

In order to obtain new knowledge about the process of differentiation of chondrocytes in CKD and, therefore, meet the following objectives, the methodology was applied to a CKD induced growth retardation rat model. Chondrocytes were analyzed in growth-retarded young rats with CKD induced by adenine (AD), pair-fed with the AD group (PF) and CKD rats treated with growth hormone (ADGH). The results obtained showed that: (1) The cell volume that chondrocytes reach at the end of hypertrophy was reduced in AD rats, but treatment with GH was able to normalize it; (2) Uremia produced in chondrocytes an alteration of the pattern of variation in the density of the cell cytoplasm that implied a delay in the beginning of the hypertrophy process; (3) Uremia produced a decrease in the expression of the Igf1 and Aqp1 proteins; (4) GH treatment was effective in reversing the impaired maturation of chondrocytes in CKD by restoring the normal onset of the hypertrophy process; (5) The effect of GH was partially mediated by its action on the expression of the membrane cotransporter Nkcc1, which plays an important role in the increase in volume of chondrocytes during hypertrophy. Additionally, to study the formation of the epiphyseal bone plate we performed a time course analysis of tibias of rats at different stages of growth and found that formation of the epiphyseal bone plate occurs in a manner that may be considered as intramembranous-like ossification.

In conclusion, the new method developed in this thesis allowed to obtain additional information to the common measurements of chondrocytes and improved the understanding of the sequence of events that take place during the differentiation process of these cells. When

applying this three-dimensional approach for the first time to study abnormalities in uremic chondrocyte maturation, we have seen that uremic chondrocytes experience a delayed entry into hypertrophy, preventing them from reaching a normal size at the end of the differentiation process. Growth hormone treatment improves growth impairment and reverts the effects of uremia on the final chondrocyte volume, likely by triggering an early chondrocyte enlargement that could be mediated by Nkcc1.

# | RESUMEN

El retraso del crecimiento sigue siendo una complicación importante en los pacientes pediátricos con enfermedad renal crónica (ERC) ya que solo el 30% de los adultos con ERC de inicio en la infancia alcanza una altura final normal. La ERC modifica la morfología y función de la placa de crecimiento (GP) de los huesos largos al alterar el proceso de maduración de los condrocitos.

El objetivo general de esta tesis fue contribuir a esclarecer el mecanismo de retraso del crecimiento secundario a la ERC, así como el efecto que la hormona de crecimiento (GH) ejerce sobre la placa de crecimiento para revertir este retraso. Además, los objetivos específicos: (1) desarrollar un nuevo procedimiento que permitiera el uso de la microscopía confocal para investigar el proceso de hipertrofia de condrocitos; (2) estudiar el mecanismo de retraso del crecimiento en la enfermedad renal crónica experimental; (3) analizar la expresión de marcadores de hipertrofia, (4) conocer el efecto de la administración de GH en las fases mencionadas y (5) analizar la formación y función de la placa de hueso epifisaria.

En una primera fase del estudio, desarrollamos una nueva técnica basada en la microscopía confocal que permitió la discriminación objetiva de distintos grupos de poblaciones de condrocitos en la placa de crecimiento. Al aplicar esta metodología a ratas en crecimiento normal, clasificamos los condrocitos en siete clústeres diferentes, con cuatro subfases en la zona prehipertrófica y tres en la zona hipertrófica. Para obtener nuevos conocimientos sobre el proceso de diferenciación de condrocitos en la ERC y, por tanto, cumplir con los objetivos restantes, se aplicó la metodología a un modelo de rata con hipocrecimiento inducido por ERC. Se analizaron los condrocitos en ratas jóvenes con retraso del crecimiento con ERC inducida por adenina (AD), con restricción de alimentación, pareada con el grupo AD (PF) y ratas con ERC tratadas con hormona del crecimiento (ADGH). Los resultados obtenidos mostraron que: (1) El volumen celular que los condrocitos alcanzaron al final de la hipertrofia se redujo en el grupo AD, pero el tratamiento con GH pudo normalizarlo; (2) La uremia produjo en los condrocitos una alteración del patrón de variación en la densidad del citoplasma celular que implica un retraso en el comienzo del proceso de hipertrofia; (3) La uremia produjo una disminución de la expresión de las proteínas Igf1 y Aqp1; (4) El tratamiento con hormona de crecimiento fue eficaz para revertir la alteración de la maduración de los condrocitos en la ERC mediante la restitución del comienzo normal del proceso de hipertrofia; (5) El efecto de la GH está parcialmente mediado por su acción sobre la expresión del cotransportador de membrana Nkcc1, que juega un papel importante en el incremento de volumen de los condrocitos durante la hipertrofia. Además, para estudiar la formación de la placa ósea epifisaria, realizamos un análisis del curso temporal de las tibias de ratas en diferentes etapas de crecimiento y encontramos que la formación de la placa ósea epifisaria se produce de una manera que puede considerarse como una osificación intramembranosa.

En conclusión, el nuevo método desarrollado en esta tesis ha permitido obtener información adicional a las mediciones comunes de condrocitos y ha mejorado la comprensión de la secuencia de eventos que tienen lugar durante el proceso de diferenciación de estas células. Al aplicar por primera vez este enfoque tridimensional para estudiar las anomalías en la maduración de los condrocitos urémicos, hemos visto que los condrocitos urémicos experimentan una entrada retardada en la hipertrofia, impidiendo que alcancen un tamaño normal al final del proceso de diferenciación. El tratamiento con GH compensó esto al desencadenar un agrandamiento temprano de los condrocitos mediante un mecanismo no totalmente establecido, pero en el que el cotransportador de membrana Nkcc1 podría tener un papel importante.

# I.INTRODUCTION

# | GROWTH

## Phases of Normal Growth

Children increase in height because of longitudinal bone growth that occurs at the GP. Growth is not a linear process but fluctuates according to age and maturation, longitudinal bone growth occurs rapidly in early life but then slows and, eventually, ceases. During the prenatal/fetal life, growth occurs at the fastest velocity, especially between gestational weeks 20 and 24, when the human fetus growth rate averages 2.5cm per week [1]. Fetal growth depends on maternal factors including placenta and chronic diseases of the mother, such as malnutrition, diabetes, arterial hypertension and toxics, as tobacco or alcohol, have the potential to decrease the size of the new-born **(Figure 1).**

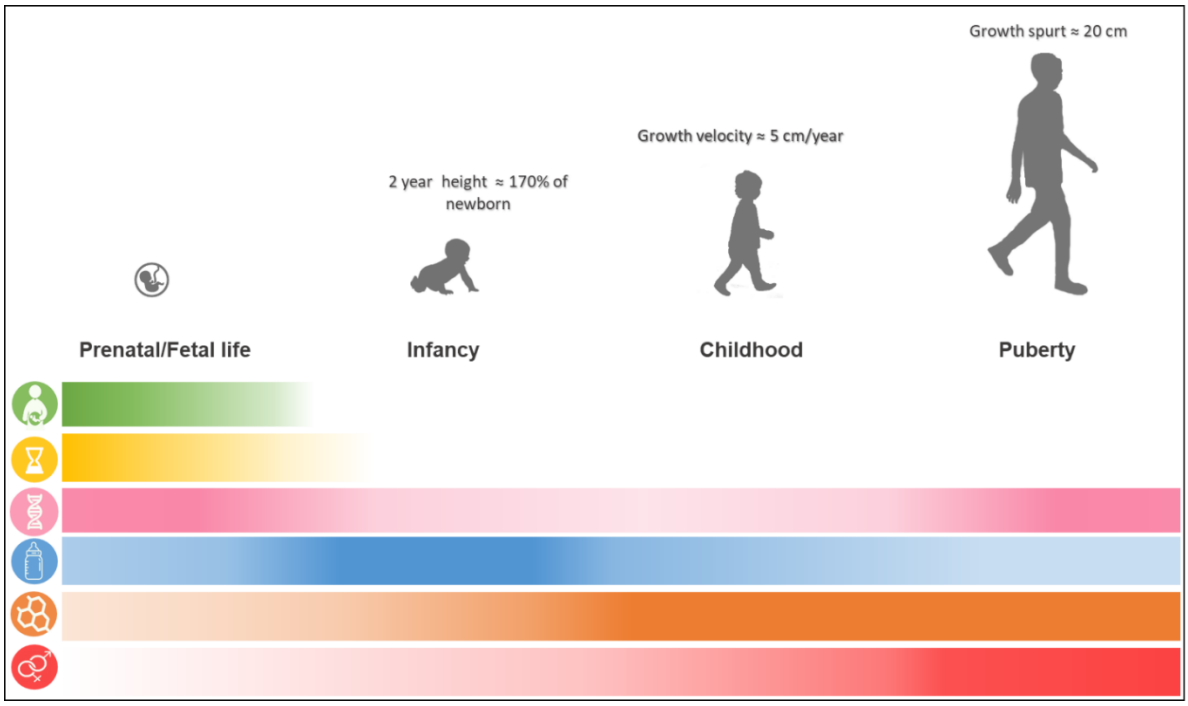


**Figure 1. Phases of normal growth and regulating factors.** Colour legend: Green, maternal factors. Yellow, gestational age. Pink, genetics. Blue, nutrition. Orange, hormones. Red, sexual differences. Colour intensity determines the importance of the factor for each phase of growth.

Postnatal growth takes place in three partly overlapping periods: infancy, childhood and puberty **(Figure 1)** [2]**.** In infancy, growth averages 25 cm per year and is influenced predominantly by nutrition [3]. Growth during childhood is primarily dependent on thyroid hormones (TH) and growth hormone (GH), nutrition playing a permissive role [4]. After infancy, the maximum growth rate, occurs during later stages of puberty at around 12 years in girls and 14 years in boys [5]. Growth in puberty is influenced by genetic factors and, more importantly,

by changes in sexual hormones [6]. During this final phase, growth in height accelerates, then peaks, and finally falls to zero. The peak of growth is named the pubertal growth spurt and is a time of rapid increase in bone length followed by the cessation of longitudinal growth. In boys, signs of puberty appear before the growth spurt begins whereas in girls both run in parallel.

## Growth Alterations in Disease

There are about two hundred different conditions that can cause alterations in the normal growth patterns, each having different causes, symptoms and treatments. These conditions can be grouped into three main types, depending on the overall cause of the condition. These are:

- Problems with the growth process itself, also known as primary growth disorders.
- Problems caused by external factors such as malnutrition or long-term illness, also known as secondary growth disorders.
- Unknown causes – when it is not possible to identify the cause of the growth disorder, also known as idiopathic growth disorders.

## Bone Development

Growth implies an increase in volume of the organs by hyperplasia (cell number increase), hypertrophy (cell size increase) and/or extracellular matrix synthesis. Most organs of the body are non-rigid and new elements can be added to any internal area, in a process named volumetric interstitial growth. By contrast, rigid organs are unable to grow by adding material internally, but new elements must be added to the external surface. This process is called appositional (or surface) growth and implies a significant limitation in the area of new material incorporation, so that, it is less efficient for rapid growth. Since bones are very rigid organs, they must grow by apposition.

Based on the development of bone, formation can be divided in two types, called endochondral and intramembranous bone formation/ossification. During **intramembranous ossification**, the connective tissue membrane of undifferentiated mesenchymal cells changes into bone and matrix bone cells, resulting in the formation of the flat bones of the cranial vault [7,8].

Conversely, during **endochondral ossification,** the tissue that will become bone is firstly formed from cartilage, a tissue with high growth potential. Endochondral ossification is an essential process during the rudimentary formation of long bones, the growth of the length of long bones, and the natural healing of bone fractures. It can be summarized in six stages **(Figure 2)**:

1. Mesenchymal cells of either neural crest in the craniofacial region or mesoderm elsewhere in the body condense and form a shape template of the future bone.
2. Mesenchymal cells in the core differentiate into chondrocytes and cells in the periphery form the perichondrium.
3. Chondrocytes start differentiating and the centers of the epiphyses begin to calcify. Chondrocytes show hypertrophic changes and calcification from the cartilage matrix continues.
4. The calcification of the extracellular matrix prevents nutrients from reaching the chondrocytes and causes them to undergo apoptosis. The resulting cell death voids in the cartilage template and allows blood vessels to invade. Blood vessels carry in osteogenic cells that trigger the transformation of the perichondrium into the periosteum. The primary ossification centre (POC) forms, a region deep in the periosteal collar where ossification begins.
5. Whereas bone is replacing cartilage in the diaphysis, cartilage continues to proliferate at the ends of the bone, increasing bone length. These proliferative areas become the epiphyseal GPs, which provide longitudinal growth of bones after birth and into early adulthood.
6. After birth, the same process is basically recapitulated in the epiphysis where; where the secondary ossification centre (SOC) forms.

**Figure 2. Overview of development of a bone by endochondral ossification.** (1) Mesenchymal cells of either neural crest in the craniofacial region or mesoderm elsewhere in the body condense and form a shape template of the future bone. (2) Mesenchymal cells in the core differentiate into chondrocytes and cells in the periphery form the perichondrium. (3) Chondrocytes start differentiating and calcified matrix with calcified central cartilage primordium matrix is formed. Chondrocytes show hypertrophic changes and calcification from the cartilage matrix continues. (4) The calcification of the extracellular matrix prevents nutrients from reaching the chondrocytes and causes them to undergo apoptosis. The resulting cell death voids in the cartilage template and allows blood vessels to invade. Blood vessels carry in osteogenic cells that trigger the transformation of the perichondrium into the periosteum. The primary ossification center forms, a region deep in the periosteal collar where ossification begins. (5) While bone is replacing cartilage in the diaphysis, cartilage continues to proliferate at the ends of the bone, increasing bone length. These proliferative areas become the epiphyseal growth plates, which provide longitudinal growth of bones after birth and into early adulthood. (6) After birth, this entire process repeats itself in the epiphyseal region; where the secondary ossification center forms (SOC).

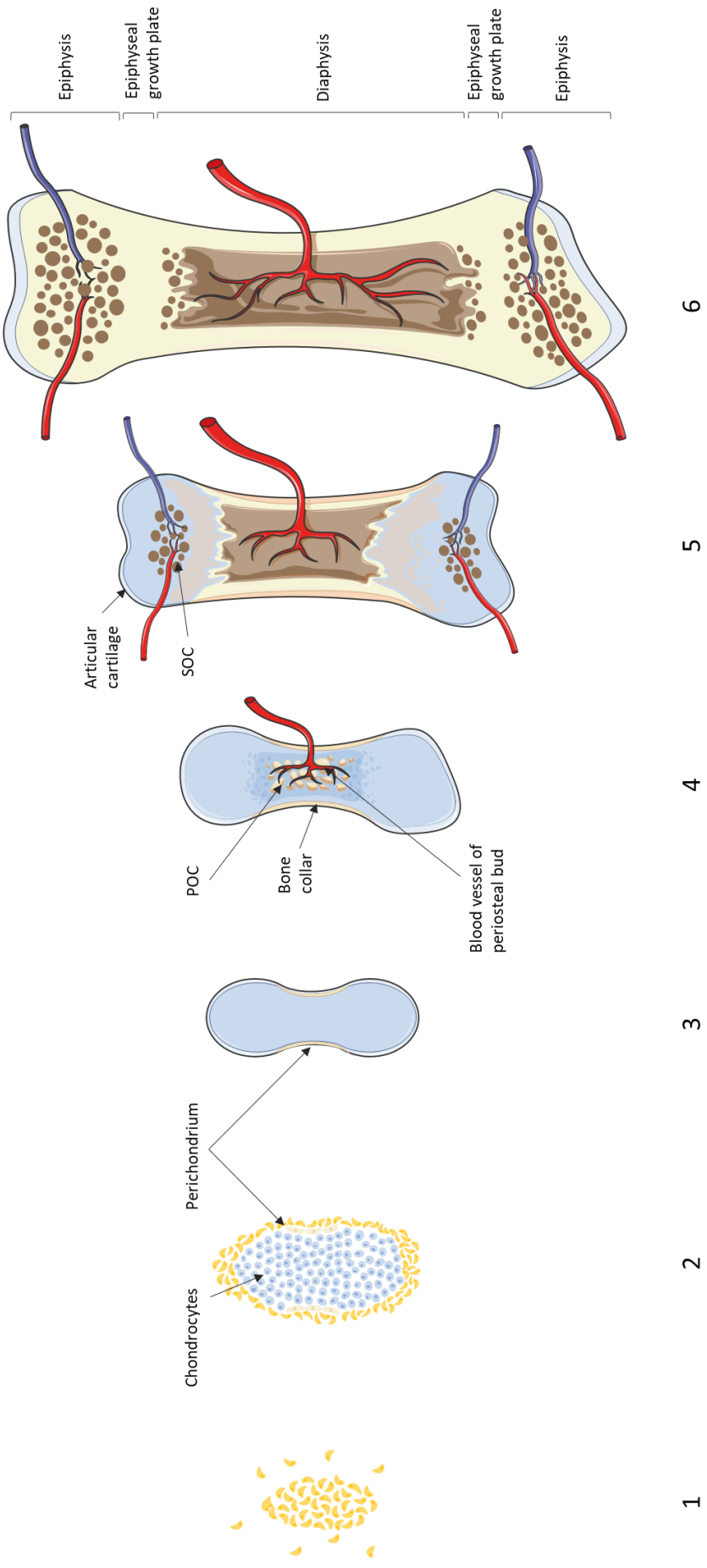
Epiphysis
Epiphyseal growth plate
Diaphysis
Epiphyseal growth plate
Epiphysis
Articular cartilage
SOC
POC
Bone collar
Blood vessel of periosteal bud
Perichondrium
Chondrocytes
6
5
4
3
2
1

## Growth Plate: Physiology and Regulation

The **growth plate** (or epiphyseal growth plate, *physis* or growth cartilage) is the area of growth in a postnatal long bone (**Figure 3**). It is a hyaline cartilage located in the metaphyseal end of long bones. This structure is found in children and adolescents, whereas it disappears and is replaced by an epiphyseal line in adults when height growth stops. This replacement is known as epiphyseal closure.

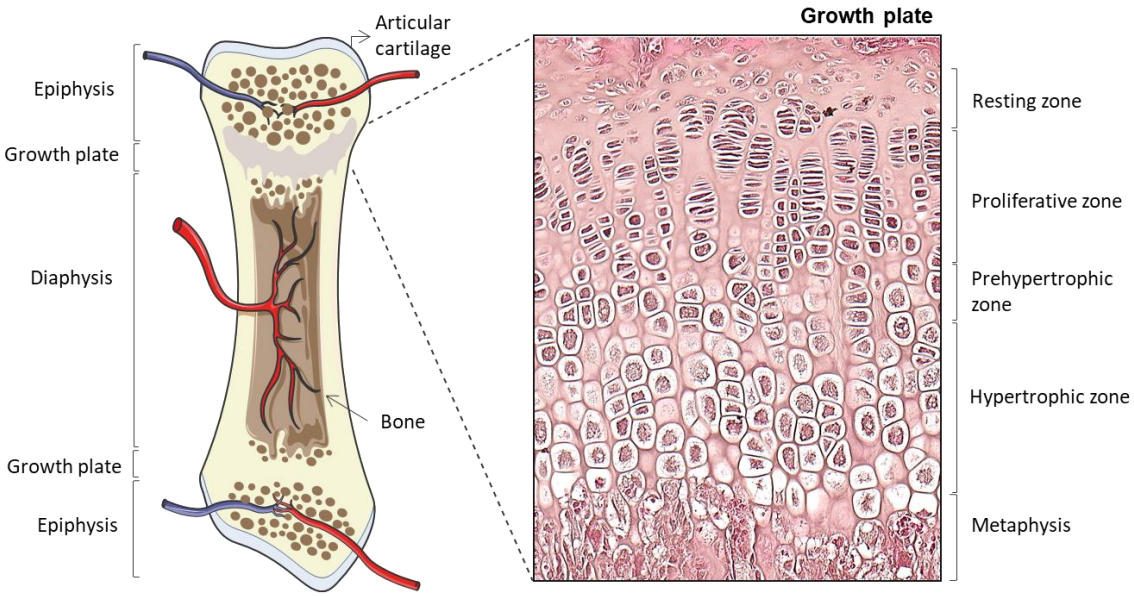


**Figure 3. Growth plate structure and regulation.** The growth plate is a thin cartilage structure situated in the ends of long bones between the epiphysis and diaphysis. Four distinct zones can be distinguished: resting, proliferative, prehypertrophic and hypertrophic zones.

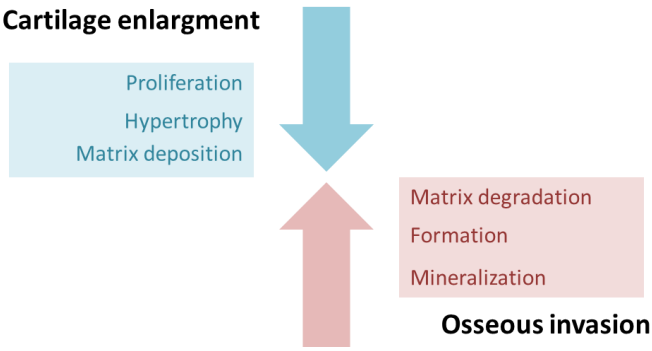


**Figure 4.** The balance between cartilage enlargement and osseous invasion is essential to maintain the adequate dynamic of endochondral growth.

Chondrocytes within the GP elongate the bone by proliferation, progression, hypertrophy, and synthesis of extracellular matrix. The continual production of cartilage is coordinated with a process of cartilage replacement by bone at the chondro-osseous junction,

leading to the lengthening of the bone by progressive apposition of the osseous tissue [8] (**Figure 4**).

In growth cartilage, chondrocyte proliferation occurs near the epiphysis and chondrocyte hypertrophy occurs close to the diaphysis. This spatial distribution leads to the identification of four strata or zones according to the characteristics of chondrocytes: reserve, proliferative, prehypertrophic and hypertrophic zones **(Figure 3).** At the epiphyseal end of the GP, the **reserve zone,** also called germinal or stem cell zone, contains the resting chondrocytes, crucial for the orientation of the underlying columns of chondrocytes [9]. Upon some unknown trigger, the stem cells enter the **proliferating zone.** In this matrix-rich zone, the flattened chondrocytes undergo cell divisions in a direction parallel to the long axis of bone and organize in a typical columnar disposition. GP chondrocytes synthesize substantial amounts of extracellular matrix proteins, which are essential for the structure of the GP. At a given moment, either by a finite predetermined number of cell divisions or by changes in the exposure to local growth factors, proliferating chondrocytes lose their capacity to divide, start to increase in size and differentiate to **prehypertrophic chondrocytes**. Then, they further progress in the differentiation pathway to become **hypertrophic chondrocytes**, having a longitudinal axis greater than the transversal axis, and secrete large amounts of matrix proteins. The rate of bone elongation is to a large extent dependent upon the velocity and magnitude of this chondrocyte volume enlargement [10–14]. Simultaneously, blood vessels, osteoclasts, and osteoblasts, invade the distal hypertrophic zone and remodel it into bone [15]. The net result is that new bone is formed at the boundary between the growth cartilage and the metaphysis, causing the bones to grow longer and the child to become taller.

### | Hypertrophy of Chondrocytes

The rate of longitudinal bone growth is determined by the number of proliferative and hypertrophic cells, the rate of division of proliferative chondrocytes, the rate of volume increase of the hypertrophic zone cells and the final volume attained by this cells [11]. Nevertheless, is the final step of chondrocyte maturation, hypertrophy, that is the primary driver behind bone elongation, being responsible for more of 60% of longitudinal bone growth [13,14,16]. Surprisingly, little attention has been paid to the way in which the proper volume increase occurs and the intracellular mechanisms underlying volume enlargement and cell-shape change during chondrocyte hypertrophy remain much less understood. Early electron microscopic studies showed that hypertrophic chondrocytes have markedly more lucent cytoplasm and subsequent stereological studies reported that only the 15% of the total cell volume increment can be accounted for by the increase of cytoplasmic organelles. Such observations suggested that the cell volume increase of hypertrophic chondrocytes could be mostly due to unbalanced water accumulation or swelling [10]. However, later studies revealed that the osmotic fractions did not change as chondrocytes progress from proliferative to hypertrophic regions of the GP. These

authors postulated that a directional cell volume increase may occur through a combination of both true hypertrophy and swelling [17].

Cooper et al. (2013) found that the increase of chondrocyte volume to result from three sequential stages by using tomographic phase microscopy [18]: two stages of ***true hypertrophy*** (phases 1 and 3) when chondrocytes increase their volume with active synthesis of cytoplasmic components separated by a stage of ***swelling*** (phase 2), when volume keeps increasing but synthesis ceases and the cytoplasm density decreases (Figure 5). IGF-I was found to specifically affect chondrocyte hypertrophy during phase 3. This last phase of true hypertrophy differs from phase 1 in that it occurs at unusual low density. These findings supported the view of chondrocyte hypertrophy as a sequence of events, each susceptible of independent regulation, and enabled new possibilities for understanding growth regulation and growth disorders. Membrane proteins such as $Na^+$, $K^+$, $2Cl^-$ cotransporter (Nkcc1) and aquaporin 1 (Aqp1) have been recently shown to be expressed at the hypertrophic zone and likely play and important role in the process of chondrocyte volume increase [19,20].

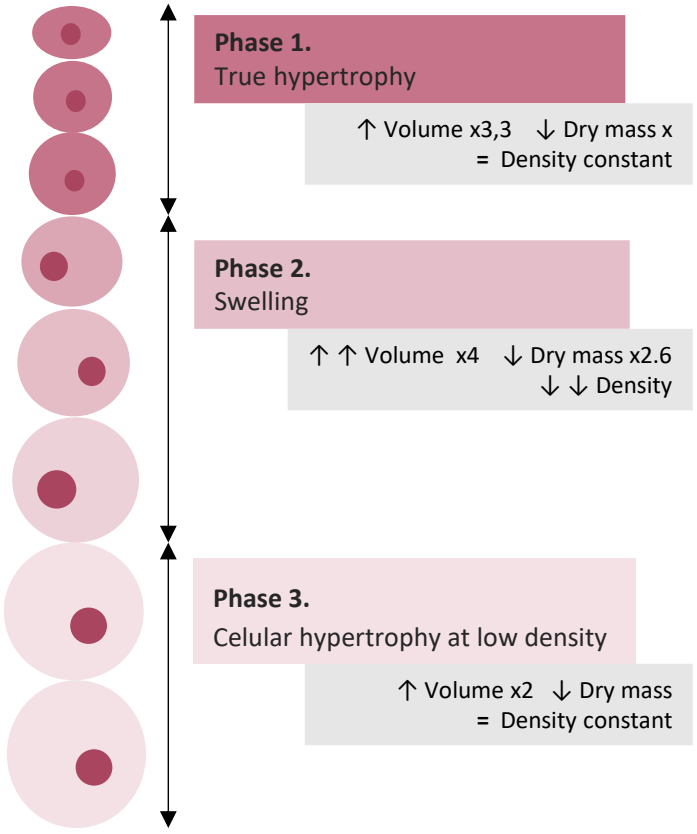


**Figure 5. Hypertrophy of chondrocytes**. The process is divided in two stages of true hypertrophy (phases 1 and 3) when chondrocytes increase their volume with active synthesis of cytoplasmic components separated by a stage of swelling (phase 2), when volume keeps increasing but synthesis ceases and the cytoplasm density decreases.

### | Regulation of the Growth Plate

The functions of chondrocytes are tightly regulated by circulating hormones, such as GH, insulin-like growth factor I (IGF-I), thyroid hormones, estrogens and androgens and vitamin D, as well as inflammatory cytokines and autocrine and paracrine factors produced locally by chondrocytes themselves [8]. These factors elicit their control over chondrocyte function during their differentiation cascade and may have variable importance according to the species and stage of life. Locally produced transcription factors (e.g., Sox9 and Runx2) and other peptides produced by chondrocytes (e.g., Indian hedgehog protein, parathyroid hormone-related peptide, fibroblast growth factors, and bone morphogenetic proteins) are important for proper development and regulation of the morphological heterogeneity of GP chondrocytes in a not well defined way [8,21]. Thus, alterations of many of these hormones and local factors have been associated with disorders causing GP dysfunction and short stature [22,23]. An overview of the most relevant systematic and local factors that have been proposed by experimental procedures to regulate the GP functions are depicted in **Figure 6**.

## The Epiphyseal Bone Plate

The epiphyseal bone plate is a flat bony structure located between the epiphysis and the metaphysis of the long bones [24]. It holds the GP, providing the weakest area of the growing bone with strength and stability. In addition to structural support, the epiphyseal bone plate also has a nutritional role by allowing the passage of blood vessels from the epiphysis to form a capillary network that supplies the growth cartilage with oxygen, nutrients and chemical signaling.

The epiphyseal bone plate is formed by ossification of the lower part of the epiphyseal cartilage after the development of the SOC. At the beginning, the SOC expands in all directions to form spongy bone trabeculae with a radial orientation. However, the mode of ossification substantially changes when the front approaches the region facing the resting cartilage of the GP. At this location, cartilage is directly transformed into compact bone tissue to generate a flat plate with several layers of densely packed bony lamellae-oriented transverse to the long axis of the bone [25]. The formation of the epiphyseal bone plate has some peculiar characteristics that make it different from a standard endochondral ossification process. Firstly, it is considered as a specialized extension of the cortical bone [26], which is usually formed through direct-intramembranous ossification. Secondly, it is oriented perpendicular to the long axis of the bone, an unusual orientation since most bone structures are oriented such that they are stronger in the direction in which they support load [27]. Thirdly, it develops very quickly, so that transformation of cartilage into bone occurs faster than anywhere else in the bone [28]. Finally, it is formed in the region immediately adjacent to the resting cartilage of the GP and this close

spatial proximity suggests that the latter could exert a great deal of influence on its development [29].

Despite the above considerations and the fact that the epiphyseal bone plate could be considered a structural component of the growth plate that influences its function, it has been largely unexplored and is one of the least understood parts of the long bones. Even little is known about how it is affected by diseases associated with growth failure and bone abnormalities.

**Figure 6. Regulation of the growth plate.** The regulation of the GP involves a complex interplay of systemic and local factors acting at the different stages of the chondrocyte differentiation process to maintain the dynamics of the endochondral growth. The figure represents most factors involved in the endochondral growth process that are described in the literature to date. RZ, resting zone; PZ, proliferative zone; PHZ, prehypertrophic zone; HZ, hypertrophic zone; LHZ, late hypertrophic zone; OB, osteoblasts; OCL, osteoclasts; OC, osteocyte; P, periosteum. Colored bar: Stratum where the factor is being expressed; Stripped bar: Stratum where the factor exerts its function; Color stripped bar: Stratum where the factor is being expressed and exerts its function.

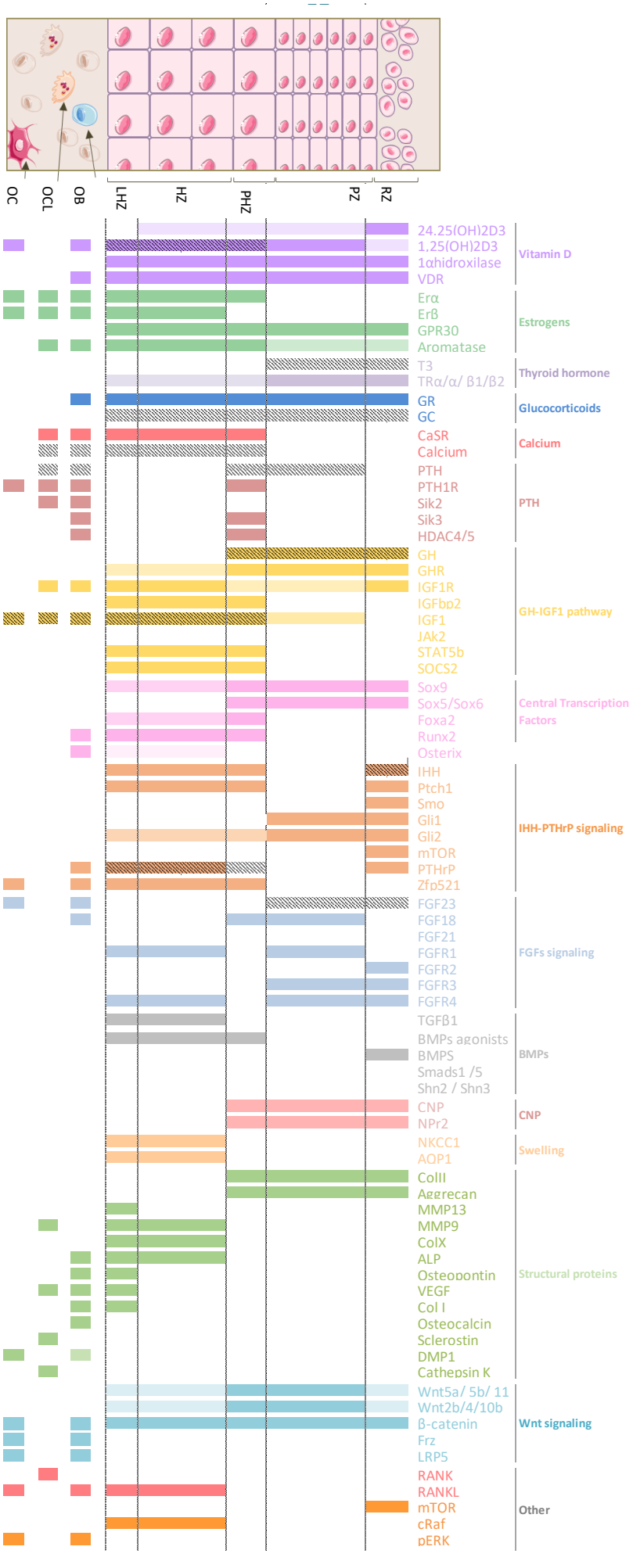
OC
OCL
OB
LHZ
HZ
PHZ
PZ
RZ
24.25(OH)2D3
1,25(OH)2D3
1αhidroxilase
VDR
Vitamin D
Erα
Erβ
GPR30
Aromatase
Estrogens
T3
TRα/α/ β1/β2
Thyroid hormone
GR
GC
Glucocorticoids
CaSR
Calcium
Calcium
PTH
PTH1R
Sik2
Sik3
HDAC4/5
PTH
GH
GHR
IGF1R
IGFbp2
IGF1
JAk2
STAT5b
SOCS2
GH-IGF1 pathway
Sox9
Sox5/Sox6
Foxa2
Runx2
Osterix
Central Transcription Factors
IHH
Ptch1
Smo
Gli1
Gli2
mTOR
PTHrP
Zfp521
IHH-PTHrP signaling
FGF23
FGF18
FGF21
FGFR1
FGFR2
FGFR3
FGFR4
FGFs signaling
TGFβ1
BMPs agonists
BMPS
Smads1 /5
Shn2 / Shn3
BMPs
CNP
NPr2
CNP
NKCC1
AQP1
Swelling
ColII
Aggrecan
MMP13
MMP9
ColX
ALP
Osteopontin
VEGF
Col I
Osteocalcin
Sclerostin
DMP1
Cathepsin K
Structural proteins
Wnt5a/ 5b/ 11
Wnt2b/4/10b
β-catenin
Frz
LRP5
Wnt signaling
RANK
RANKL
mTOR
cRaf
pERK
Other

# | CHRONIC KIDNEY DISEASE AND GROWTH

## General Aspects

Chronic kidney disease (CKD) is defined by current international guidelines as decreased kidney function shown by glomerular filtration rate (GFR) of less than 60ml/min per 1.73m$^2$ or markers of kidney damage, or both, of at least 3 months duration, regardless of the underlying cause [30]. Its classification is made based on the cause, category of glomerular filtration and category of albuminuria according to the criteria of the "Kidney Disease Improving Overall results" [31].

Even though the treatment for CKD has improved over the years, impairment of lineal growth remains a prevalent problem in pediatric patients, and only 30% of the adults with childhood onset CKD reach a normal final height [32,33]. Along with the psychological effects of short stature, growth retardation is associated with greater morbidity and mortality in CKD patients, so that for each reduction in the height standard deviation score (SDS) of 1 SD, mortality has been shown to increase by 14% and risk of death to double when the height stands below percentile 1 [34].

Children who have congenital CKD are of small size at birth and/or typically fall below the 3$^{rd}$ length percentile during infancy and then their rate of growth parallels the normal growth curve staying below the 3$^{rd}$ percentile. In these patients, the pubertal spurt is also delayed and associated with a reduced growth velocity, contributing to the loss of growth potential and reduced final height in adulthood [35]. Children receiving dialysis have more profound growth retardation and although growth velocity improves after transplantation, catch-up growth post-transplantation depends on age, graft function, and systematic steroid exposure [36].

The pathogenesis of growth retardation in CKD is multifactorial and only partially understood [37,38]. A schematic description of what is known about its pathogenesis is provided in **Figure 7.**

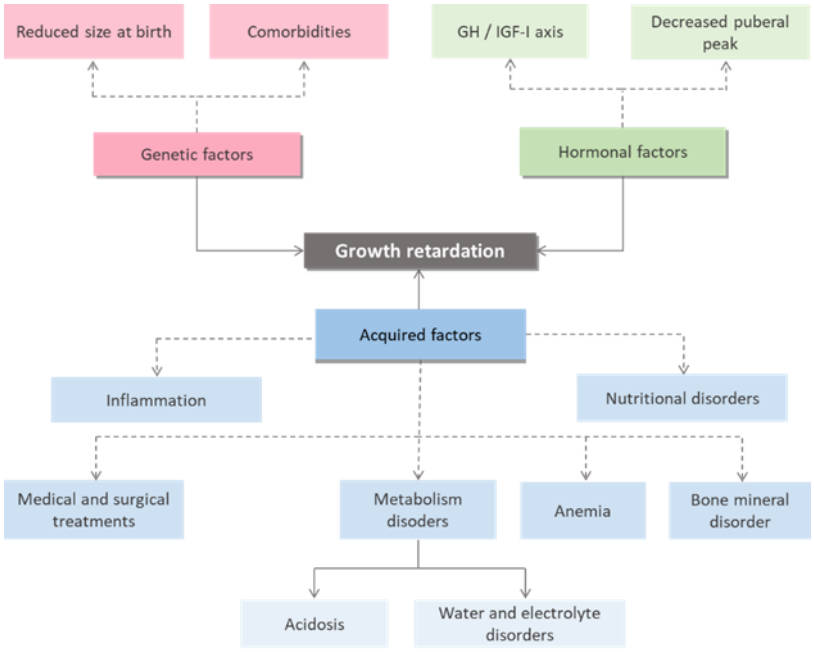


**Figure 7. Schematic representation of the pathogenesis of growth impairment in CKD.** Causes of growth failure in children with CKD include genetic factors and syndromes, delay and/or lack of a pubertal growth spurt, GH and insulin-like growth factor (IGF)-I axis abnormalities, nutritional abnormalities metabolic derangements such as acidosis and electrolyte imbalance, bone mineral disorder or anemia.

## Growth Plate in Uremia

There is limited information on the alterations of the morphology and dynamics of the GP and in the factors regulating chondrocyte proliferation and differentiation in CKD **(Table 1).** The anatomic characteristics of the GP make its study extremely difficult in the clinical setting and what is known about its pathogenesis. Available data in humans are limited to necropsy studies in individual patients showing an expanded and profoundly disorganized GP in end-stage renal disease [39]. Young rats made uremic by 5/6 nephrectomy or, more recently, by intake of adenine are habitually used as animal model to investigate growth retardation in CKD [40,41].

In brief, the height of the GP cartilage has been described to be increased, reduced or unchanged compared to normal renal function pair-fed rats [42–49]**.** The variability in growth cartilage size depends to a great extent on the time of sacrifice and the severity of uremia [50]. When the GP is greater than normal, it results from an expansion of the hypertrophic zone and seems to depend on a delay in the progression of the hypertrophic chondrocytes rather than from modifications in the proliferative activity, which is also reduced in CKD [44].

More importantly, chondrocytes of uremic rats achieve a lower final size than those of control rats. This is crucial because longitudinal growth rate in mammals, as discussed in the *Growth* chapter, has been described to be dependent on the volume increase of GP terminal hypertrophic chondrocytes [14]. Further understanding of the process of chondrocyte maturation and hypertrophy as well as the participation of proteins involved in the regulation of the different phases of cell enlargement are necessary to unravel the cellular and molecular basis of growth impairment secondary to CKD. Membrane protein transporters such as *NKCC1* and *AQP1* have been recently shown to be expressed at the hypertrophic zone and likely play

and important role in the process of chondrocyte volume increase [19,20]. However, no noticeable changes in the pattern of Aqp1 and Nkcc1 protein distribution have been found in growth-retarded young uremic rats [20].

High pharmacological doses of GH accelerate growth velocity [51] and improve, although do not normalize, final height of patients with CKD [52]. GH administration accelerates growth rate as a result of stimulating the proliferation of GP chondrocytes and reversing the inhibiting action of uremia on the process of maturation and enlargement of chondrocytes. GH treatment does not decrease the growth cartilage height but it seems to cause a beneficial effect on chondrocyte maturation, as shown by normalization of the size of most distal chondrocytes and a more organized aspect of the cartilage/metaphyseal bone junction on experimental animal models [20,53].

## | Alterations of the GH-IGF1 Axis

GH is the key regulator of postnatal growth. Children who lack GH have short stature and GH therapy given before puberty increases their rate of growth and ultimate height. The secretion of GH from the anterior pituitary is pulsatile and under a variety of hormonal influences, such as stimulatory hypothalamic GHRH, ghrelin and sex steroids, and inhibitory somatostatin, IGF-1 and glucocorticoids. GH interacts with GP through GH receptors (GHR) located in chondrocytes and, indirectly, through systemic and local stimulation of IGF-I [54].

Upon binding to GHR at the GP's chondrocytes, GH activates several intracellular signal transduction pathways, including four signal transducers and activators of transcription pathways (STAT1, -3, -5a and -5b), the mitogen-activated protein kinase (MAPK) and the phosphoinositide-3 kinase (PI3K) pathways, which regulate the transcription of GH target genes, including IGF-I [55], IGF binding protein 3 (IGFBP3) or acid labile subunit, ALS (IGFALS).

The Janus kinase 2/signal transducers and activators of transcription (JAK2/STAT) signaling pathway is required for the GH stimulus of IGF-I production [55]. Upon binding to GHR at the GP's chondrocytes, it induces dimerization of the receptor, resulting in tyrosine phosphorylation of Janus-associated kinase 2 (JAK2), a tyrosine kinase associated with the intracellular domain of the receptor. Phosphorylation induces the kinase activity of JAK2, which in turn phosphorylates/activates a group of molecules known as signal transducers and activators of transcription (STATs).

**Table 1. Growth plate alterations in advanced chronic kidney disease (CKD) and effect of growth hormone (GH) treatment**

| | Description |
|---|---|
| **General structure** | ▪ Increased, reduced or unchanged height depending on the severity and duration of CKD<br>▪ Disorganization of the columnar arrangement<br>▪ Marked irregularity of the metaphyseal bone/cartilage interface<br>▪ Expansion of the hypertrophic zone |
| **Dynamics** | ▪ Reduced velocity in the advance of chondrocytes<br>▪ Disequilibrium between bone apposition rate and cartilage production and progression |
| **Chondrocytes** | ▪ Reduction of the proliferative activity<br>▪ Alteration of the maturation process<br>▪ Low height of terminal chondrocytes |
| **GH-stimulated JAK2/STAT pathway** | ▪ Reduced expression of GH receptor<br>▪ Impaired phosphorylation of JAK2.<br>▪ Impaired phosphorylation and nuclear translocation of STAT5 proteins.<br>▪ Reduced expression of IGF-I |
| **GH treatment** | ▪ Accelerated growth velocity<br>▪ Improved final height<br>▪ Stimulation of the proliferation of growth cartilage chondrocytes<br>▪ Normalized size of terminal chondrocytes<br>▪ Reorganization of the cartilage/metaphyseal bone junction |

*See text for further details.

Upon activation, the STATs dimerize and translocate to the nucleus, where they regulate the expression of target genes responsible for GH action, including IGF-I [55]. Although Stat1, -3, 5a and -5b can all be activated by GH, Stat5b is essential for the GH-stimulated IGF-1 expression in rats [56,57] and for normal growth, as shown by the discovery of individuals with profound growth failure, short stature, and loss of responsiveness to GH, who had mutations within the STAT5B gene [58] (**Figure 8**).

The JAK2/STAT signaling pathway is regulated by several factors, including signal transducers and suppressor of cytokine signaling (SOCS) proteins. SOCS-2 has been found to bind to cytokine receptor-JAK2 complexes and inhibit JAK2 kinase activity [59]. GH stimulates the expression of some members of the SOCS family through activation of the JAK2/STAT pathway, providing, in turn, a negative feedback loop regulating GH activity.

Alterations in the GH-stimulated JAK2/STAT pathway likely contribute to the partial resistance to GH action characteristic of advanced CKD. In the GP of young uremic rats, reduced expression of GH receptor [60] and IGF-I [61] have been found. Phosphorylation of JAK2 and the downstream proteins phosphorylated by this kinase, namely the GHR, STAT5, STAT3, and

STAT1, were impaired in liver and the STAT5 phosphorylation was depressed by 50%–75% [62]. In addition, Troib *et al* [63] reported a defect in GH signal transduction characterized by impaired phosphorylation and nuclear translocation of GH-activated STAT proteins in the chondrocytes of uremic rats. Since activation of STAT5b is crucial for normal growth [64], this defect contributes to the local tissue insensitivity to GH and points to a post-receptorial defect as a mechanism responsible for growth retardation in CKD [62,63].

Recent studies have proposed SOC-2 as a major cause of attenuated JAK-STAT signaling. Elevated expressions of SOC-2 and SOC-3 mRNA in skeletal muscle, liver and GP have been found in uremic rats [62,63,65]. If this increase in gene expression were accompanied by an increase in protein expression, this would provide a potential explanation for the depressed signal transduction. An acquired defect in GHR-JAK2-STAT signaling with upregulation of SOCS expression has also been described in inflammatory conditions. This may be relevant to GH resistance in uremia as patients with advanced CKD often have chronic inflammation [66] The mechanism accounting for the increase in SOCS gene expression in uremia remains unclear. One possible mechanism could involve the action of inflammatory cytokines that stimulate signal transduction via other members of the Janus kinase family such as JAK1, JAK3 and Tyrk2, not demonstrated to be affected in renal failure [67]. Accordingly, the proinflammatory cytokine IL-6, together with its signaling transducer STAT3 and its gene product SOC-3, were found to be significantly increased in uremia. SOC-3 is a potent negative feedback inhibitor of IL-6 and GH signaling and may well contribute to the GH-resistant state in CKD [68].

It is also of note that children with advanced CKD have marked alterations in the pattern of circulating insulin-like growth factor binding proteins (IGFBP) leading to decreased IGF bioactivity [58]. IGFBPs in CKD serum inhibit IGF action in cultured GP chondrocytes likely by competition with the type 1 IGF receptor for IGF binding [58]. Interference of unsaturated IGFBPs with the IGF action might be a mechanism contributing to GH resistance in uremia.

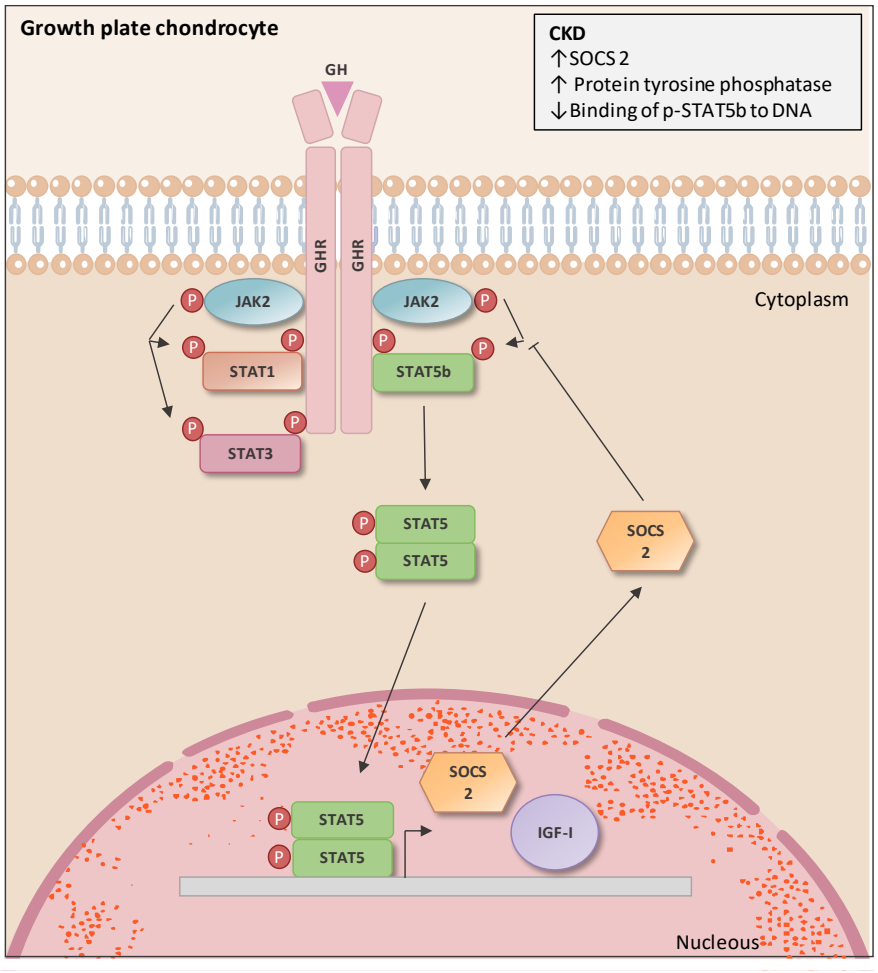


**Figure 8. GH mediates its effects in growth plate's chondrocytes by the JAK/STAT5b signaling pathway.** Upon binding to GHR at the growth plate's chondrocytes, GH activates the JAK2/STAT signaling pathway, required for the GH stimulus of IGF-I production. SOC2 are induced by GH and act as a negative feedback regulator of the signaling pathway.

# II.HYPOTHESIS

On the basis that:

1. The increase in volume of chondrocytes during hypertrophy is the major determinant of the rate and extent of bone lengthening.
2. CKD interferes with the maturation and change in size of the GP chondrocytes.
3. This effect is related to the growth impairment secondary to CKD.
4. The administration of GH increases the longitudinal growth rate and reverses, at least in part, this adverse effect of the CKD.
5. The GP's chondrocytes enlargement is related to processes of cellular hypertrophy, in its final phase IGF1-dependant, and intracellular fluid accumulation.
6. The epiphyseal bone plate could be considered a structural component of the growth plate that influences its function.

It is proposed that the development of a model of growth impairment secondary to chronic renal failure and the comparison of the experimental groups will allow to analyze the effects of the renal failure and the treatment with GH on growth. Also, the development of a new histological technique to approach the growth plate cartilage will offer original and relevant data on the maturation process of chondrocytes and the influence of chronic renal failure and GH treatment on this process.

# III.OBJECTIVES

# | GENERAL

To contribute to clarify the mechanism of growth retardation secondary to CKD and the growth-promoting effect of GH treatment on this entity.

# | SPECIFIC

(1) To develop a new procedure that would allow the use of confocal microscopy to investigate the process of chondrocyte hypertrophy.

(2) To study the mechanism of growth retardation in experimental chronic kidney disease and analyze if the decrease in the longitudinal growth rate is associated with an alteration of the chondrocytic hypertrophy pattern.

(3) To analyze the expression of hypertrophy markers.

(4) To know the effect of GH administration on the above-mentioned phases.

(5) To analyze the formation of the epiphyseal bone plate

# IV.MATERIALS AND METHODS

# | THREE-DIMENSIONAL ANALYSIS OF CHONDROCYTES

## Animals

The study was carried out in six weeks old female Sprague-Dawley rats (Charles River Laboratories, L´Arbresle, France). Procedures involving animals and their care were conducted according to Spanish law on the use of experimental animals, which acknowledges the European Directive 86/609. The project proposal was approved by the Ethical Committee of University of Oviedo, Spain. Rats were housed in individual cages under controlled conditions of light (12 light/dark cycles) and temperature (21–23 °C) with free access to rats' standard diet and tap water. Animals were sacrificed under lethal dose of Dolethal® anesthesia.

This work comprised three consecutive steps. First, we established a procedure for processing the GP which would result in the preservation of the structure of the hypertrophic chondrocytes and be suitable to obtain three-dimensional images of whole (non-sectioned) chondrocytes inside their native lacunae by using confocal microscopy. A group of twelve rats was used for this first study. The second step was to apply the procedure for analysis of cell changes during chondrocyte proliferation and hypertrophy in the GP. A cluster analysis was performed to classify chondrocytes according to quantitative analysis of volume, shape, and cytoplasm density. Finally, an immunohistochemical study of the expression of proteins associated with the process of chondrocyte differentiation in the GP cartilage was performed to further characterize the different classes of subpopulations discriminated by their morphological features.

## Procedure

### | Tissue Collection

The tibia and femur of each leg were separated at the knee joint immediately after death and were then bisected sagittally with the aid of a stereomicroscope using high quality sharp blades. Next, the two halves of each bone were cut again parallel to the parasagittal plane to obtain two slices of about 2 mm in thickness, a medial one and a lateral one. Two medial slices and two hemispherical-like caps of about 2 mm in thickness were obtained from each bone. Medial slices were used to compare the effectiveness of a series of fixation and staining solutions whereas hemispherical-like caps were used as negative controls to characterize background fluorescence. One of the four hemispherical-like caps in each bone was not fixed and embedded without staining to control fluorescence due to the intrinsic biomolecules of the chondrocytes (native autofluorescence) and the other three were fixed each with one of the three fixatives (see later) and embedded without staining to control fluorescence due to fixation (induced autofluorescence). A total number of forty-eight tibial samples and forty-eight femoral samples were obtained for positive analysis and the same number for background fluorescence controls.

Bone slices were placed without delay in the fixative solution to minimize the time lapse between surgical excision of the specimen and fixation. Fixation, staining and dehydration were carried out at 4ºC to retard autolysis and prevent extraction of cytoplasm material during the procedure. Likewise, the osmolarity of the solutions were always adjusted to be isotonic with the tissue (300 mOsm) to preserve the normal volume/morphology of the chondrocytes. Samples were individually placed in glass vials 10 ml, 24.5 mm diameter x 41 mm high with clip-on caps (Taab G060). Samples remained in the same glass vial until they were moved into the moulds for polymerization. The procedure does not include demineralization, or conventional sectioning. It consists of a sequence of five steps: (1) fixation, (2) In-block staining, (3) embedding and block formation, (4) ground section preparation, and (5) analysis with confocal microscopy.

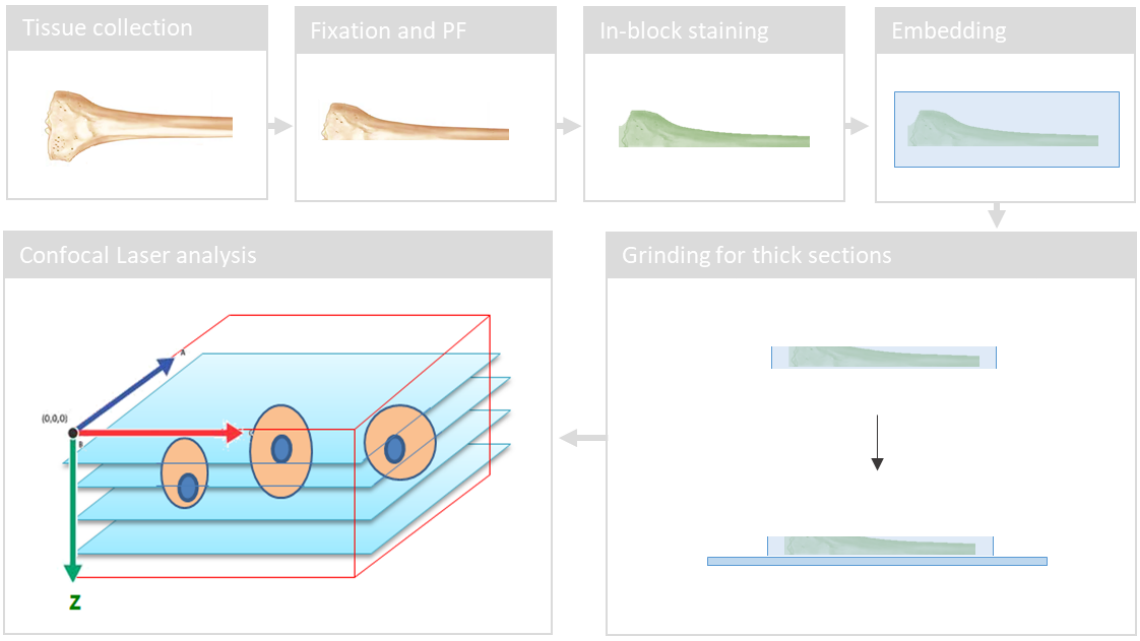


**Figure 9. Schematic description of the methodological procedure to obtain three-dimensional images of chondrocytes.** The rats' right tibias are collected immediately after sacrifice, fixated in glutaraldehyde 2%, ruthenium hexaammine trichloride 0.5%, and calcium chloride 5 mM in 0.025 M sodium cacodylate buffer. Then, they are in-block stained with a solution of 0.5% eosin, after which they are embedded in epoxy resin Durcupan (Sigma) and thinned by grinding to obtain thick bone sections. *See text for further details.

## | Fixation

Three fixative solutions were tested, all containing ruthenium hexaammine trichloride (RHT) and glutaraldehyde and adjusted to 300 mOsm [69,70]:

F1: Paraformaldehyde 0.5%, glutaraldehyde 1.2 % and ruthenium hexaammine trichloride 0.5% in 0.025 M sodium cacodylate buffer (pH 7.4).

F2: Glutaraldehyde 2.5 % and ruthenium hexaammine trichloride 0.7% in 0.03 M sodium cacodylate buffer (pH 7.4).

F3: Glutaraldehyde 2%, ruthenium hexaammine trichloride 0.5% and calcium chloride 5mM in 0.025 M sodium cacodylate buffer (pH 7.4).

Fixatives were always freshly prepared and cooled to 4°C prior to use. The pH was adjusted to 7.4 with cacodylate buffer, which does not tend to form precipitates in presence of calcium ions [71]. Paraformaldehyde was restricted to low concentrations because a 1% unbuffered solution exerts an osmotic pressure of 300 mOsm. It was always dissolved in hot water immediately before use to keep the concentrations of polymers low. Calcium chloride ($CaCl_2$) was included in one fixative because of its effect on phospholipid preservation[72] and also to test a hypothetical contribution of the divalent calcium cation to aggrecan precipitation and shrinkage prevention. Total bone samples were divided in three equal groups, each containing sixteen tibial samples and sixteen femoral samples, and each group was treated with one of the three fixative solutions. Bone samples were individually placed in tubes containing 5 ml of the fixative solution for 12 hours at 4°C. After this time, the fixative was decanted and replaced by new/fresh fixative solution in which tissues remained 5 additional hours (4ºC). Samples were then washed three times of 30 min each with the post fix buffer consisting of sodium cacodylate 0.1 M, MgCl2 3mM and sucrose 2.5% (osmolarity 300 mOsmols, 4ºC). The quality of preservation of the hypertrophic chondrocytes in each fixative solution was subsequently evaluated under the confocal microscope, as detailed later.

### | In-block Staining

Epoxy-resin was used as embedding medium. Tissue staining was performed prior to embedding. Eosin Y was assessed as a potential fluorescent probe for in-block staining. This xanthene dye obtained by halogenization of fluorescein has high-fluorescence emission and selectively marks cell constituents of protein nature because of the electrostatic interactions between its carboxylic and phenolic groups to arginine, histidine, lysine, and tryptophan residues of proteins. Since both the spectral behaviour of eosin and its fluorescence quantum yield slightly vary in different solvent media [73], several eosin solutions and incubation times were tested. Bone samples were incubated with two eosin concentrations (0.5 and 1%) at two different pH (4.8 and 5.5) and during two staining times (2 and 4 hours), so a total of eight possible combinations were tested. In order to not increase excessively number of staining solutions, eosin was always diluted in acetate buffered ethanol 60% (based on previous experience in our lab) and both staining and post-staining washes were always carried out at 4°C. After staining, bone samples were washed two times of 15 min each with ethanol 80% followed by two changes of 15 mins each in ethanol 90%, two changes of 30 mins each in ethanol 100% and two changes of 30 mins each in acetone. With the aim of evaluate the effect of the

fixative on downstream staining, the samples were subdivided in a total of twenty-four groups (n=4, two tibias and two femurs) and each was treated with one of the combinations of three fixative solutions and the eight staining conditions (**Table 1, II**). The quality of the fluorescent signal was subsequently evaluated in each group under the confocal microscope, as detailed later.

## | Embedding

Bone samples were embedded in epoxy resin. A soft Durcupan ACM mixture (Sigma, St Louis, MO, USA) was chosen based on previous experience in our laboratory. Infiltration was performed in a mixture consisting of 12.2 g epoxy monomers (A/M), 9.5 g hardener (B) and 0.3 g plasticizer (D) that was prepared at least 15 minutes before use. It was applied to the bone samples by first mixing with equal parts of acetone. Bone samples remained in resin/acetone for 2 hours at room temperature. Then, the mixture was removed from each glass tube and replaced by pure resin mixture. Tubes were then incubated at 40°C for 5 hours. Afterwards, the resin was wiped and replaced by a new mixture with the same components as the primary plus 0.4 g of accelerator (C). This mixture was prepared 15 minutes before use and warmed to 40°C. After the samples had remained in this last mixture for 5 hours at 40 ºC, they were individually placed in silicone rubber molds with round cavities of 14 mm diameter x 3 mm deep (Taab E070) filled with freshly prepared resin. Each bone sample was carefully positioned so that it laid perfectly flat against the bottom of the mold to ensure that the block was properly oriented. Next, samples were put in an oven at 50°C and allowed to polymerize for 48 h. After this time, the molds were taken out of the oven and allowed to cool at room temperature before demolding.

## | Grinding for Thick Sections

The embedded bone samples appeared as a 3 mm thick disc with one slightly concave face corresponding to the upper side of the mold and a flat one corresponding to the bottom. They were mounted on a specimen holder (Struers AccuStop) with the concave face oriented upwards and grinding was performed by using a commercial grinding machine (LaboPol-1, Struers A/S, Ballerup, Denmark) to a thickness of 0.5 mm. Fine sandpaper with a constant grit size of P800 was used (Buehler GmbH, Düsseldorf, Germany). Once grinded, the sample was glued by the no-grinded face to a histological slide with cyanoacrylate. To eliminate the effect of grinding contamination, the slide was mounted on an automated microtome with tungsten carbide blades (Technovit® Histoblade Ref 66045730) and 1µm thick sections were made to carefully trim the tissue down to a level where the tissue had no sign of grinding. Finally, Permount mounting media (Permount) was applied and the slides coverslipped and stored in a dark box until observation.

## | Confocal Laser Analysis

Thick bone sections were imaged with a confocal microscope Leica TCS SP8 (Leica Microsystems, Germany) equipped with a pulsed white light laser (470–670 nm), Acousto-Optical Beam Splitter (AOBS) and two internal hybrid single photon counting detectors and operated by Leica Application Suite X program (Leica Microsystems, Wetzlar, Germany). Excitation and emission lambda scans were obtained by scanning the excitation (absorbance) spectrum of the sample while simultaneously acquiring the fluorescence emission spectrum at each excitation wavelength coordinate. Excitation-emission maps were obtained for positive samples resulting from different fixative and staining combinations and for controls samples for native and induced autofluorescence. The image acquisition settings for negative controls were designed to maximize the ratio of fluorescence over autofluorescence. Autofluorescence-corrected images were obtained by digital subtraction of the autofluorescence from the fluorescence of positive samples.

Samples for confocal microscopy were first scanned at low magnification (20×) to locate GP cartilage. Confocal slide scanning was then performed using a 63X oil immersion objective with 1.4 NA at two different areas of hypertrophic cartilage. The pixel intensity, ranging from 0 to 255, was set to be the mean value of four scans. The increment of the Z-axis optical section was 0.5 µm to obtain 100 continuous images and those images were sequentially overlapped along the z-axis to form a stack of 184.52 µm (x) × 184.52 µm (y) × 50 µm (z) with X/Y resolution of 1024×1024 pixels. Twenty chondrocytes, all situated in the last three rows of the hypertrophic cartilage adjacent to the invading front, were analyzed in each sample. A trained operator, the same for all samples, used a semi-automated, hand-drawn contouring system to delineate each chondrocyte. The Leica LAS X 3D software and the IMARIS v.7.1.1. software (Bitplane, Switzerland) image reconstruction software was used for the 3D projection and analysis of the confocal micrographs, respectively. In **Supplementary Videos 1 and 2**, the image stacks were displayed using the "Ortho Slice" function, and the video was made via the "Movie Maker" function with the increase in display time in association with the depth of the optical section. Structural parameters, including cell volume, sphericity and ellipticity were obtained by using the SURPASS tool available in IMARIS v.7.1.1. software (Bitplane, Switzerland). The quality of the preservation was evaluated in each sample by scoring 20 chondrocytes located in the last two rows of the hypertrophic chondrocyte layer. Three issues were considered: structural integrity (SI), cytoplasm preservation (CP) and integrated optical density (IOD). SI was considered optimal when hypertrophic chondrocytes were regularly attached to the pericellular matrix border so that they completely fill their lacunae and neither irregular shrinkage nor cell collapse or lysing were observed. It was rated by using a semiquantitative scale ranging from 1–4 (1 poor; 2 fair; 3 good; and 4 excellent). CP was considered optimal when the cells were not vacuolated and had a homogeneous content and semiqualitative evaluation was performed in the same way (1 poor; 2 fair; 3 good; and 4 excellent). IOD was considered as an indicator of cytoplasmic density and was calculated by quantifying the fluorescent signal. The entire volume of the chondrocytes

was measured, and every pixel was used to calculate IOD from which was subtracted the fluorescence of the background control. Values of IOD obtained for all chondrocytes of the different were ranged in descending order and rated from 1–4 (4 for the top 25% of the distribution; 3 for those between 25% and 50%; 2 for those between 50% and 75%; and 1 for those between 75% and the bottom of the distribution). The cumulative score was calculated as the sum of SI, CP and IOD (range 3–12) to determine the final score (FS) value. Values obtained from the chondrocytes in each group (n = 20) were expressed as X ± SD and the group with the highest X and lowest SD was finally selected.

## Transmission Electron Microscopy

Ultrastructural images of the cytoplasm of chondrocytes were alto obtained by transmission electron microcopy and these images were used as a reference for judging the quality of the micro-structural data in images obtained from confocal microscopy. Tibial samples for electron microscopy were fixed in a solution of 2.5% glutaraldehyde and 0.7% RHT (Strem Chemicals, Newburyport, MA) in 0.05 M cacodylate buffer, pH 7.4, for 3 hours at 4ºC. Then, the samples were washed in buffer and postfixed in a solution of 1% osmium tetroxide and 0.7% RHT in cacodylate buffer for 2 hours at room temperature, dehydrated with a graded series of acetone and embedded in Durkupan-ACM (Sigma). Ultrathin sections were cut on a Reicher Ultracut E ultramicrotome, stained with lead citrate, and viewed with a Jeol JEM-2000 EX II electron microscope.

## Analysis of Cell Changes during Chondrocyte Hypertrophy

Once the procedure was established, it was applied to a group of five rats to analyze changes in cell volume, cell shape and cytoplasm density during chondrocyte maturation. To this end, both tibias of each rat were processed as previously described to obtain a total of 20 positive and 20 autofluorescence-control samples that were analyzed with confocal microscopy. Four complete columns of chondrocytes, extending from proliferating to the hypertrophic zones, were scanned in each sample using the same objective (63×) and image acquisition settings previously reported. Two or three scans were performed along the XY plane, sequential in the Y axis, to obtain an image reconstruction of a complete column and the sequence of cell structural variation along a vertical column, by measuring a total of 500 chondrocytes, was analyzed. **In Supplementary Videos 3 and 4.**

## Immunohistochemistry

In order to connect volume, shape and cytoplasm density changes in specific chondrocyte subsets with chondrocyte progression through proliferation and hypertrophy we

performed immunohistochemistry of some well-defined molecular landmarks of distinct stages of chondrocyte differentiation.

We analyzed the immunolocalization of collagen type II (Col2a1), collagen type X (Col10a), transcription factor Sox9, Igf1, Aqp1 Nkcc1 with respect to the seven clusters of chondrocytes objectively graded by the quantitative analysis. To this end, an additional group of five rats was used. Tibias were dissected, fixed in 4% paraformaldehyde, and embedded in methyl-methacrylate, as previously described by our group [74].

Immunodetection was carried out on 5-µm-thick methyl methacrylate sections. Antigen retrieval was performed with citrate buffer pH 8, 35 min at 60°C for Sox9, proteinase K 1mg/ml 15 min at 37ºC for Col2a1, proteinase K 1mg/ml 10 min at 37ºC for ColX, proteinase K 1mg/ml 16 min at 37°C for Igf-1, hyaluronidase 2mg/ml 30 min 37°C for NKCC1, citrate buffer pH 8 30 min at 60°C for Aqp1. TNB blocking buffer (75 min, RT) made from TSA blocking reagent (Perkin Elmer, MA, USA) was used. The primary antibodies used were anti-Sox9 (#PA5-81966, Invitrogen, California, USA) at 1:50 dilution, anti-Col2a1 (#MA5-12789, Invitrogen, California, USA) at 1:20 dilution, anti-ColX (A6889, Abclonal, MA 01801, USA) at 1:20 dilution, anti-IGF-I (#PA5-27207, Invitrogen, California, USA) at 1:200 dilution, anti-Aqp1 (ab15080, Abcam, Cambridge, UK) at 1:100 dilution and anti-NKCC1 (ab59791, Abcam, Cambridge, UK) at 1:100 dilution. Goat anti-mouse Alexa 594 (A-21155, Invitrogen, California, USA), goat anti-rabbit Alexa 594 (#A-11012, Invitrogen, California, USA) and goat anti-rabbit Alexa 488 (A11034, Invitrogen, California, USA) were used as secondary antibodies and sections were finally mounted with Vectashield Mounting Medium with DAPI (Vector Laboratories, Burlingame, California, USA). Sections were examined and pictures taken with a confocal microscope Leica TCS SP8 (Leica Microsystems, Germany) with the 20x magnification objective. Image J (National Institutes of Health, Bethesda, Maryland, USA) was used to measure the fluorescence intensity on whole chondrocyte columns.

## Statistical Analyses

To investigate differences in the quality of the preservation and labelling of hypertrophic chondrocytes, X and SD of the final rating were obtained for each of the 24 groups resulting from combinations of fixative and staining solutions. Comparison among groups was performed using the one-way ANOVA following by a Turkey's Multiple Comparison test. All statistical analyses utilized a 95% confidence level and were conducted using GraphPad Prism statistical software v.7 (La Jolla, California, USA).

A cluster analysis was used for classifying chondrocytes according to the values obtained for the cell parameters on the basis of the distance between them in a multidimensional array. A hierarchical dendrogram showing the order of successive agglomerations was generated and the cluster number was chosen by applying the Ward's linkage algorithm in combination with

Manhattan distances. The statistical significance among clusters was assessed by one-way ANOVA followed by a Turkey's Multiple Comparison test.

# | ANALYSIS OF THE UREMIC GROWTH PLATE

## Animals

Female weaning Spragüe-Dawley rats weighing 65±5 g obtained (Charles River Laboratories, L'Arbresle, France) were housed in light (12 light/dark cycles) and temperature-controlled rooms (21-23ºC). After 3 days of adaptation in individual cages with *ad libitum* access to deionized drinking water and standard diet, animals were classified into 4 groups, summarized in **Table 2.**

**Table 2. Groups of animals used for the experimental protocol.**

| Group | Diet | Treatment |
|---|---|---|
| **Control group (C)** | Normal diet | Vehicle |
| **Adenine group (AD)** | 0.5% adenine diet | Vehicle |
| **Adenine group + GH (ADGH)** | 0.5% adenine diet | rhGH (3.3 mg/kg/day) |
| **Pair fed group (PF)** | Normal diet pair fed with AD | Vehicle |

The experimental protocol lasted 21 days, after the 3 days adaptation period, and animals were sacrificed and exsanguinated under lethal doses of anaesthesia (Dolethal ©) on day 21 of the protocol. Animals, water and food were weighed daily. The length of the rats was measured from the snout to the end of the tail on day 0 of protocol and day 21, coinciding with the day of sacrifice.

Recombinant human GH (rhGH) (Norditropin®), gently provided by Novo Nordisk Pharma, Madrid, Spain), was administered intraperitoneally to the ADGH group from day 14 to day 21 of the protocol, at a dosage of 3.3 mg/kg/day, given at 09.00 h and 17.00 h [75]. The other groups received the vehicle following an identical protocol of administration. Animals were sacrificed under a lethal dose of Dolethal® anesthesia after 21 days. Bromodeoxyuridine (BrdU) (100 mg/kg; Sigma Aldrich, Madrid, Spain) was injected intraperitoneally 1 and 8 h before sacrifice. Five days before sacrifice, 20 mg/kg of intraperitoneal calcein (Sigma, St Louis, MO, USA) was injected for the measurement of the OFA.

## Serum Biochemistry

Blood was centrifuged at 3500 rpm at 4ºC for 10 minutes and the resulting serum was stored in aliquots of 500µl at -20°C for subsequent measurement. Serum concentrations of creatinine, urea nitrogen, calcium and phosphate were measured by IDEXX laboratories (Barcelona, Spain).

## Growth and Nutritional Studies

Growth during the experimental protocol was assessed by measuring the total gained weight between days 0 and 21. Animals were weighed daily using a scale. Likewise, the length from the snout to the distal end of the tail was measured under anesthesia on day 21 of the protocol using a millimeter rule. Longitudinal growth rate (µm/day) was assessed by OFA in frontal sections from the right tibias. Sections were examined under an Olympus incident light fluorescent microscope (Olympus BX61, Olympus Optical, Barcelona, Spain) to detect calcein labels. Images were captured and measurements were made using Image J (National Institutes of Health, Bethesda, Maryland, MD, USA). The mean value measurement divided by 5 days was considered the osseous front advance per day, representing the daily longitudinal bone growth rate in each animal.

Food efficiency was calculated as the ratio between weight gained and food consumed (g/g) by each animal between days 0 and 24 of the protocol.

## Three-Dimensional Uremic Chondrocytes

### | Sample Harvest and Tissue Processing

The rats' right tibias were fixated in glutaraldehyde 2%, ruthenium hexaammine trichloride 0.5%, and calcium chloride 5 mM in 0.025 M sodium cacodylate buffer (pH 7.4, osmolarity 300 mOsm). Then, they were in-block stained with a solution of 0.5% eosin in acetate buffered ethanol for 2 h at 4◦C, after which they were embedded in epoxy resin Durcupan (Sigma, St Louis, MO, USA) and thinned by grinding to obtain 100-µm thick bone sections, as described in the | THREE-DIMENSIONAL ANALYSIS OF CHONDROCYTES Chapter.

### | Three-Dimensional Reconstruction of Uremic Chondrocytes

The bone thick sections were imaged with a confocal microscope Leica TCS SP8 (Leica Microsystems, Germany) equipped with a pulsed white light laser (470–670 nm), Acousto-Optical Beam Splitter (AOBS), and two internal hybrid single photon counting detectors, which was operated by Leica Application Suite X program (Leica Microsystems, Wetzlar, Germany). Z-stacks of 184.52 µm (x) × 184.52 µm (y) × 50 µm (z) with an X/Y resolution of 1024 × 1024 pixels were obtained by the sequential overlapping of 100 continuous images at an increment of Z-axis optical section of 0.5 µm. Two scans were performed along the XY plane, sequential in the Y axis, to obtain an image reconstruction of a complete column; see **Supplementary Videos 5-10**. The Leica LAS X 3D software was used for the 3D projection and the IMARIS v. 7.1.1. software (Bitplane, Switzerland) to obtain the cell structural parameters of the chondrocytes: cell volume, integrated optical density (IOD), and sphericity. The sequence of structural variation along a

complete column was analyzed by measuring a total of 300 chondrocytes for each experimental group.

## Histology and Histomorphometry

### | Sample Processing

The left tibias were fixed in 4% paraformaldehyde (PFA). At the end of the PFA fixation process, the samples were washed in autoclaved miliQ water. Samples were dehydrated in 70% ethanol, 90% ethanol, 100% ethanol and Histoclear® (National Diagnostics, Atlanta, GA, USA). After dehydration, the samples were submerged sequentially in three different solutions of MMA with increasing concentrations of benzoyl peroxide (Sigma, St Louis, MO, USA), to be placed in MMA-based glass tubes and covered with a polymerization mixture composed of MMA and N, N Dimethyl-p-toluidine (Sigma, St Louis, MO, USA). The polymerization was carried out at -20°C for 3 weeks.

### | Immunofluorescence of GP Markers

The fluorescent immunodetection of Col2a1, Col10a1, Nkcc1, Aqp1, Igf1, Stat5b, SOCS2, Sox9, PTHrP (Parathyroid hormone related protein) and IHH (Indian hedgehog) was performed in 5 µm thick sections of methyl-methacrylate embedded left tibias. Antigen retrieval was performed with proteinase K 1 mg/mL 16 min at 37 ◦C for Igf1, hyaluronidase 2 mg/mL 30 min 37 ◦C for Nkcc1, citrate buffer pH 8 30 min at 60 ◦C for Aqp1, citrate buffer pH 8 30 min at 60 ◦C for Stat5b, proteinase K 0.1mg/ml 18 min at 37ºC for SOCS2, citrate buffer pH 8 35 mins at 60°C for Sox9, EDTA pH 8 45 min 60ºC for PTHrP and proteinase K 0.15 mg/ml 27 min at 37ºC for IHH. A TNB blocking buffer made with 0.1 M TRIS-HCl, pH 7.5 0.15 M NaCl 0.5% TSA Blocking Reagent (FP1012, Perkin Elmer, Waltham, Massachusetts, MA, USA) was used. The primary antibodies used were as follows: anti-Col2a1 (#MA5-12789, Invitrogen, California, USA) at 1:20 dilution, anti-Col10a1 (A6889, Abclonal, MA 01801, USA) at 1:20 dilution, anti-Igf1 (#PA5-27207, Invitrogen, California, CA, USA) at 1:200 dilution, anti-Aqp1 (ab15080, Abcam, Cambridge, UK) at 1:100 dilution, anti-Nkcc1 (ab59791, Abcam, Cambridge, UK) at 1:100 dilution, anti-Stat5b (ST5b-10G1, Invitrogen California, USA) at 1:20 dilution, anti-SOCS2 (MBS462132, MyBiosource, San Diego, USA) at 1:10 dilution, anti-Sox9 (#PA5-81966, Invitrogen, California, USA) at 1:50 dilution, anti-PTHrP (PC09, Merck KGaA, Darmstadt, Germany), anti-IHH (PA5-19680, Invitrogen, California, USA). Goat anti-mouse Alexa 594 (A-21155, Invitrogen, California, CA, USA), goat anti-rabbit Alexa 594 (#A-11012, Invitrogen, California, CA, USA), and goat anti-rabbit Alexa 488 (A11034, Invitrogen, California, CA, USA) were used as secondary antibodies, and sections were finally mounted with Vectashield Mounting Medium with DAPI (Vector Laboratories, Burlingame, California, CA, USA).

Sections were examined and pictures taken with a confocal microscope, Leica TCS SP8 (Leica Microsystems, Germany), with the 20× magnification objective. Image J (National Institutes of Health, Bethesda, Maryland, MD, USA) was used to measure the fluorescence intensity on the whole chondrocyte columns and the position of chondrocytes in the GP.

## Statistical Analysis

All statistical analyses utilized a 95% confidence level and were conducted using GraphPad Prism v. 7 (La Jolla, California, CA, USA).

To analyze the structural variation along the vertical column, chondrocytes were classified into the previously described differentiation clusters | Confocal Laser Analysis Chapter], based on their distance to the osseous invasion front. Means and standard deviations (SD) of the different structural parameters were determined for each cluster. Comparison among experimental groups was performed using a one-way ANOVA, followed by Tukey's multiple comparison test.

# | FORMATION OF THE EPIPHYSEAL BONE PLATE

## Animals

Male Sprague-Dawley rats were obtained from the animal facility building of the University of Oviedo. Rats were sacrificed on days 3, 5, 8, 11, 14, 19, 24 and 35 after birth. We used five animals per age group except in the age-group of 35 days in which an additional rat was included (n=6). Rats were injected intraperitoneally with calcein 20 mg/kg (Sigma, St Louis, MO, USA) three days before sacrifice. The procedures involving animals and their care were conducted according to Spanish law on the use of experimental animals, which acknowledges the European Directive 86/609. The project proposal was approved by the Ethical Committee of the University of Oviedo, Spain (14 July 2015, PROAE 19/2015).

## Histology and Histomorphometry

### | Sample processing

Tibiae were isolated and cut through the sagittal plane of the proximal epiphysis into two equal sized parts, obtaining four tibial halves from each animal. One tibial half was embedded in paraffin to obtain sections which were used for both histochemical and in situ hybridization studies. The second tibial half was processed for mineralization studies. The third tibial half was processed to obtain semithin sections and the last tibial half was processed for confocal microscopy. Tibiae of the additional rat of the 35 days old group were processed for scanning electron microscopy.

For histochemical, immunohistochemical and in situ hybridization studies, tissues were fixed by immersion in 4% paraformaldehyde at 4ºC for 12 h, rinsed in PBS, decalcified in 10% EDTA (pH 7.0) for 48 h at 4ºC, dehydrated through a graded ethanol series, cleared in xylene and embedded in paraffin. Sections were serially cut at a thickness of 5 µm and mounted on Superfrost Plus slides (Menzel-Glaser).

### | Trichromic Staining

Trichromic staining was carried out by using Weigert's hematoxylin/Alcian blue/picrofuchsin, which distinguished cartilage matrix (blue) from bone matrix (red).

### | Elements with Alkaline Phosphatase Activity

For analysis of alkaline phosphatase (AP) staining, sections were pretreated with 10 mM MgCl2 solution to reactivate the enzyme and subsequently incubated with a substrate solution containing containing 0.16 mg/ml 5 bromo 4 chloro 3 indolylphosphate and 0.33 mg/ml nitroblue tetrazolium in 100 mM Tris, 100 mM NaCl, 50 mM MgCl2, pH 9.5, for 30 min at room temperature.

### | Elements with Tartrate Resistant Acid Phosphatase (TRAP) activity

Tartrate resistant acid phosphatase (TRAP) activity, a marker of osteoclast precursor cells and mature osteoclasts, was also determined histochemically by incubation of sections with 50 mM sodium acetate (pH 5.2) containing 0.15% Napthol AS TR phosphate, 50 mM sodium tartrate, and 0.1% Fast Red T.R. (Sigma).

### | Matrix Mineralization

For studies of matrix mineralization, tissues were fixed in 4% paraformaldehyde in PBS for 5 hours at 4ºC, dehydrated in acetone, embedded in Durkupan-ACM (Sigma) and sectioned at 2 µm on a Reicher Ultracut E ultramicrotome. The von Kossa staining was used to detect mineralization by setting sections in 1% AgNO3 for 60 min at room temperature and fixed with 5% sodium hyposulfite.

### | Toluidine Blue Staining

Semithin sections were obtained from tissues fixed in 2% glutaraldehyde and 0.7% ruthenium hexamine trichloride (RHT) (Strem Chemicals) in 0.05 M cacodylate buffer, pH 7.4, for 3 hours at 4ºC. They were then postfixed in 1% osmium tetroxide and 0.7% RHT in cacodylate buffer for 2 hours. After washing, they were dehydrated with acetone, embedded in Durkupan-ACM (Sigma), sectioned at 0.5 µm on a Reicher Ultracut E ultramicrotome and stained with toluidine blue.

### | Immunohistochemistry

Immunohistochemistry for CD31 was applied by using a rabbit polyclonal antibody (Abcam, Cambridge, MA). Sections were deparaffinized, hydrated and treated with a solution of 0.05% pepsin (Sigma) in 0.01 M HCl (pH 2) at 37° C for 15 min for antigen retrieval. After H2O2 inactivation and unspecific antibodies blocking, slices were incubated overnight with the primary antibody (1:100). Immunostaining was then performed by using an ExtrAvidin Peroxidase Staining Kit for rabbit antibodies (Sigma-Aldrich).

### | *In situ* hybridization

In situ hybridization studies were performed as reported previously [52]. Sections were hybridized to 35S-labeled antisense riboprobes and subsequently exposed to photographic emulsion at 4ºC for several days, developed, fixed, cleared and counterstained with 0.02% toluidine blue. Sections hybridized with a labeled sense riboprobe were used as negative controls. Either sense or antisense 35S-uridine triphosphate-labeled RNA probes were synthesized from the corresponding linearized DNA using the appropiate RNA polymerases. Probes for in situ hybridization were as follows: The probe for type II collagen was a 550 bp Pst I fragment from the amino-terminal portion of rat pro-α1(II) chain cloned in PGEM 3Zf-vector. Type X collagen probe was a 650-bp HindIII fragment containing containing 360 bp of non-collagenous (NC1) domain and 290 bp of 3´-untranslated sequence of the mouse type X collagen

gene, subcloned into the HindIII site of pBluescript. The rat and mouse genes (RGD ID:2371 vs RGD ID: 735282) share 96.0-97.0 sequence similarity (ncbi.nlm.nih.gov/genome). The gelatinase B probe was generated by subcloning into pBluescript a 1353 BamHI fragment obtained by RT-PCR from embryo RNA with the following oligonucleotides: 5' TGGCACCATCATAACATCACCT and 5' AGAAGAAAATCTTCTTGGGCTG (GenBank acces. nb. NM_031055). The probe for murine osteocalcin consisted of a 212-bp fragment amplified from embryo RNA with the oligonucleotides 5'-TCTCTCTGCTCACTCTGCTGG and 5'AGCAGGGTTAAGCTCACACTand subcloned into pBluescript vector. Digoxigenin-11-UTP-labeled single-stranded RNA probes were also used for type-II collagen to get a better spatial resolution of chondrocytes freed form the cartilage matrix. Probes were prepared with the DIG RNA labeling mix (Boehringer Mannheim), and the hybridized probe was detected with the alkaline-phosphatase-coupled anti-DIG antibody (Boehringer Mannheim).

## Three-dimensional Analysis

Bone samples for confocal microscopy were processed as previously reported [51]. Briefly, tibial samples were fixated in glutaraldehyde 2%, RHT 0.5%, and calcium chloride 5 mM in 0.025 M sodium cacodylate buffer (pH 7.4, osmolarity 300 mOsm). Then, they were embedded in epoxy resin Durcupan (Sigma), thinned by grinding to obtain 100-µm thick bone sections and imaged with a confocal microscope Leica TCS SP8 (Leica Microsystems, Germany) equipped with a pulsed white light laser (470–670 nm), Acousto-Optical Beam Splitter (AOBS), and two internal hybrid single photon counting detectors, which was operated by Leica Application Suite X program (Leica Microsystems, Wetzlar, Germany).

## Scanning Electron microscopy

Bone samples for scanning electron microscopy were dehydrated in a graded series of acetone and critical-point dried in a Bomar SPC-900 EX critical-point dryer. Samples were glued to standard SEM stubs, coated with gold in a Sputtering Balzers SCD 004 and viewed with a JEOL JSM-5600 scanning electron microscope operated at 20 kV. 5.

# V.PUBLISHED ARTICLES

# I. Educational Review: Growth Plate Alterations in Chronic Kidney Disease

Growth retardation is a major feature of CKD of onset in infants or children and is associated with increased morbidity and mortality. Several factors have been shown to play a causal role in the growth impairment of CKD. All these factors interfere with growth by disturbing the normal physiology of the GP of long bones. To facilitate the understanding of the pathogenesis of growth impairment in CKD, this review discusses cellular and molecular alterations of the GP during uremia, including structural and dynamic changes of chondrocytes, alterations in their process of maturation and hypertrophy, and disturbances in the GH signaling pathway.

**Article 1. Ángela Fernández-Iglesias** & José Manuel López & Fernando Santos. "Growth Plate Alterations in Chronic Kidney Disease"

Pediatr Nephrol. 2020 Mar;35(3):367-374. doi: 10.1007/s00467-018-4160-7.

Journal metrics 2019:

2-year impact factor: 2.676

5-year impact factor: 2.686

# II. Three-Dimensional Analysis of Growth Plate Chondrocytes

This manuscript reports a novel procedure to imaging GP chondrocytes by using confocal microscopy. The method is based on fixed undecalcified bone samples, in-block staining with eosin, epoxy resin embedding and grinding to obtain thick sections. It is simple, inexpensive and provides three-dimensional images of entire chondrocytes inside their native lacunae. Quantitative analysis of volume, shape and cytoplasm density of chondrocytes at different strata of the GP allowed to objectively grade chondrocytes of the GP in seven different clusters. These seven categories of chondrocytes were subsequently evaluated by immunohistochemistry of some well-defined molecular landmarks of chondrocyte differentiation. Furthermore, immunohistochemical analysis of proteins responsible for ionic changes and water transport allowing chondrocyte swelling during hypertrophy was also performed. Results obtained indicate that four subphases can be defined in the pre- hypertrophic zone and three subphases in the hypertrophic zone, a fact that raises that chondrocytes of the GP are less homogeneous than usually considered when different zones are defined according to subjective cell morphological criteria. Results in the present study provide a technological innovation and gives new insights into the complexity of the process of chondrocyte differentiation in the GP.

**Article 2. Ángela Fernández-Iglesias, Rocío Fuente, Helena Gil-Peña, Laura Alonso-Duran, María García-Bengoa, Fernando Santos & José M. López.** "A simple method based on confocal microscopy and thick sections recognizes seven subphases in growth plate chondrocytes"

Sci Rep. 2020 Apr 24;10(1):6935. doi: 10.1038/s41598-020-63978-6.

Journal metrics 2019

2-year impact factor: 3.998

5-year impact factor: 4.576

SCIENTIFIC REPORTS
nature research

Check for updates

OPEN

# A simple method based on confocal microscopy and thick sections recognizes seven subphases in growth plate chondrocytes

Ángela Fernández-Iglesias[1,2], Rocío Fuente[1], Helena Gil-Peña[4], Laura Alonso-Duran[1], María García-Bengoa[1], Fernando Santos[1,4] & José M. López[3] ✉

**This manuscript reports a novel procedure to imaging growth plate chondrocytes by using confocal microscopy. The method is based on fixed undecalcified bone samples, in-block staining with eosin, epoxy resin embedding and grinding to obtain thick sections. It is simple, inexpensive and provides three-dimensional images of entire chondrocytes inside their native lacunae. Quantitative analysis of volume, shape and cytoplasm density of chondrocytes at different strata of the growth plate allowed to objectively grade chondrocytes of the growth plate in seven different clusters. These seven categories of chondrocytes were subsequently evaluated by immunohistochemistry of some well-defined molecular landmarks of chondrocyte differentiation. Furthermore, immunohistochemical analysis of proteins responsible for ionic changes and water transport allowing chondrocyte swelling during hypertrophy was also performed. Results obtained indicate that four subphases can be defined in the pre-hypertrophic zone and three subphases in the hypertrophic zone, a fact that raises that chondrocytes of the growth plate are less homogeneous than usually considered when different zones are defined according to subjective cell morphological criteria. Results in the present study provide a technological innovation and gives new insights into the complexity of the process of chondrocyte differentiation in the growth plate.**

Hypertrophy of the chondrocytes of the growth plate is the major contributor to bone lengthening[1]. This process is characterized by a widespread increase of cell volume and has been widely studied, especially with respect to its regulation[2]. However, information regarding how the cell volume increase occurs is relatively scarce. Hypertrophic chondrocytes have great amount of cytoplasm with sparse organelles and numerous membrane transporters, and volume increase is due to unbalanced water accumulation or swelling[3,4] as well as to synthesis of cytoplasmic components or true hypertrophy[5]. Increase of chondrocyte volume was found to result from three sequential stages by using tomographic phase microscopy[6]: two stages of true hypertrophy (phases 1 and 3) when chondrocytes increase their volume with active synthesis of cytoplasmic components separated by a stage of swelling (phase 2), when volume keeps increasing but synthesis ceases and the cytoplasm density decreases. IGF-I was found to specifically affect chondrocyte hypertrophy during phase 3. These findings supported the view of chondrocyte hypertrophy as a sequence of events, each susceptible of independent regulation, and enabled new possibilities for understanding growth regulation and growth disorders. Unfortunately, no further studies in this line of work have been published. A possible cause is that diffraction phase microscopy is not commercially accessible and is not available in most laboratories. Thus, we have developed a procedure based on confocal microscopy that allows the analysis of cell volume, cell shape and cytoplasm density during chondrocyte maturation. This approach is simple, inexpensive, provides three-dimensional images of chondrocytes that maintain their shape and size inside their native lacunae and enables objective morphological discrimination of discrete groups of chondrocyte populations in the growth plate cartilage. For further molecular characterization, the expression

[1]Division of Pediatrics, Department of Medicine, Faculty of Medicine, University of Oviedo, CP 33006, Oviedo, Asturias, Spain. [2]Fundacion para la Investigación Sanitaria del Principado de Asturias (FINBA), Oviedo, Spain. [3]Department of Morphology and Cellular Biology, Faculty of Medicine, University of Oviedo, Oviedo, Asturias, Spain. [4]Pediatric Nephrology, Department of Pediatrics, Hospital Universitario Central de Asturias (HUCA), Oviedo, Asturias, Spain. ✉e-mail: jmlopez@uniovi.es

profiles of well-defined molecular landmarks of distinct stages of chondrocyte differentiation were immunohistochemically analyzed with respect to populations of chondrocytes graded by the quantitative analysis. Our study corroborates that chondrocyte hypertrophy is a multistage process and reports for the first time that four subphases can be defined in the pre-hypertrophic zone and three subphases in the hypertrophic zone.

## Materials and Methods

**Animals.** The study was carried out in six weeks old female Sprague-Dawley rats (Charles River Laboratories, L´Arbresle, France). Procedures involving animals and their care were conducted according to Spanish law on the use of experimental animals, which acknowledges the European Directive 86/609. The project proposal was approved by the Ethical Committee of University of Oviedo, Spain. Rats were housed in individual cages under controlled conditions of light (12 light/dark cycles) and temperature (21–23 °C) with free access to rats' standard diet and tap water. Animals were sacrificed under lethal dose of Dolethal® anaesthesia.

This work comprised three consecutive steps. First, we established a procedure for processing the growth plate which would result in the preservation of the structure of the hypertrophic chondrocytes and be suitable to obtain three-dimensional images of whole (non-sectioned) chondrocytes inside their native lacunae by using confocal microscopy. A group of twelve rats was used for this first study. The second step was to apply the procedure for analysis of cell changes during chondrocyte proliferation and hypertrophy in the growth plate. A cluster analysis was performed to classify chondrocytes according to quantitative analysis of volume, shape and cytoplasm density. Finally, an immunohistochemical study of the expression of proteins associated with the process of chondrocyte differentiation in the growth plate cartilage was performed in order to further characterize the different classes of subpopulations discriminated by their morphological features.

**Procedure.** Undecalcified bones were fixed under osmotically controlled conditions, *in block* stained, embedded with epoxy resin and thinned by grinding to obtain 100-μm thick bone sections. Different techniques for fixation, staining and post-processing were tested for their effectiveness and were systematically optimized for best synergy. Detailed information about the studies, including bone sampling, fixative solutions, dye concentrations and pH, staining times, embedding and ground section preparation is presented in Supplementary Information.

Thick bone sections were imaged with a confocal microscope Leica TCS SP8 (Leica Microsystems, Germany) equipped with a pulsed white light laser (470–670 nm), Acousto-Optical Beam Splitter (AOBS) and two internal hybrid single photon counting detectors and operated by Leica Application Suite X program (Leica Microsystems, Wetzlar, Germany). Excitation and emission lambda scans were obtained by scanning the excitation (absorbance) spectrum of the sample while simultaneously acquiring the fluorescence emission spectrum at each excitation wavelength coordinate. Excitation-emission maps were obtained for positive samples resulting from different fixative and staining combinations and for controls samples for native and induced autofluorescence. The image acquisition settings for negative controls were designed to maximize the ratio of fluorescence over autofluorescence. Autofluorescence-corrected images were obtained by digital subtraction of the autofluorescence from the fluorescence of positive samples. Ultrastructural images of the cytoplasm of chondrocytes were alto obtained by transmission electron microcopy and these images were used as a reference for judging the quality of the micro-structural data in images obtained from confocal microscopy. Tibial samples for electron microscopy were fixed in a solution of 2.5% glutaraldehyde and 0.7% RHT (Strem Chemicals, Newburyport, MA) in 0.05 M cacodylate buffer, pH 7.4, for 3 hours at 4 °C. Then, the samples were washed in buffer and postfixed in a solution of 1% osmium tetroxide and 0.7% RHT in cacodylate buffer for 2 hours at room temperature, dehydrated with a graded series of acetone and embedded in Durkupan-ACM (Sigma). Ultrathin sections were cut on a Reicher Ultracut E ultramicrotome, stained with lead citrate and viewed with a Jeol JEM-2000 EX II electron microscope.

Samples for confocal microscopy were first scanned at low magnification (20×) to locate growth plate cartilage. Confocal slide scanning was then performed using a 63X oil immersion objective with 1.4 NA at two different areas of hypertrophic cartilage. The pixel intensity, ranging from 0 to 255, was set to be the mean value of four scans. The increment of the Z-axis optical section was 0.5 μm to obtain 100 continuous images and those images were sequentially overlapped along the z-axis to form a stack of 184.52 μm (x) × 184.52 μm (y) × 50 μm (z) with X/Y resolution of 1024×1024 pixels. Twenty chondrocytes, all situated in the last three rows of the hypertrophic cartilage adjacent to the invading front, were analyzed in each sample. A trained operator, the same for all samples, used a semi-automated, hand-drawn contouring system to delineate each chondrocyte. Structural parameters, including cell volume, sphericity and ellipticity were obtained by using the SURPASS software. The Leica LAS X 3D software and the IMARIS v.7.1.1. software (Bitplane, Switzerland) image reconstruction software were used for the 3D projection and analysis of the confocal micrographs. In Supplementary Videos 1 and 2, the image stacks were displayed using the "Ortho Slice" function, and the video was made via the "Movie Maker" function with the increase in display time in association with the depth of the optical section. The quality of the preservation was evaluated in each sample by scoring 20 chondrocytes located in the last two rows of the hypertrophic chondrocyte layer. Three issues were considered: structural integrity (SI), cytoplasm preservation (CP) and integrated optical density (IOD). SI was considered optimal when hypertrophic chondrocytes were regularly attached to the pericellular matrix border so that they completely fill their lacunae and neither irregular shrinkage nor cell collapse or lysing were observed. It was rated by using a semiquantitative scale ranging from 1–4 (1 poor; 2 fair; 3 good; and 4 excellent). CP was considered optimal when the cells were not vacuolated and had a homogeneous content and semiqualitative evaluation was performed in the same way (1 poor; 2 fair; 3 good; and 4 excellent). IOD was considered as an indicator of cytoplasmic density and was calculated by quantifying the fluorescent signal. The entire volume of the chondrocytes was measured, and every pixel was used to calculate IOD from which was subtracted the fluorescence of the background control. Values of IOD obtained for all chondrocytes of the different were ranged in descending order and rated from 1–4 (4 for the top 25% of the distribution; 3 for those between 25% and 50%; 2 for those between 50% and 75%; and 1 for those between 75% and the bottom of the

distribution). The cumulative score was calculated as the sum of SI, CP and IOD (range 3–12) to determine the final score (FS) value. Values obtained from the chondrocytes in each group (n = 20) were expressed as X ± SD and the group with the highest X and lowest SD was finally selected.

**Analysis of cell changes during chondrocyte hypertrophy.** Once the procedure was established, it was applied to a group of five rats to analyze changes in cell volume, cell shape and cytoplasm density during chondrocyte maturation. To this end, both tibias of each rat were processed as previously described to obtain a total of 20 positive and 20 autofluorescence-control samples that were analyzed with confocal microscopy. Four complete columns of chondrocytes, extending from proliferating to the hypertrophic zones, were scanned in each sample using the same objective (63×) and image acquisition settings previously reported. Two or three scans were performed along the XY plane, sequential in the Y axis, to obtain an image reconstruction of a complete column and the sequence of cell structural variation along a vertical column, by measuring a total of 500 chondrocytes, was analyzed. In Supplementary Videos 3 and 4.

**Immunohistochemistry.** In order to connect volume, shape and cytoplasm density changes in specific chondrocyte subsets with chondrocyte progression through proliferation and hypertrophy we performed immunohistochemistry of some well-defined molecular landmarks of distinct stages of chondrocyte differentiation. We analyzed the immunolocalization of collagen type II (Col2a1), collagen type X (Col10a), transcription factor Sox9, insulin like growth factor 1 (Igf1), aquaporin 1 (Aqp1) and Na-K-Cl cotransporter 1 (NKCC1) with respect to the seven clusters of chondrocytes objectively graded by the quantitative analysis. To this end, an additional group of five rats was used. Tibias were dissected, fixed in 4% paraformaldehyde and embedded in methyl-methacrylate, as previously described by our group[7]. Immunodetection was carried out on 5-μm-thick methyl methacrylate sections as further described in Supplementary methods.

**Statistical analyses.** To investigate differences in the quality of the preservation and labelling of hypertrophic chondrocytes, X and SD of the final rating were obtained for each of the 24 groups resulting from combinations of fixative and staining solutions. Comparison among groups was performed using the one-way ANOVA following by a Turkey's Multiple Comparison test. All statistical analyses utilized a 95% confidence level and were conducted using GraphPad Prism statistical software v.7 (La Jolla, California, USA).

A cluster analysis was used for classifying chondrocytes according to the values obtained for the cell parameters on the basis of the distance between them in a multidimensional array. A hierarchical dendrogram showing the order of successive agglomerations was generated and the cluster number was chosen by applying the Ward's linkage algorithm in combination with Manhattan distances. The statistical significance among clusters was assessed by one-way ANOVA followed by a Turkey's Multiple Comparison test.

## Results and Discussion

**Processing procedure.** Analysis of bone samples at the spectral confocal microscope showed that both the quality of the preservation and the IOD of hypertrophic chondrocytes varied noticeably depending on fixation and staining conditions (Table 1). The FS varied between 6.4 and 9.9 (12 being the theoretical maximum). Two procedures reached the highest value (9.9): (1) fixation in glutaraldehyde 2%, ruthenium hexaammine trichloride 0.5% and calcium chloride 5 mM in 0.025 M sodium cacodylate buffer (pH 7.4, osmolarity 300 mOsm) (F3) followed by staining with a solution of eosin 0.5% in acetate buffered ethanol 60% pH 4.8 during 2 hours at 4 °C and (2) the same fixation followed by staining with a solution of eosin of higher concentration (1%) at the same pH (4.8) for a longer time (4 hours). When values for the three simple parameters in the two procedures were compared it was found that both SI and CP were higher in the first procedure (3.40 vs 3.25 and 3.60 vs 3.45, respectively) whereas the second procedure showed a higher value for IOD (3.2 vs 2.9). The quality of cell preservation was prioritized over fluorescence intensity and the procedure using lower eosin concentration during less time was selected. Although the penetrating properties of formaldehyde are stronger than those of glutaraldehyde, this distributed homogeneously into the slices of about 2 mm in thickness of the growth plate and effectively preserved the structure of hypertrophic chondrocytes giving good overall cytoplasmic and nuclear detail. Formaldehyde, limited to low concentrations because of its high osmolarity, did not improve structural preservation, slightly increased cell shrinkage and considerably decreased signal-to-background fluorescence ratios. Ruthenium hexammine trichloride was effective to prevent the loss of matrix proteoglycans and shrinkage of chondrocytes at the two concentrations tested (0.5 and 0.7%) and thus, the 0.5% concentration was chosen. Addition of calcium chloride to the fixative improved structural preservation of chondrocytes while not decreasing signal-to-background autofluorescence ratio. These results confirm that minor changes during tissue processing induce noticeable changes in the preservation of hypertrophic chondrocytes[8].

Chondrocytes showed a strong and clean fluorescence signal dispersed throughout the cytoplasm (Fig. 1A). The fluorescence signal appeared diffused in the intercellular matrix and almost absent in the nuclear region. Fluorescence signal was more intense in the perinuclear region and appeared constituted by a network of granulo-filamentous structures. Comparative analysis of confocal and electron micrographs (Fig. 1A–C) revealed that fluorescent signal correspond to the area where organelles were concentrated. Perinuclear cytoplasm contained abundant rough endoplasmic reticulum, scattered mitochondria and some lipid droplets. The excitation-emission map of the samples treated with the selected procedure (Fig. 1D–F) showed a broad range of effective excitation wavelengths and peaks in intensity at excitation/emission wavelengths of 531/556 nm. Matched control samples fixed in the same way but without eosin staining showed a clear different map in which the peak at 531/556 nm disappeared and a smaller one was found at 649/674, a result that demonstrates that a substantial fraction of the fluorescence signal in the first sample came from eosin labelling.

| | | | STAIN | | | | | | | |
|---|---|---|---|---|---|---|---|---|---|---|
| | | | Eosin 0.5% | | | | Eosin 1% | | | |
| | | | pH 4.8 | | pH 5.5 | | pH 4.8 | | pH 5.5 | |
| | | Parameters | 2 h | 4 h | 2 h | 4 h | 2 h | 4 h | 2 h | 4 h |
| FIXATIVE | F1 | SI | 2.45 ± 0.51 | 2.50 ± 0.51 | 2.55 ± 0.51 | 2.45 ± 0.51 | 2.30 ± 0.47 | 1.90 ± 0.55 | 2.15 ± 0.67 | 2.00 ± 0.46 |
| | | CP | 2.65 ± 0.49 | 2.75 ± 0.44 | 2.75 ± 0.44 | 2.65 ± 0.49 | 2.75 ± 0.55 | 2.25 ± 0.55 | 2.40 ± 0.60 | 2.25 ± 0.44 |
| | | IOD | 2.45 ± 1.28 | 2.70 ± 1.13 | 1.70 ± 0.80 | 2.00 ± 1.03 | 2.75 ± 1.21 | 2.95 ± 1.10 | 1.85 ± 0.88 | 2.20 ± 1.06 |
| | | FS | 7.55 ± 1.70 | 7.95 ± 1.43 | 7.00 ± 1.26 | 7.10 ± 1.55 | 7.80 ± 1.54 | 7.10 ± 1.29 | 6.40 ± 1.31 | 6.45 ± 1.23 |
| | F2 | SI | 3.30 ± 0.47 | 3.15 ± 0.59 | 2.80 ± 0.52 | 2.65 ± 0.49 | 3.00 ± 0.46 | 2.95 ± 0.51 | 2.70 ± 0.47 | 2.40 ± 0.68 |
| | | CP | 3.40 ± 0.50 | 3.35 ± 0.49 | 3.10 ± 0.45 | 2.85 ± 0.37 | 3.10 ± 0.31 | 3.00 ± 0.46 | 3.00 ± 0.56 | 2.55 ± 0.51 |
| | | IOD | 2.50 ± 1.36 | 2.75 ± 1.16 | 1.85 ± 0.93 | 2.65 ± 1.18 | 3.00 ± 1.03 | 3.15 ± 0.93 | 2.05 ± 0.83 | 2.30 ± 1.08 |
| | | FS | 9.20 ± 1.64 | 9.25 ± 1.37 | 7.75 ± 1.37 | 8.15 ± 1.39 | 9.10 ± 0.97 | 9.10 ± 1.25 | 7.75 ± 1.33 | 7.25 ± 1.41 |
| | F3 | SI | 3.40 ± 0.60 | 3.30 ± 0.57 | 3.45 ± 0.51 | 3.10 ± 0.64 | 3.20 ± 0.62 | 3.25 ± 0.64 | 3.15 ± 0.59 | 3.20 ± 0.70 |
| | | CP | 3.60 ± 0.50 | 3.55 ± 0.51 | 3.30 ± 0.47 | 3.20 ± 0.52 | 3.40 ± 0.50 | 3.45 ± 0.51 | 3.30 ± 0.47 | 3.35 ± 0.59 |
| | | IOD | 2.90 ± 1.12 | 2.95 ± 1.00 | 1.95 ± 0.89 | 2.65 ± 1.14 | 3.15 ± 0.93 | 3.20 ± 0.89 | 2.10 ± 0.97 | 2.30 ± 1.03 |
| | | FS | 9.90 ± 1.21 | 9.80 ± 1.47 | 8.70 ± 1.22 | 8.95 ± 1.67 | 9.75 ± 1.07 | 9.90 ± 1.37 | 8.55 ± 1.15 | 8.85 ± 1.31 |

**Table 1.** Effect of different fixation/staining protocols on the preservation quality and staining of hypertrophic chondrocytes. Three fixative solutions (F1, PFA 0.5%, Glu 1.2% and RHT 0.5% in 0.025 M SCB; F2, Glu 2.5% and RHT 0.7% in 0.03 M SCB; and F3, Glu 2%, RHT 0.5% and $CaCl_2$ 5 mM in 0.025 M sodium cacodylate buffer), two eosin concentrations (0.5% and 1%) at two different pH (4.8 and 5.5) and two staining times (2 and 4 h), in a total of 24 groups. PFA, paraformaldehyde; Glu, glutaraldehyde; RHT, ruthenium hexaammine trichloride; SCB, sodium cacodylate buffer; $CaCl_2$, calcium chloride. SI, structural integrity; CP, cytoplasm preservation; IOD, integrated optical density; FS, final score, (see text for details). Each point is the mean value of 20 hypertrophic chondrocytes ± SD

Fluorescent labelling was observed in chondrocytes throughout the growth plate, with highest levels in proliferative chondrocytes and a progressively decreasing levels towards the hypertrophic zone (Fig. 2). Analysis of thick sections with the confocal microscopy avoids damage to the integrity of the chondrocytes caused by mechanical sectioning and this allows to visualize entire chondrocytes inside their native lacunae preserving cell-matrix interactions. Eosin has quite good penetration into thick tissue sections of growth plate cartilage and stains the cytoplasm of the chondrocytes providing a strong fluorescent signal that resisted solvent dehydration, epoxy resin embedding and heat polymerization. Eosin is usually not regarded as a fluorochrome but results in the present work shows its utility for fluorescence labelling of chondrocytes, and this agrees with some previous studies in which eosin staining and confocal microscopy were used to analyze the three-dimensional distribution of cytoplasmic constituents of protein nature[9–11] and also for tissue pathology diagnosis[12,13]. Although eosin possesses only 20% the fluorescence quantum yield of more conventional fluorophores, such as fluorescein and rhodamine, eosin conjugated to either an immunoglobulin G (IgG) or steptavidin has been also proposed as an alternative to fluorescein in immunofluorescence[14,15]. Furthermore, eosin forms protein–dye complexes whose absorbance is proportional to the concentration of protein[16–18] and it has been used as a fluorescent probe for estimating a wide range of proteins by spectroscopy[19–21].

It is also of note that embedding of the growth plate in epoxy resin reduced refractive disparity between the different tissue constituents and this decreased random light scattering and increased penetration of light for imaging. Analysis of the maximum depth at which images can be obtained in the samples revealed that there was effective photon penetration along the Z-axis up to 70 microns depth for both the excitation laser and the emission fluorescence, being the detector gain was adjusted from 36% (surface) to 57% (Z: 70 μm). As a result, the three-dimensional reconstruction of focal image stacks of hypertrophic chondrocytes allowed to obtain images of intact entire chondrocytes inside their lacunae with a relatively smooth surface and minimal irregular shrinkage or cell collapse even for those adjacent to the vascular invasion front. The complete serial optical sections, from the surface to depth = 70 μm, are shown in Supplementary video 1.

The findings obtained in this study support the usefulness of this easy and inexpensive approach based on *in block* eosin staining followed by embedding in epoxy resin and grinding to analyze growth plate chondrocytes by confocal microscopy.

**Analysis of cell changes during chondrocyte proliferation and hypertrophy.** Size, shape and cytoplasm density of the chondrocytes disposed in vertical columns exhibit a range of continuous variation from the top to the bottom. Growth plate shows a multilayered horizontal stratification but precise transition lines between contiguous zones cannot be established because variation is continuous. Quantitative values of cell volume, shape and cytoplasmic density obtained from each chondrocyte were used to perform a hierarchical cluster analysis and to objectively grade the chondrocytes of the growth plate. Comparison in a multidimensional array of quantitative values allowed to define distances between chondrocytes and to establish seven categories or clusters. Chondrocytes in a particular cluster share common characteristics and are more similar to each other than to those in the other clusters. A hierarchical dendrogram showing the order of successive agglomerations and

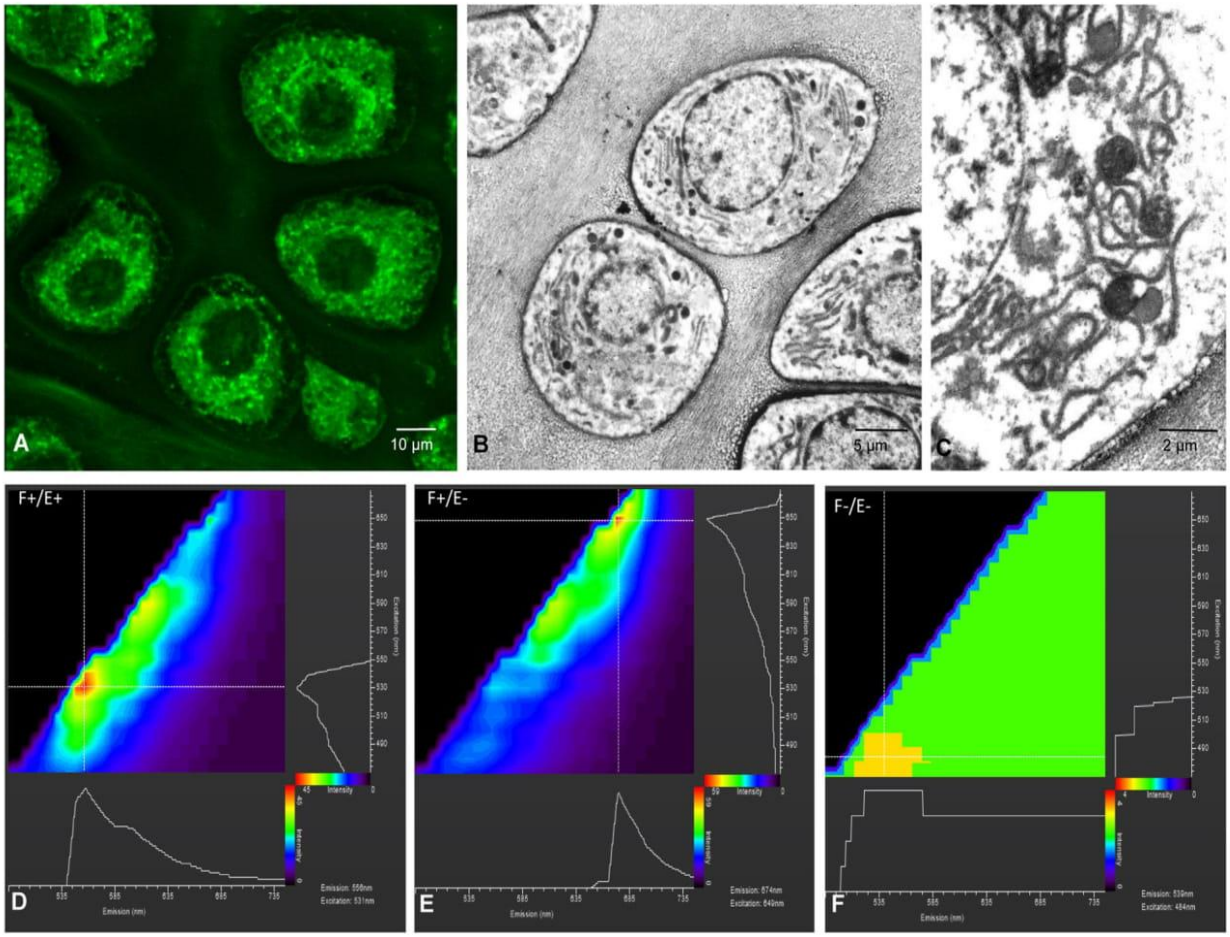


**Figure 1.** (**A**) Confocal micrograph of a single optical section 10 µm from the surface of the block showing prehypertrophic chondrocytes with fluorescent labelling in form of a reticular network around the nucleus. (**B**,**C**) are transmission electron micrographs of prehypertrophic chondrocytes with rough endoplasmic reticulum, scattered mitochondria and some lipid droplets. A correspondence is found between the fluorescent labelling and the Intracellular organelles viewed with the electron microscopy. (**D**–**F**) are excitation-emission maps of a positive sample (F+/E+) and two control samples for background fluorescence: F+/E−, fixed non-eosin stained; F−/E−, non-fixed and non-eosin stained. The map of F+/E+ shows a broad range of effective excitation wavelengths and peaks in intensity at excitation/emission wavelengths of 531/556 nm. The map of F+/E− shows a significant decrease of fluorescence and the excitation/emission peak is found at 649/674 nm. Native autofluorescence due to the intrinsic components of the chondrocytes (F−/E−) was low. Color scale bar represents fluorescence intensity in arbitrary units.

a cluster plot are shown in Fig. 3. Four layers corresponding to different stages of differentiation are classically considered in the growth plate: resting, proliferating, prehypertrophic, and hypertrophic. Results obtained in the present analysis show some of these layers defined by subjective cell morphological criteria can be subdivided into several subphases. According to our results, chondrocyte cell volume remains unchanged in the clusters 1 to 4 and then a statistically significant increase takes place in the transition from cluster 4 to cluster 5 (Fig. 4). Since cell enlargement triggers the switch to hypertrophy, it could be considered that transition from cluster 4 to cluster 5 corresponds to the transition from the proliferating to the hypertrophic stage. Thus, cluster analysis allows to differentiate four subphases in the pre-hypertrophic stage (clusters 1 to 4) and three subphases in the hypertrophic stage (clusters 5 to 7). When clusters of the hypertrophic stage were analyzed it was found that transition from cluster 4 to cluster 5 was associated with a significant increase in cell volume without significant change in cytoplasm density. However, an increase of cell volume and decrease of the cytoplasmic density, both statistically significant, took place in the transition from cluster 5 to cluster 6. Finally, cell volume increase without cytoplasmic density variation occurred in the transition from cluster 6 to cluster 7.

The seven categories of chondrocytes were evaluated by immunohistochemistry of chondrocyte markers of maturity and activity, including Col2a1, a structural component of the cartilage matrix that may act as an extracellular signaling molecule suppressing chondrocyte hypertrophy; Col10a1, a short-chain collagen associated with hypertrophy of chondrocytes and involved in the ossification of cartilage; Sox9, a transcription factor essential for chondrocyte differentiation; Igf1, a growth factor that stimulates both proliferation and hypertrophy of chondrocytes by paracrine/autocrine mechanisms; Aqp1, a water channel protein that is responsible for high water permeability of chondrocyte membrane during hypertrophy; and NKCC1, a secondary active transport system that is responsible for cell volume regulation. Immunohistochemical analysis of growth plate cartilage

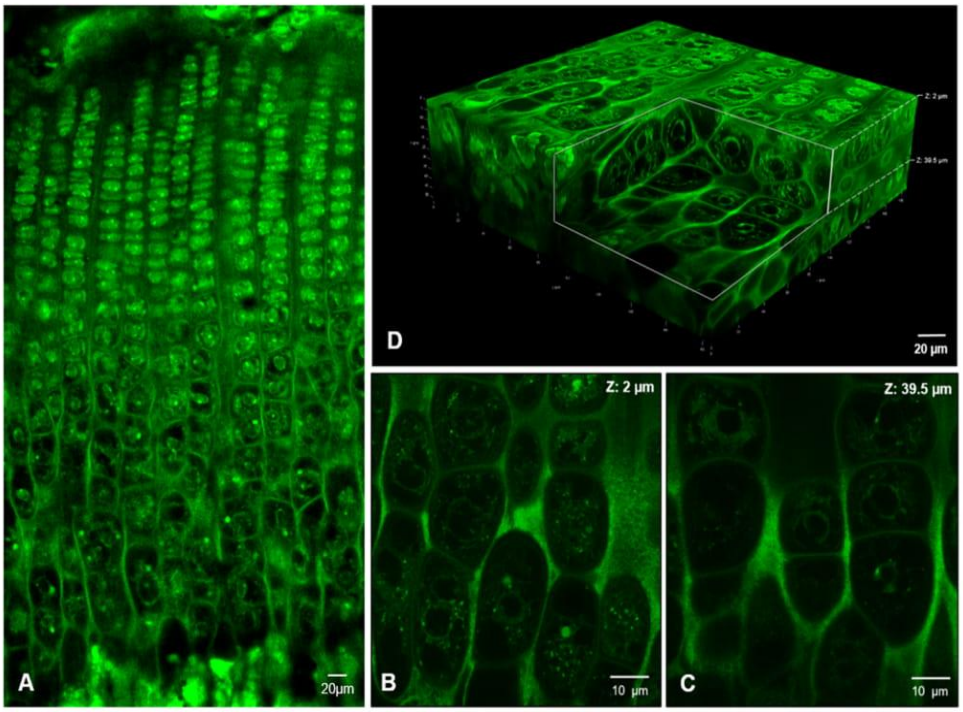


**Figure 2.** Confocal imaging of the growth plate cartilage. (**A**) Low-power micrograph showing the characteristic arrangement of the chondrocytes stacked in columns and the gradual variation in size, shape and cytoplasm density. (**B**,**C**) are two optical sections of the same field at different focal planes (2 and 39.5 µm, respectively). 3D projection of the thick section of the growth plate columns. Three-dimensional visualization is shown in Supplementary Videos.

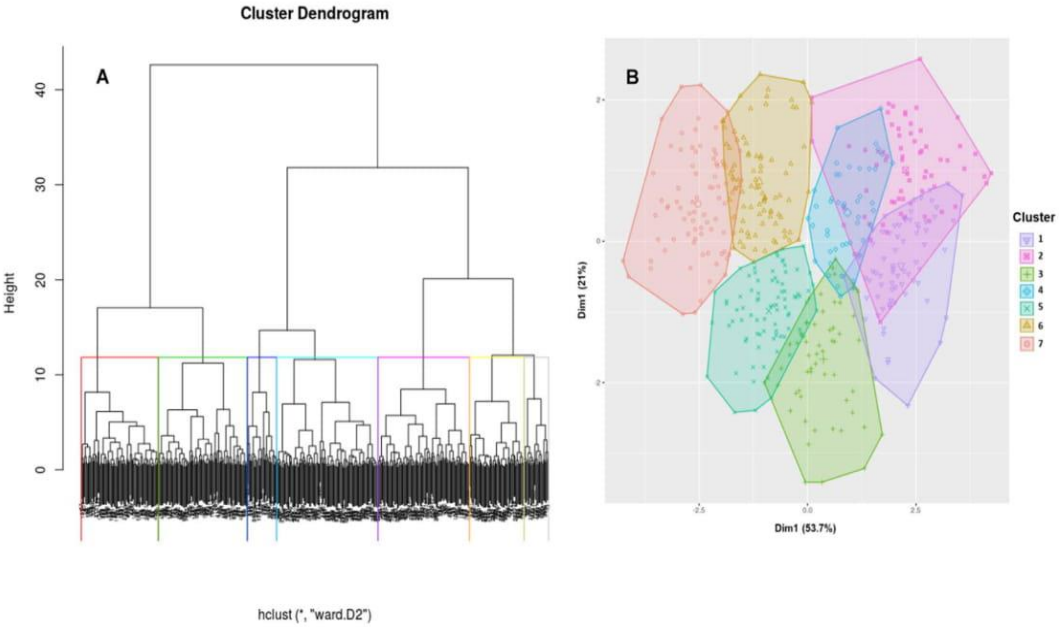


**Figure 3.** Representation of the cluster analysis. (**A**) Dendrogram showing the order in which chondrocytes were clustered by applying the Ward's linkage algorithm in combination with Manhattan distances. (**B**) Two-dimensional representation of the cluster solution. Chondrocytes are represented by points in the plot, using principal parameters and an ellipse was drawn around each cluster.

(Fig. 5) showed that Col2a1 is expressed throughout the growth plate but it decreases as chondrocytes become hypertrophic and ceases in the chondrocytes near the zone of mineralization. Analysis of immunohistochemical staining demonstrated intense signal in clusters 1 to 5 but it significantly decreased in the transition from cluster 5 to cluster 6 whereas no signal was observed in the cluster 7. By contrast, Col10a1 had the inverse distribution of Col2a1, signal was absent in clusters 1 to 3, raised in cluster 4, increased in cluster 5 and reached high levels in clusters 6 and 7. The restricted expression of Col10a1within the hypertrophic zone of the growth plate supports

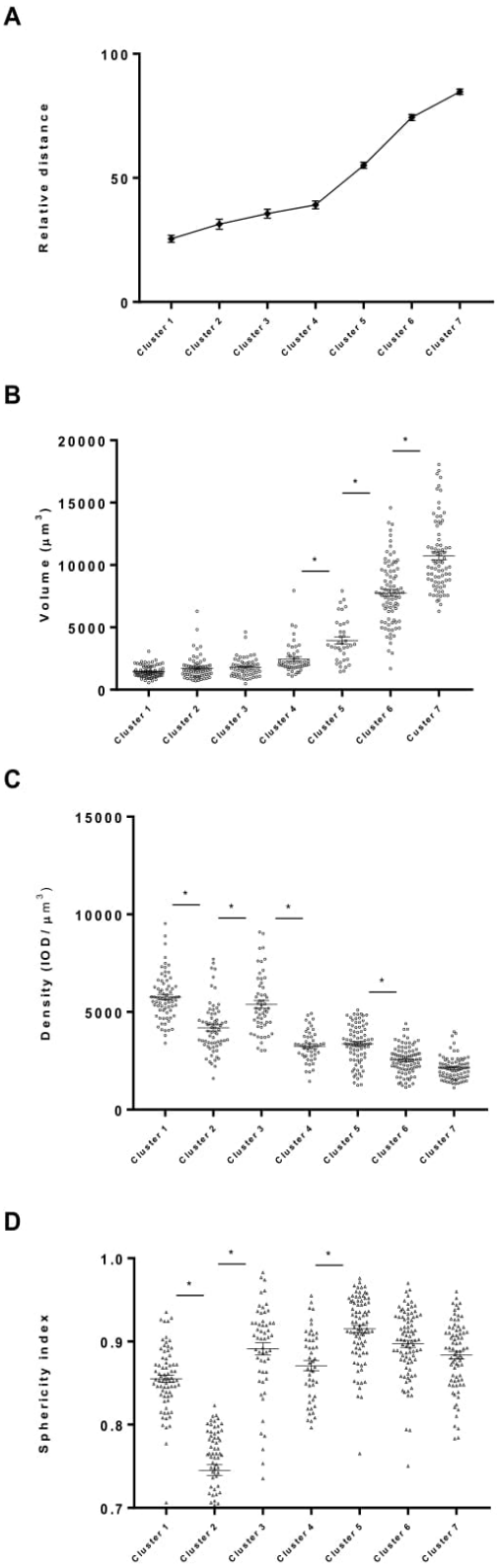


**Figure 4.** Quantitative values of relative distance, volume, cytoplasm density and sphericity index of chondrocytes in the seven categories that resulted for the cluster analysis. Data obtained from a total of 500 chondrocytes measured. Asterisks indicate significance ($P < 0.05$) when compared to preceding cluster.

that it enables the removal of type II collagen fibrils and participates in the mineralization process. Sox 9 was observed throughout the growth plate in all chondrocyte layers, with low values in clusters 1 to 4 and significant increases in the transitions from cluster 4 to cluster 5 and from cluster 5 to cluster 6 where it peaks. Finally, it significantly decreased in the transitions from cluster 6 to cluster 7. These results are coincident with previous reporting that Sox9 has essential roles in successive steps of the chondrocyte differentiation pathway[22,23]. Aqp1 and NKCC1 proteins showed equally low signal levels in clusters 1 to 4 but NKCC1 exhibited a significant increase in the transition from cluster 4 to cluster 5 whereas Aqp1 expression remained low in the cluster 5. Both transport

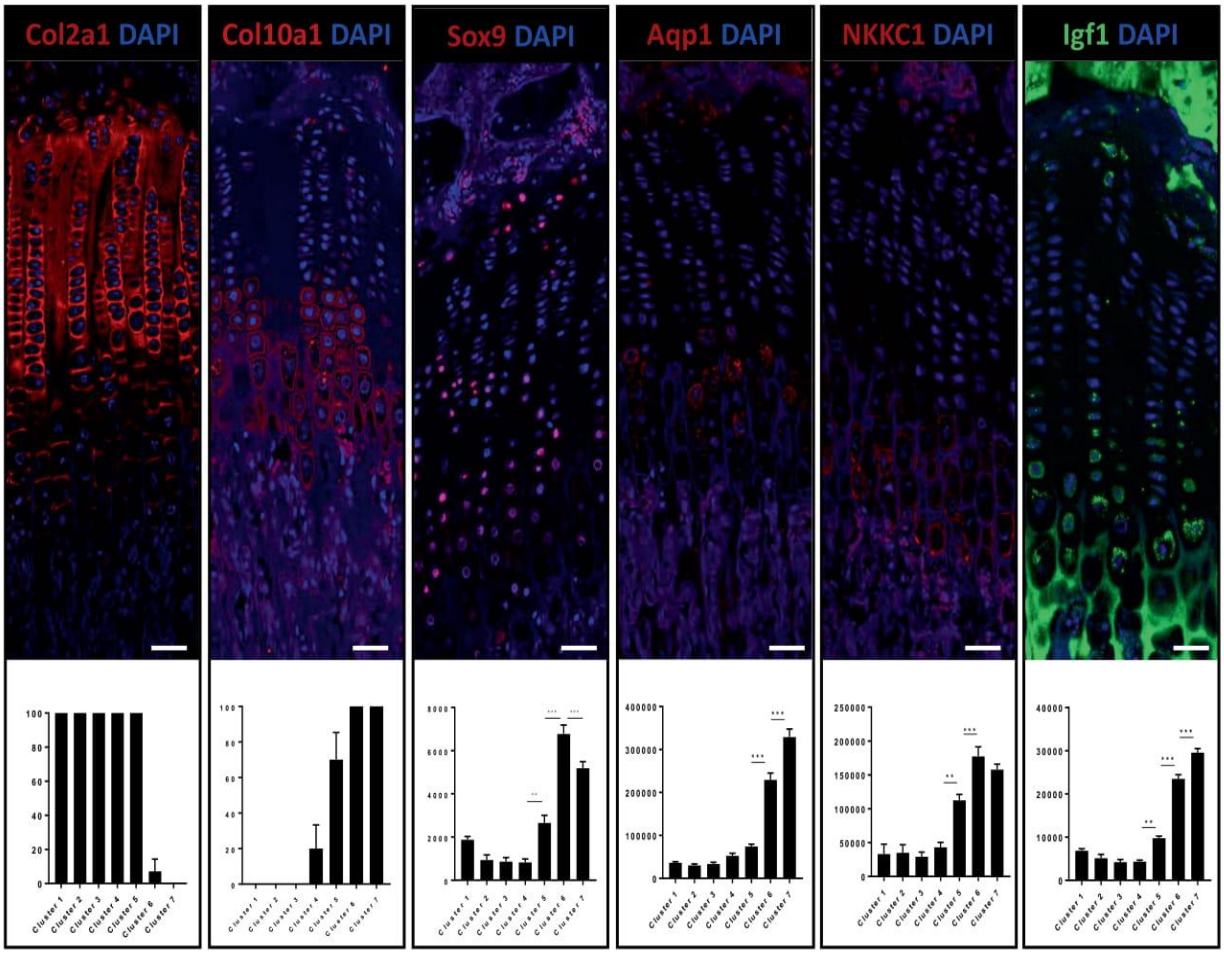


**Figure 5.** Immunohistochemical analysis of the expression of Col2a1, Col10a1, Sox9, Aqp1, NKCC1 and Igf1 in the seven categories that resulted for the cluster analysis. Asterisks indicate significance ($P < 0.05$) when compared to preceding cluster.

proteins showed high signal levels in cluster 6, where NKCC1 reached the peak level to slightly decrease in cluster 7, although without significant difference. However, Aqp1 signal continuously increased during hypertrophy and reached the highest level in cluster 7. Such differences in the expression profiles during chondrocyte hypertrophy suggest that NKCC1 may have a major role in the onset of cell volume expansion (cluster 5) whereas Aqp1 may have its main function in the later stages of the process (cluster 7). One major factor that determines ion mobility and the net movement of water into the chondrocyte is the interaction with an ionic microenvironment with high cationic content due to the concentration of fixed negative charges on proteoglycans of the cartilage extracellular matrix. Interactions between transported molecules with the microenvironment and both active and passive membrane transport proteins have been documented in cell volume regulation of chondrocytes[4,5]. Igf1 expression was in the clusters 1 to 4 and a significant increase occurred in the transition from cluster 4 to cluster 5. Likewise, significant increases were also found in the transition from cluster 5 to cluster 6 and in the transition from cluster 6 to cluster 7, where reached the highest expression level. This data supports the view that Igf1 promotes the anabolic actions associated with the increased biosynthetic activity of chondrocyte hypertrophy[24].

The occurrence of four clusters in the pre-hypertrophic stage is remarkable because only two categories of chondrocytes, resting and proliferating, have so far been defined. This result implies that proliferating zone has a less uniform structure than usually considered. Previous works have reported that chondrocytes possess nearly the same structure from the beginning to the end of the proliferating zone[25]. However functional differences among the various segments of the columns have also been reported. The establishment of clonal columns of chondrocytes is a major process that precisely occurs at the transition from the resting to the proliferating zone. Likewise, the rate of cell proliferation varies through the proliferating zone of the growth plate and changes in gene expression associated with regional differences in proliferative activity have been reported[26,27]. Since cells approximately double in size prior to mitosis and this involves both protein synthesis and energy production, it is expected that different proliferation activity may result in structural differences. Immunohistochemical analysis revealed that no differences among clusters 1 to 3 are found for Col2a1, Col10a1 or Sox9. Type II collagen and Sox9 remained unchanged at cluster 4 but Col10a1expression was first found at some chondrocytes of this cluster. Since chondrocyte cell volume remained unchanged in the clusters 1 to 4 and significantly increased in the transition from cluster 4 to cluster 5, it could be concluded that Col10a1expression is turned on before the beginning of cell volume increment. Results obtained in the present work suggest that quantitative analysis of volume, shape

and cytoplasm of chondrocytes could be a specific and sensitive method to detect differences in the activity of proliferative chondrocytes.

Our results obtained on chemically-fixed *in situ* chondrocytes are basically coincident with those obtained by Cooper and colleagues on living chondrocytes dissociated from the growth plate[6]. Fixed cells conserve their three-dimensional interaction with the surrounding extracellular matrix and preserve their shape and size but lose some of their low-molecular-weight intracellular constituents and lipids. Living chondrocytes dissociated from the growth plate maintain life functions but lose their specific shape and acquire spherical shape. The fact that two approaches with different advantages and disadvantages lead to the same conclusion reinforces the assumption that chondrocyte volume enlargement during hypertrophy is a multistage process consisting of three phases. Furthermore, our results show that NKCC1 expression is involved in the beginning of the increment in cell volume and the expression profiles of NKCC1 and Aqp1 specifically changed during different phases of chondrocyte hypertrophy.

In summary, the new method reported in the present work allows obtaining additional information to common measurements of chondrocytes and improves the understanding of the sequence of events during the process of differentiation of these cells. This is remarkable because chondrocytes go through a series of orderly changes where each stage depends on successful completion of the stage before and the correct sequence of changes is of major importance for the proper formation of the bones.

Received: 2 October 2019; Accepted: 8 April 2020;
Published online: 24 April 2020

## References

1. Hall, B. K. *Bones and Cartilage: Developmental and Evolutionary Skeletal Biology* (2015).
2. Kronenberg, H. Developmental regulation of the growth plate. *Nature* **423**, 332–336 (2003).
3. Bush, P. G., Pritchard, M., Loqman, M. Y., Damron, T. A. & Hall, A. C. A key role for membrane transporter NKCC1 in mediating chondrocyte volume increase in the mammalian growth plate. *J. Bone Miner. Res.* **25**, 1594–1603 (2010).
4. Loqman, M. Y., Bush, P. G., Farquharson, C. & Hall, A. C. Suppression of mammalian bone growth by membrane transport inhibitors. *J. Cell. Biochem.* **114**, 658–668 (2013).
5. Bush, P. G., Parisinos, C. A. & Hall, A. C. The osmotic sensitivity of rat growth plate chondrocytes *in situ*; clarifying the mechanisms of hypertrophy. *J. Cell. Physiol.* **214**, 621–629 (2008).
6. Cooper, K. L. *et al*. Multiple phases of chondrocyte enlargement underlie differences in skeletal proportions. *Nature* **495**, 375–8 (2013).
7. Fuente, R. *et al*. Marked alterations in the structure, dynamics and maturation of growth plate likely explain growth retardation and bone deformities of young Hyp mice. *Bone* **116**, 187–195 (2018).
8. Loqman, M. Y., Bush, P. G., Farquharson, C. & Hall, A. C. A cell shrinkage artefact in growth plate chondrocytes with common fixative solutions: importance of fixative osmolarity for maintaining morphology. *Eur. Cell. Mater.* **19**, 214–227 (2010).
9. de Carvalho, H. F. & Taboga, S. R. Fluorescence and confocal laser scanning microscopy imaging of elastic fibers in hematoxylin-eosin stained sections. *Histochem. Cell Biol.* **106**, 587–592 (1996).
10. Wu, Y., Li, B. & Gao, X. M. Selective fluorescence of zymogen granules of pancreatic acinar cells stained with hematoxylin and eosin. *Biotech. Histochem.* **77**, 291–293 (2002).
11. Capani, F. *et al*. Phalloidin-eosin followed by photo-oxidation: a novel method for localizing F-actin at the light and electron microscopic levels. *J. Histochem. Cytochem.* **49**, 1351–1361 (2001).
12. Luo, T., Lu, Y., Liu, S., Lin, D. & Qu, J. Enhanced Visualization of Hematoxylin and Eosin Stained Pathological Characteristics by Phasor Approach. *Anal. Chem.* **89**, 9224–9231 (2017).
13. Castellanos, M. R., Nehru, V. M., Pirog, E. C. & Optiz, L. Fluorescence microscopy of H&E stained cervical biopsies to assist the diagnosis and grading of CIN. *Pathol. Res. Pract.* **214**, 605–611 (2018).
14. Hulspas, R., Bioconsulting, C. T. & Keij, J. F. Avidin-EITC: an alternative to avidin-FITC in confocal scanning laser microscopy. *J. Histochem. Cytochem.*, https://doi.org/10.1177/41.8.7687265 (1993).
15. Deerinck, T. J. *et al*. Fluorescence photooxidation with eosin: a method for high resolution immunolocalization and *in situ* hybridization detection for light and electron microscopy. *J. Cell Biol.* **126**, 901–910 (1994).
16. Waheed, A. A., Rao, K. S. & Gupta, P. D. Mechanism of dye binding in the protein assay using eosin dyes. *Anal. Biochem.* **287**, 73–79 (2000).
17. Waheed, A. A. & Gupta, P. D. Application of an eosin B dye method for estimating a wide range of proteins. *J. Biochem. Biophys. Methods* **33**, 187–196 (1996).
18. Jordanides, X. J., Lang, M. J., Song, X. & Fleming, G. R. Solvation Dynamics in Protein Environments Studied by Photon Echo Spectroscopy. *J. Phys. Chem. B* **103**, 7995–8005 (1999).
19. Waheed, A. A. & Gupta, P. D. Estimation of submicrogram quantities of protein using the dye eosin Y. *J. Biochem. Biophys. Methods* **42**, 125–132 (2000).
20. Ni, Y., Liu, Q. & Kokot, S. Spectrophotometric study of the interaction between chlorotetracycline and bovine serum albumin using Eosin y as site marker with the aid of chemometrics. *Spectrochim. Acta - Part A Mol. Biomol. Spectrosc.* **78**, 443–448 (2011).
21. Birla, L., Cristian, A. M. & Hillebrand, M. Absorption and steady state fluorescence study of interaction between eosin and bovine serum albumin. *Spectrochim. Acta - Part A Mol. Biomol. Spectrosc.* **60**, 551–556 (2004).
22. Hallett, S. A., Ono, W. & Ono, N. Growth plate chondrocytes: Skeletal development, growth and beyond. *Int. J. Mol. Sci.* **20**, 1–17 (2019).
23. Akiyama, H., Chaboissier, M. C., Martin, J. F., Schedl, A. & De Crombrugghe, B. The transcription factor Sox9 has essential roles in successive steps of the chondrocyte differentiation pathway and is required for expression of Sox5 and Sox6. *Genes Dev.* **16**, 2813–2828 (2002).
24. Yakar, S., Werner, H. & Rosen, C. J. Insulin-like growth factors: Actions on the skeleton. *J. Mol. Endocrinol.* **61**, T115–T137 (2018).
25. Farquharson, C. & Loveridge, N. Cell proliferation within the growth plate of long bones assessed by bromodeoxyuridine uptake and its relationship to glucose 6-phosphate dehydrogenase activity. *Bone Miner.* **10**, 121–130 (1990).
26. Aizawa, T., Kokubun, S. & Tanaka, Y. Apoptosis and proliferation of growth plate chondrocytes in rabbits. *J. Bone Joint Surg. Br.* **79**, 483–486 (1997).
27. Tchetina, E., Mwale, F. & Poole, A. Changes in gene expression associated with matrix turnover, chondrocyte proliferation and hypertrophy in the bovine growth plate. *Acta Naturae* **6**, 89–97 (2014).

## Acknowledgements

We thank Henry Kronenberg (Endocrine Unit, Massachusetts General Hospital) for his comments on a former version of the manuscript, as well as the Statistical Consulting Unit of the University of Oviedo for assistance with the cluster analysis. This study was supported by Fundacion Nutrición y Crecimiento, by grants PI18/01757 (Plan Estatal I + D + I 2017–2020) from the Instituto de Salud Carlos III (Madrid, Spain) and GRUPIN14–20 from Fondos Europeos de Desarrollo Regional (FEDER), by Marie Skłodowska-Curie European Commission, by Fundación de la Universidad de Oviedo (FUO) and by Fundación para la Investigación Biomédica en Asturias (FINBA).

## Author contributions

F.S. and J.M.L. conceived and supervised the study. A.F.I. and J.M.L. implemented the method and ran evaluations with contributions from R.F., H.G.P., L.A.D. and M.G.B. A.F.I., L.A.D. and M.G.B. performed the immunohistochemical analysis. A.F.I. analyzed the data with contributions from R.F., H.G.P., L.A.D. and M.G.B. J.M.L. wrote the manuscript with input from all the authors.

## Competing interests

The authors declare no competing interests.

## Additional information

**Supplementary information** is available for this paper at https://doi.org/10.1038/s41598-020-63978-6.

**Correspondence** and requests for materials should be addressed to J.M.L.

**Reprints and permissions information** is available at www.nature.com/reprints.

**Publisher's note** Springer Nature remains neutral with regard to jurisdictional claims in published maps and institutional affiliations.

# III. Analysis of Uremic Growth Plate Chondrocytes

Chronic kidney disease (CKD) alters the morphology and function of the GP of long bones by disturbing chondrocyte maturation. GP chondrocytes were analyzed in growth-retarded young rats with CKD induced by adenine intake (AD), control rats fed ad libitum (C) or pair-fed with the AD group (PF), and CKD rats treated with growth hormone (ADGH). In order to study the alterations in the process of GP maturation, we applied a procedure recently described by our group to obtain high-quality three-dimensional images of whole chondrocytes that can be used to analyze quantitative parameters like cytoplasm density, cell volume, and shape. The final chondrocyte volume was found to be decreased in AD rats, but GH treatment was able to normalize it. The pattern of variation in the cell cytoplasm density suggests that uremia could be causing a delay to the beginning of the chondrocyte hypertrophy process. GH treatment appears to be able to compensate for this disturbance by triggering an early chondrocyte enlargement that may be mediated by Nkcc1 action, an important membrane cotransporter in the GP chondrocyte enlargement.

**Article 2. Ángela Fernández-Iglesias,** Rocío Fuente, Helena Gil-Peña, Laura Alonso-Duran, María García-Bengoa, Fernando Santos & José M. López. “Innovative Three-Dimensional Microscopic Analysis of Uremic Growth Plate Discloses Alterations in the Process of Chondrocyte Hypertrophy: Effects of Growth Hormone Treatment.”

Int J Mol Sci. 2020 Jun 25;21(12):4519. doi: 10.3390/ijms21124519.

**Journal metrics (2019)**

2-year impact Factor 4.556

5-year impact Factor: 4.653

International Journal of
*Molecular Sciences*

MDPI

*Article*

# Innovative Three-Dimensional Microscopic Analysis of Uremic Growth Plate Discloses Alterations in the Process of Chondrocyte Hypertrophy: Effects of Growth Hormone Treatment

**Ángela Fernández-Iglesias [1,2], Rocío Fuente [1], Helena Gil-Peña [1,2,3], Laura Alonso-Durán [1,2], María García-Bengoa [1], Fernando Santos [1,2,3,*] and José Manuel López [1,4]**

1 Division of Pediatrics, Department of Medicine, Faculty of Medicine, University of Oviedo, CP 33006 Oviedo, Asturias, Spain; angelafiglesias@gmail.com (A.F.-I.); rociofuenteperez@gmail.com (R.F.); hgilpena@gmail.com (H.G.-P.); laurita.alonso86@gmail.com (L.A.-D.); mariagbengoa18@gmail.com (M.G.-B.); jmlopez@uniovi.es (J.M.L.)
2 Instituto de Investigación sanitaria del Principado de Asturias (ISPA), 33012 Oviedo, Spain
3 Department of Pediatrics, Hospital Universitario Central de Asturias (HUCA), 33013 Oviedo, Asturias, Spain
4 Department of Morphology and Cellular Biology, Faculty of Medicine, University of Oviedo, CP 33006 Oviedo, Asturias, Spain
* Correspondence: fsantos@uniovi.es; Tel.: +34-985102728

Received: 23 May 2020; Accepted: 23 June 2020; Published: 25 June 2020


**Abstract:** Chronic kidney disease (CKD) alters the morphology and function of the growth plate (GP) of long bones by disturbing chondrocyte maturation. GP chondrocytes were analyzed in growth-retarded young rats with CKD induced by adenine intake (AD), control rats fed ad libitum (C) or pair-fed with the AD group (PF), and CKD rats treated with growth hormone (ADGH). In order to study the alterations in the process of GP maturation, we applied a procedure recently described by our group to obtain high-quality three-dimensional images of whole chondrocytes that can be used to analyze quantitative parameters like cytoplasm density, cell volume, and shape. The final chondrocyte volume was found to be decreased in AD rats, but GH treatment was able to normalize it. The pattern of variation in the cell cytoplasm density suggests that uremia could be causing a delay to the beginning of the chondrocyte hypertrophy process. Growth hormone treatment appears to be able to compensate for this disturbance by triggering an early chondrocyte enlargement that may be mediated by Nkcc1 action, an important membrane cotransporter in the GP chondrocyte enlargement.

**Keywords:** chronic kidney disease; CKD; uremia; chondrocyte; hypertrophy; GH

## 1. Introduction

Growth impairment remains a major complication in pediatric patients with chronic kidney disease (CKD) and only 30% of adults with childhood onset CKD reach a normal final height [1,2]. Several factors play a causal role in this growth retardation, including small infant size at birth, metabolic acidosis, salt and water deficits, anorexia, malnutrition and cachexia, anemia, and resistance to anabolic hormones such as growth hormone (GH), insulin-like growth factor 1 (IGF1), and sexual hormones.

Longitudinal growth is the product of an elaborate cascade of events, many of them taking place in the cartilaginous center of long bones, the epiphyseal growth plate (GP) [3]. Chondrocytes within the GP elongate the bone by the proliferation, progression, hypertrophy, and synthesis of the extracellular matrix [4]. The columnar or proliferative chondrocytes exit the cell cycle and begin to increase their cell volume and change their cell shape to form prehypertrophic and hypertrophic

chondrocytes. The hypertrophic cells mineralize their extracellular matrix and either they are degraded by osteoclasts and replaced by invading osteoblasts or they transdifferentiate into bone-forming osteoblasts [5].

The investigation of GP in CKD-induced growth retardation requires animal models because the analysis of GP is not feasible in children. The proximal GP of the tibiae of prepubertal rats has been used, although there is limited information on the alterations in the morphology and dynamics of GP and on the effect of CKD on the factors that regulate chondrocyte proliferation and differentiation. However, the chondrocytes of uremic rats are known to achieve a lower final size than those of control animals. This is crucial because the volume increase during chondrocyte hypertrophy is the main contributor to the longitudinal growth rate in mammals [6]. The increase in chondrocyte volume was found to result from three sequential stages: two stages of true hypertrophy (phases 1 and 3), when chondrocytes increase their volume in parallel with the active synthesis of cytoplasmic components, separated by a stage of swelling (phase 2), when the volume increases more than the synthesis, causing a decrease in the cytoplasm density. IGF1 was found to specifically affect chondrocyte hypertrophy during phase 3 [7].

We have recently developed a novel procedure that enables the objective discrimination of distinct groups of chondrocyte populations in the GP [8]. By applying this methodology to normal growing rats, we graded GP chondrocytes in seven different clusters, with four subphases in the pre-hypertrophic zone and three in the hypertrophic zone. In the present study, we apply this methodology to obtain new insights into the process of chondrocyte differentiation in a rat model of growth retardation induced by CKD. We also analyze the effects of GH treatment on the GP disturbances. For further molecular characterization of the alterations in the GP differentiation process in CKD, we analyze the immunohistochemical expression of the proteins associated with the process of chondrocyte hypertrophy.

## 2. Results

### 2.1. Renal Function and Mineral Metabolism

We used 3-week-old female rats which were grouped as follows: fed ad libitum with control diet (C); fed ad libitum with 0.5% adenine diet, either without treatment (AD) or with GH treatment (ADGH); and pair-fed with the AD group (PF). The AD and ADGH groups had similar degrees of renal failure, as shown by the similar serum creatinine and blood urea nitrogen (BUN) levels in Table 1. Phosphorus levels were significantly reduced in the AD, ADGH, and PF groups in comparison with the control group, but no significant differences in calcium levels were observed among all groups.

**Table 1.** Serum biochemical determinations in the four groups of rats ($n \geq 5$ per group).

| Groups | Serum Creatinine (mg/dL) | BUN (mg/dL) | Calcium (mg/dL) | Phosphorus (mg/dL) |
|---|---|---|---|---|
| C | 0.12 ± 0.01 | 23d ± 2 | 9.16 ± 0.22 | 10.16 ± 0.27 |
| AD | 0.59 ± 0.05 [a] | 122 ± 8 [a] | 9.45 ± 0.15 | 8.00 ± 0.47 [a] |
| ADGH | 0.51 ± 0.06 [a] | 92 ± 9 [a,b] | 9.16 ± 0.23 | 8.33 ± 0.44 [a] |
| PF | 0.10 ± 0.01 [b,c] | 40 ± 2 [b,c] | 8.96 ± 0.09 | 6.79 ± 0.25 [a,c] |

BUN, blood urea nitrogen; AD, 0.5% adenine diet; ADGH, 0.5% adenine diet and growth hormone (GH) treatment; C, normal diet; PF, normal diet pair-fed with the AD group. Values are mean ± SEM. [a] Compared with C group, $p < 0.05$. [b] Compared with AD group, $p < 0.05$. [c] Compared with ADGH group, $p < 0.05$.

### 2.2. Growth Retardation and Uremic Growth Plate

As summarized in Table 2, AD animals were growth retarded, as demonstrated by their lower length gain and growth velocity, assessed by osseous front advance (OFA), compared with the PF and C groups. GH treatment normalized body weight, growth velocity, and food efficiency in ADGH rats.

**Table 2.** Growth parameters in the groups of rats ($n \geq 5$ per group).

| Groups | Nose–Tail Length Gain (cm) | Body Weight Gain (g) | Food Efficiency (g/g) * | OFA (μm/Day) |
|---|---|---|---|---|
| C | 9.10 ± 0.28 | 107.30 ± 5.04 | 0.29 ± 0.01 | 335.7 ± 10.25 |
| AD | 4.49 ± 0.31 [a] | 54.12 ± 2.59 [a] | 0.23 ± 0.01 [a] | 210.3 ± 6.33 [a] |
| ADGH | 5.01 ± 0.44 [a] | 68.53 ± 4.71 [a,b] | 0.28 ± 0.01 [b] | 288.7 ± 17.97 [b] |
| PF | 4.96 ± 0.22 [a] | 43.28 ± 2.57 [a,c] | 0.18 ± 0.01 [a,b,c] | 206.2 ± 16.07 [a,c] |

AD, 0.5% adenine diet; ADGH, 0.5% adenine diet and GH treatment; C, normal diet; PF, normal diet pair-fed with the AD group; OFA, osseous front advance. Values are mean ± SEM. * Food efficiency was calculated as grams of gained weight divided by grams of consumed food; [a] Compared with C group, $p < 0.05$. [b] Compared with AD group, $p < 0.05$. [c] Compared with ADGH group, $p < 0.0.5$.

When we examined the histology in the proximal metaphysis of the tibiae, the height of the GP was significantly smaller in the AD and PF groups than in the C group. The AD and PF groups also showed a decrease in the height of the hypertrophic zone compared with the C group (Table 3). GH treatment restored the micro-architecture of the GP (Figure 1) as well as both its total height and that of the hypertrophic zone (Table 3).

**Table 3.** Histological characteristics of the proximal tibial growth plate in the four groups of rats ($n \geq 5$ animals per group).

| Groups | GP Height (μm) | HZ Height (μm) |
|---|---|---|
| C | 384.5 ± 12.42 | 173.8 ± 10.79 |
| AD | 323.6 ± 12.47 [a] | 132.4 ± 6.016 [a] |
| ADGH | 416.2 ± 30.82 [b] | 166.2 ± 22.18 |
| PF | 281.7 ± 9.78 [a,c] | 109.3 ± 6.04 [a,c] |

AD, 0.5% adenine diet; ADGH, 0.5% adenine diet and GH treatment; C, normal diet; PF, normal diet pair-fed with the AD group; GP, growth plate; HZ, hypertrophic zone. Values are mean ± SEM. [a] Compared with C group, $p < 0.05$. [b] Compared with AD group, $p < 0.05$. [c] Compared with ADGH group, $p < 0.05$.

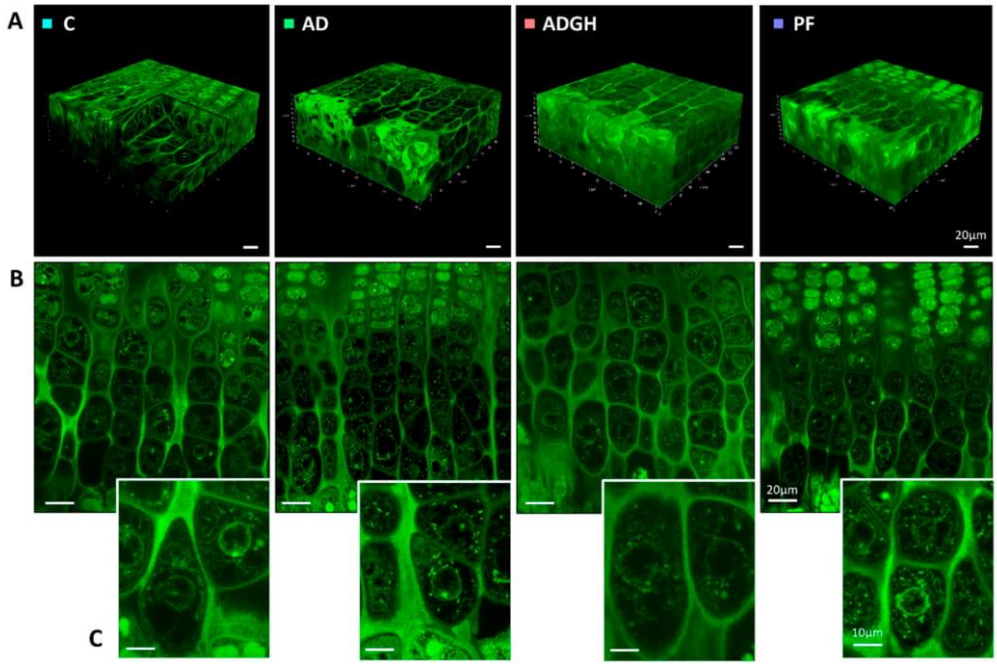


**Figure 1.** Confocal imaging of the growth plate cartilage. (**A**) A 3D projection of the thick section of the growth plate columns. Three-dimensional visualization is shown in Supplementary Videos 1–8. (**B**) Optical sections of focal planes of the hypertrophic zone. (**C**) Detail of terminal hypertrophic chondrocytes of the growth plates of the four experimental groups. C, control rats; AD, adenine 0.5% rats; ADGH, adenine 0.5% rats treated with growth hormone; PF, pair-fed rats.

### 2.3. Three-Dimensional Analysis of Uremic Chondrocytes

In order to study how uremia and GH treatment affect the differentiation pattern of chondrocytes, we applied a three-dimensional approach, as described elsewhere [8]. Changes in the cell volume, integrated optical density (IOD), and cytoplasm cell density of the three-dimensional chondrocytes were analyzed along the long axis of the GP (Figure 1) (Videos S1–6). According to our results, the AD and PF groups started with a reduced chondrocyte cell volume in cluster 1, partially normalized from cluster 2 to 3 (Figure 2A,C). In the control GP, chondrocytes started enlarging in the transition from cluster 3 to 4. Conversely, AD chondrocytes were unable to increase their volume from cluster 3 to 4. By cluster 4, AD chondrocytes presented a significantly reduced volume and increased integrated optical density (IOD) compared to the control chondrocytes. The volume increase in the AD chondrocytes appeared to be delayed up to the transition from cluster 4 to 5, when they underwent an abrupt entrance in hypertrophy, by increasing their volume (×2.2) without a proportional increase in dry mass (×1.6). This progression differed greatly from that of the control chondrocytes, having a proportional increase in volume (×1.4) and dry mass (×1.4). Subsequently, in the transition from cluster 5 to 6, the control chondrocytes underwent a marked increase in their volume (×2.3) which was not accompanied by a proportional increase in dry mass. Instead, the AD chondrocytes had a more modest increase in volume and dry mass (×1.7 and ×1.30), causing a reduction in their cell cytoplasm density. Finally, in the transition from cluster 6 to 7, normal and uremic chondrocytes displayed parallel behaviors, undergoing both a proportional increase in volume and dry density, characteristic of true hypertrophy. Thus, uremic chondrocytes reached cluster 7 with a reduced size but at a normal cell density (Figures 1C and 2A). The chondrocytes of PF animals mostly exhibited the same behavior as AD chondrocytes. They showed a similar pattern of volume and cell cytoplasm density from the prehypertrophic clusters 1 to 5 but a higher cell density from cluster 5 to 6, which was normalized in cluster 7 (Figure 2C).

The GP of the GH group (ADGH) showed a reduced chondrocyte volume in cluster 1, but the pattern of the chondrocyte volume increase was normalized from cluster 2 to 3. Chondrocytes increased their volume in the transition from cluster 3 to 4, and by cluster 4, they paralleled their volume with that of the control and significantly increased their IOD to higher values than the AD chondrocytes. In the transition from cluster 4 to 5, GH treatment caused a large volume enlargement (×2,3) which was not proportional to the increase in the IOD (×1,3), reducing the cell cytoplasm density even more than that of the AD chondrocytes. In the transitions from cluster 5 to 6 and 6 to 7, GH chondrocytes presented a similar pattern of increase in both volume (×1,7) and IOD (×1,3) than the uremic untreated chondrocytes (Figure 2A,B). By cluster 7, GH chondrocytes had a normalized chondrocyte volume (Figures 1C and 2A).

### 2.4. Immunohistochemistry of Growth Plate Markers

To connect the changes in volume, shape, and cytoplasm cell density in the chondrocyte subsets with changes in the specific proteins which are possibly implicated in the pathogenesis of growth impairment, we performed an immunohistochemical analysis (Figure 3). The pattern of the distribution of Igf1 was phenotypically similar between experimental groups, but its levels of expression were reduced in the AD group compared with the C group in all the GP clusters, except cluster 3, where levels did not differ between groups. In contrast, the PF group showed low levels, similar to those of AD, between clusters 1 to 5, but peaked in clusters 6 and 7, both with significantly more Igf1 expression than AD chondrocytes (Figure 3). GH treatment did not produce changes in the Igf1 levels between clusters 1 to 3 but increased its levels from clusters 4 to 6 compared with the AD group, to reach the highest levels in cluster 7 (Figure 3).

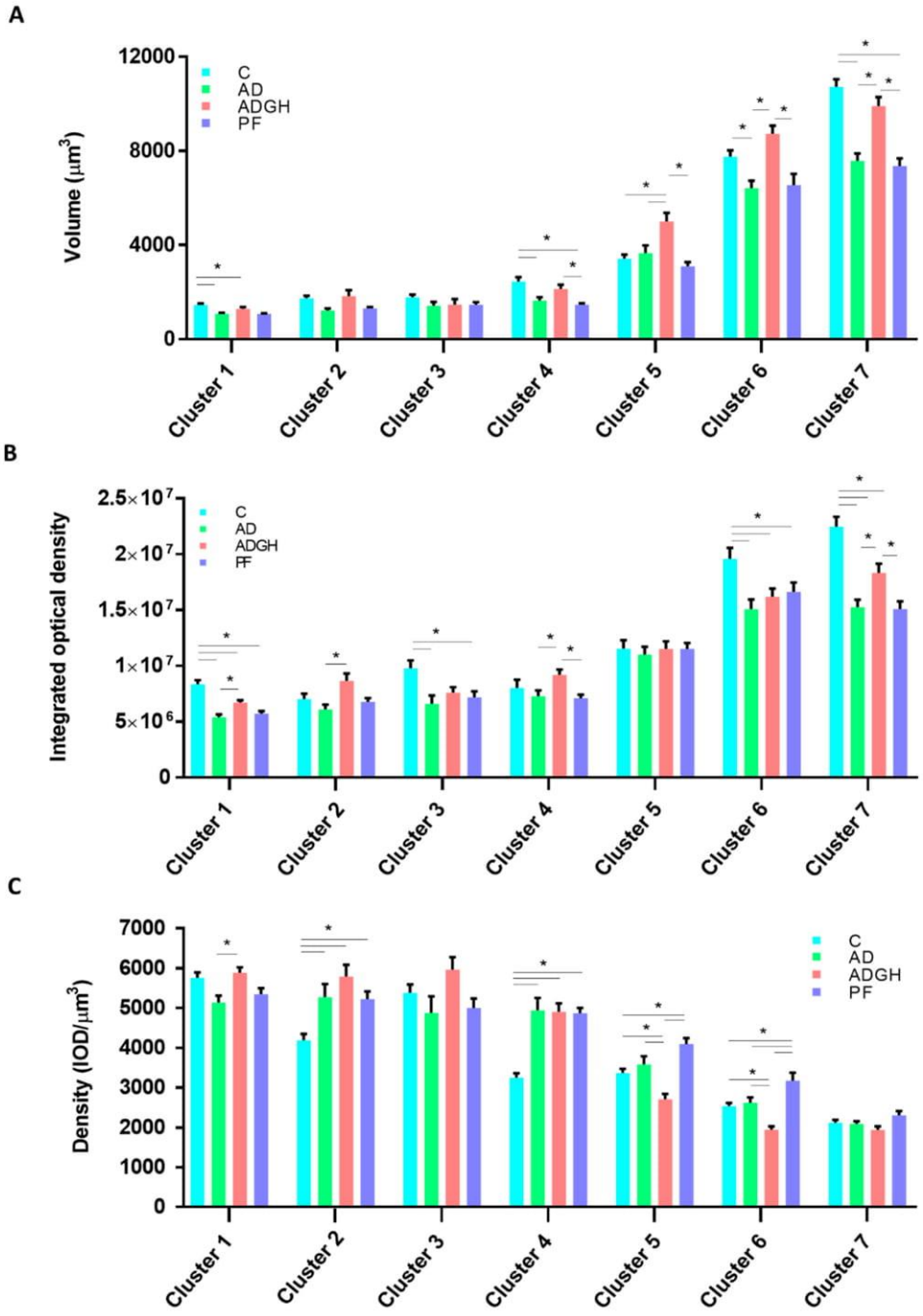


**Figure 2.** Quantitative values of chondrocytes of the four experimental groups. (**A**) Volume, (**B**) integrated optical density, and (**C**) cytoplasm density of chondrocytes of the groups organized into the seven categories of chondrocytes. Data obtained from a total of 1500 chondrocytes measured. C, control rats; AD, adenine 0.5% rats; ADGH, adenine 0.5% rats treated with GH; PF, pair-fed rats; IOD, integrated optical density. Values are mean ± SEM. * $p$ value < 0.05.

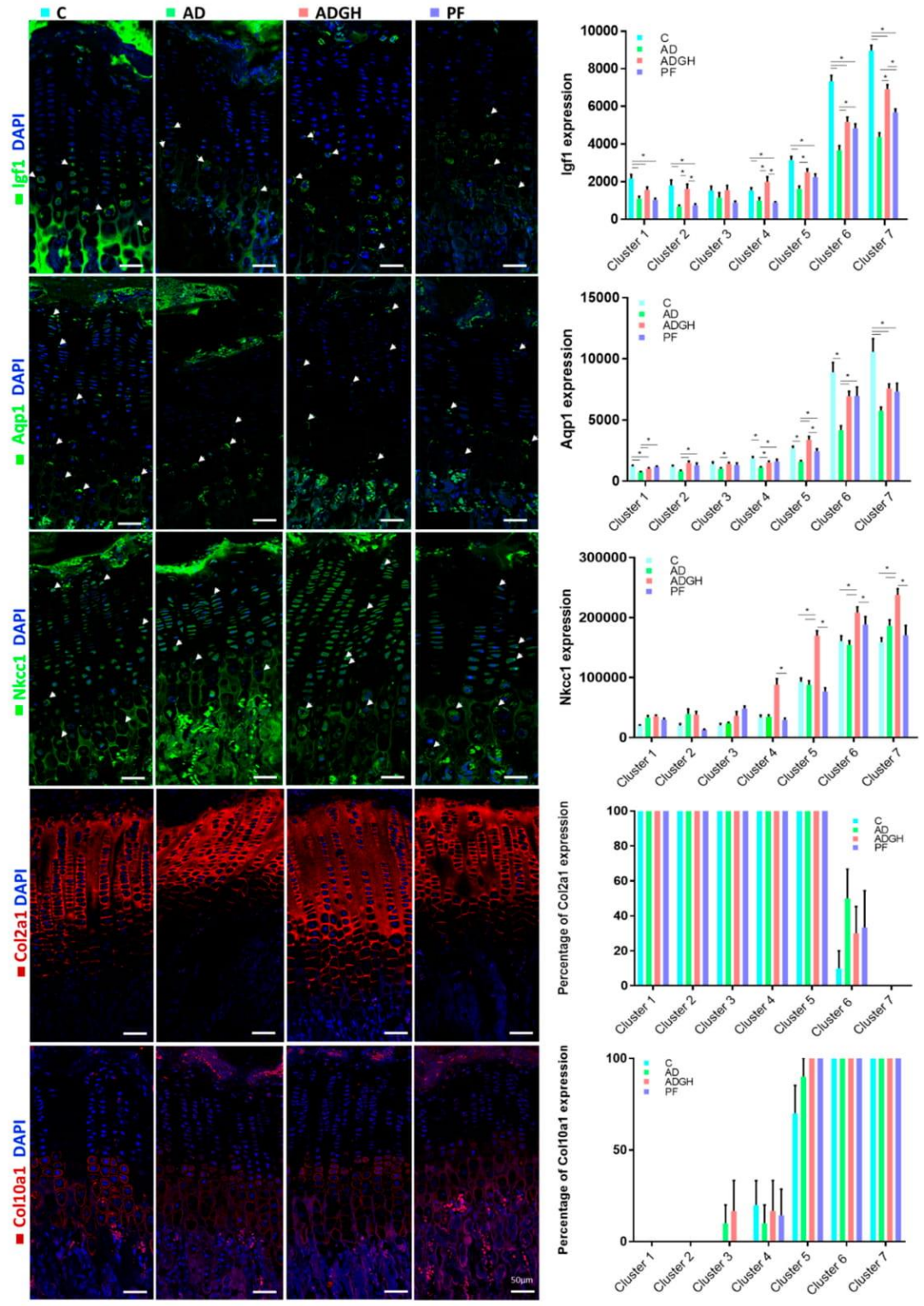


**Figure 3.** Immunohistochemical analysis of the expression of growth plate markers. Representative images are shown for Igf1 (green), Aqp1 (green), Nkcc1 (green), Col2a1 (red), and Col10a1 (red) and their corresponding quantifications in the seven described clusters. Arrowheads mark some of the labeled cells. Blue nuclei are stained by DAPI. DAPI, 4′,6-diamidino-2-phenylindole; C, control rats; AD, adenine 0.5% rats; ADGH, adenine 0.5% rats treated with GH; PF, pair-fed rats; Col2a1, collagen 2 alpha chain 1; Col10a1, collagen 10 alpha chain 1; Nkcc1, Na K $Cl^-$ cotransporter 1; Aqp1, aquaporin 1; Igf1, insulin growth factor 1. Values are mean ± SEM. * $p$ value < 0.05.

The expression of type II (Col2a1) and X (Col10a1) collagens was analyzed by inmunofluorescence (Figure 3). In control rats, Col2a1 expression was high in prehypertrophic clusters (clusters 1 to 5) and then showed a progressive decrease to reach relatively low values in the last clusters (clusters 6–7) (Figure 3). Col10a1 expression suddenly appeared in the early hypertrophy zone (cluster 4) and extended until late hypertrophy (cluster 7) (Figure 3). No apparent changes in the pattern of Col2a1 were found, but we did note an early Col10a1 expression in cluster 3, compared to the control (Figure 3).

The transporters and channels that regulate water and electrolyte traffic through the cell membrane Aquaporin (Aqp1) and $Na^+/K^+/2Cl^-$ cotransporter 1 (Nkcc1) were analyzed. The Aqp1 signal was localized within the cytoplasm and the cellular membrane of the hypertrophic chondrocytes in all groups (Figure 3). Its expression was significantly diminished in the AD group compared to the C group for all the clusters. GH treatment appeared to partly normalize levels at clusters 2 to 6, but not at cluster 7, where levels were like those of uremic chondrocytes (Figure 3). Similarly, Nkcc1 expression was found in the hypertrophic chondrocytes in all groups, mainly in the cytoplasm and the cellular membrane (Figure 3). No significant changes were found in the pattern or intensity of expression in the AD and PF groups compared with the C group. Conversely, GH significantly increased Nkcc1 levels of expression from clusters 4 to 7 in comparison with the AD, PF, and C groups.

## 3. Discussion

In the present study, a three-dimensional approach to evaluate the alterations in the chondrocyte differentiation process that underlie growth retardation in CKD was applied for the first time. As previously described, the final chondrocyte volume was decreased in uremic rats, but GH treatment was able to normalize it. Interestingly, the pattern of variation in IOD and cell cytoplasm density suggests that uremia could be causing a delay at the beginning of chondrocyte hypertrophy. Nevertheless, GH treatment appeared to be able to compensate for this disturbance by triggering an early chondrocyte enlargement, likely mediated by Nkcc1 action (Figures 2 and 3). For the experimental protocol, we used an adenine-induced CKD rat model that resulted in moderate renal failure, as reflected by BUN and serum creatinine concentrations that were about five times higher in the AD group than in the control and PF groups, and growth retardation, as previously described by our group [9]. As corresponds to the uremic state, the AD rats ate less than the ad libitum-fed rats with normal renal function (control group). It is of note that a similar degree of growth retardation was found in the AD and PF groups. In this model of uremia, a greater degree of growth impairment in the AD rats could have been achieved by a higher dose of adenine in their diets, as adenine is not well tolerated by rats and causes more severe bone diseases than in rats with subtotal nephrectomy [10].

The impairment of growth was associated with several modifications in the morphology and dynamics of the GP, as previously reported [11,12]. The height of the growth plate was significantly reduced in uremic and PF rats. It has been indistinctly described to be increased, reduced, or unchanged compared to the controls, a fact suggesting that it could be dependent to a great extent on the severity of the uremia [13]. AD rats presented smaller GPs, and this reduction was accompanied by a significantly reduced hypertrophic stratum (Table 3). Previous studies are coincident with these findings and also show that the GP height reduction is caused by alterations in the hypertrophic zone rather than by modifications in the proliferative activity, although this is also reduced in CKD [9,14].

The hypertrophy of GP chondrocytes is known to be the main contributor to bone lengthening [6]. The hypertrophic chondrocytes of uremic rats have been reported to achieve a lower final size than those of control animals [12]. This process is characterized by a widespread increase in cell volume and has been studied previously, especially with respect to its regulation [15]. However, information regarding how the cell volume increase occurs is limited. The increase in chondrocyte volume has been reported to result from three sequential phases, as mentioned above [7,8]. By applying our technique to the chemically fixed, in situ chondrocytes of uremic rats, we demonstrated here that the chondrocytes of uremic animals started with a reduced chondrocyte volume and cell density, as seen in cluster 1. The GP chondrocytes of normal growing rats started enlarging in the transition from cluster 3 to 4, when

the beginning of hypertrophy occurs. Conversely, by cluster 4, uremic chondrocytes seemed unable to start increasing and volume enlargement appeared to be delayed until the transition from cluster 4 to 5. Our results suggest that uremic chondrocytes, by cluster 4, had the same amount of proteins as normal chondrocytes (Figure 2B), but, somehow, they were unable to use this to start enlarging, causing hypertrophy to be delayed. Interestingly, the start of the hypertrophy was quite abrupt, as seen in the transition from cluster 4 to 5 and 5 to 6, when they underwent two phases of marked volume increase, causing the cell cytoplasm density to decay, compared to the control (Figure 2A,C). At a later stage of hypertrophy, the behavior of normal and uremic chondrocytes became parallel, both experiencing a phase characteristic of true hypertrophy. These results suggest that, in CKD, chondrocytes are not able to reach a normal terminal chondrocyte volume because they experience a delayed start to hypertrophy and seem unable to catch up, reaching the end of the maturation process with a reduced size. The chondrocytes of PF animals mostly show the same behavior as uremic chondrocytes, as suggested by the cell volume pattern across all the GP clusters. This could suggest that some of the GP alterations during CKD are not caused by uremia itself but are partially triggered by associated nutritional disorders. More marked differences between the chondrocytes of PF and AD rats had likely been found by inducing a more severe degree of renal failure [13]. However, in this model of uremia, this would have required a higher concentration of adenine in the diet, which is not well tolerated by rats and induces life-threatening inflammation [9].

Studies in mice lacking the GH receptor, Igf1, or both, provided conclusive evidence suggesting that only 17% of postnatal growth occurs independent of the GH/IGF-1 axis [16]. Growth impairment in CKD children has been explained mainly by a reduced IGF-I bioavailability, in part owing to a GH-resistance state caused by a postreceptorial defect in the JAK2-STAT5b signaling pathway downstream of the GH, as shown in the liver, skeletal muscle, and GP [3,17–20]. Our previous findings revealed low Igf1 expression levels in the prehypertrophic clusters and a significant increase in the transition from cluster 4 to cluster 5, coincident with the onset of chondrocyte hypertrophy in the transition from cluster 5 to cluster 6 and in the transition from cluster 6 to cluster 7, to reach the highest expression level at the later stage of the hypertrophy process [8]. In uremic chondrocytes, this pattern of expression was preserved, but there were significantly reduced levels of expression across the GP, more importantly in the hypertrophic clusters. These results are in line with those previously seen by Troib et al. [21], which showed reduced protein expression, suggesting that a decrease in the action of GH, mediated through the JAK2/STAT5 pathway in the bone during CKD, in turn, leads to a decreased local Igf1 level. GP Igf1 expression was reduced in the food-restricted, pair-fed, normal control rats compared with the ad libitum-fed, normal rats. This again indicated that the suppressed GP Igf1 expression in CKD is in part secondary to anorexia and reduced nutrient intake. Reduced levels of Igf1 mRNA and protein were associated with chronic anorexic states or prolonged fasting or food restriction [20–22]. Gevers et al. [23] demonstrated that fasting attenuates the Stat5 phosphorylation response to GH therapy in the liver and the GP cartilage of GH-deficient mice, which could partly explain the similar behavior of uremic and pair-fed animal chondrocytes.

Other factors besides GH and IGF-I contribute to the rate of bone growth through endochondral ossification, including the control of chondrocyte cell volume and proliferation rates. Type II and type X collagen are the most abundant proteins found in the GP. Type II is the predominant structural collagen present in all zones of the GP and is the main protein that is responsible for providing the tissue with a fibrillar framework to arrange chondrocytes as well as other extracellular matrix components (ECM). Type X collagen is an ECM component expressed exclusively by hypertrophic chondrocytes. No changes were observed in the pattern of expression of Col2a1 in uremic GPs, but we did note an early Col10a1 expression, by cluster 3. Interestingly, previous studies also revealed a generalized decrease in collagen expression and changes in its architecture, which were especially marked in the hypertrophic cartilage of 5/6 nephrectomized rats [24].

The distribution of the transporters and channels that regulate water and electrolyte traffic through the cell membrane was also analyzed, given its importance in the cell enlargement characteristic of

hypertrophy. Our aim was to evaluate if some proteins could be implicated in the pathogenesis of growth retardation in uremia. Water channels facilitate plasma membrane water permeability to the levels required for efficient coupling between NaCl transport and water transport in epithelia, which carries out isosmotic fluid transport [25]. Aqp1 is a widely expressed water channel whose physiological function has been most thoroughly characterized in the kidney, but it has also been found in red blood cells, the vascular endothelium, the gastrointestinal tract, sweat glands, and lungs [26]. Aqp1 expression was recently described in GP chondrocytes, mostly in the hypertrophic zone. No differences in the pattern of distribution of Aqp1 were reported in uremia or when treated with GH [12]. Our results confirmed these findings and showed that there are indeed differences in the levels of expression and that Aqp1 levels are significantly diminished in uremia in almost all the GP strata. Alternatively, we have found that uremia does not seem to alter the levels of expression of Nkcc1, an important membrane cotransporter in the GP chondrocyte enlargement [27]. There is no precise knowledge of the actions of either Nkcc1 or Aqp1 in the hypertrophy of chondrocytes, so further experiments would be required in order to unravel their mechanism of action in the cell volume enlargement.

High pharmacological doses of GH accelerate growth velocity [28] and improve the final height of patients with CKD [29]. The effects of GH therapy in the GP chondrocytes of uremic rats have not been extensively studied. The present study found that GH normalizes the growth rate, measured by OFA, and the height of both the GP and the hypertrophic stratum. Remarkably, the three-dimensional study of the uremic chondrocytes treated with GH revealed that, whereas chondrocytes, like untreated chondrocytes, start with a reduced chondrocyte volume, the pattern of chondrocyte volume increase is partly normalized at the prehypertrophic clusters compared to the control. GH appeared to be able to successfully enable uremic chondrocytes to enter hypertrophy, and in cluster 4, they present normal volumes. In the remaining phases, GH chondrocytes underwent the same volume enlargement as the untreated uremic chondrocytes, but, coming from a higher volume, they reached cluster 7 with a significantly increased volume. Even if GH was not able to normalize the pattern of hypertrophy in uremic chondrocytes from clusters 5 to 7, it was able to stimulate a chondrocyte cell volume enlargement from clusters 3 to 5. These data are consistent with the previous findings stating that GH acts locally at the GP to recruit resting chondrocytes into a proliferative state [30], as well as to stimulate local Igf1 production, which then stimulates the proliferation of chondrocytes [4,30,31]. In turn, our data suggest that GH treatment stimulates protein synthesis at the prehypertrophic stages of chondrocytes, causing an early increase in the volume of chondrocytes and allows them to complete the maturation process with normal parameters of volume and cytoplasm cell density. Moreover, GH increases Igf1 levels. Thus, Igf1 may play a role in the GH's compensatory mechanism of chondrocyte volume increase. Findings in experimental animals and in humans have shown that the absence or mutations of the STAT5b gene, the major mediator of the GH-regulated IGF-1 gene expression, are associated with diminished postnatal growth, GH resistance, and reduced IGF-I synthesis [32].

In this study, GH was able to raise Aqp1 levels at the prehypertrophic stages and allow chondrocytes to enter hypertrophy with significantly increased levels compared to uremic chondrocytes (cluster 4 to 5), a result that differs from previously published studies [10]. The level of Aqp1 expression in GH-treated chondrocytes, even if significantly lower than the control in most of the GP, has the same pattern of variation across the GP than untreated chondrocytes, indicating that, even though Aqp1 is still functioning, it could not be a part of the mechanism by which GH normalizes the chondrocyte volume in uremic conditions. However, it is interesting to note that, whereas uremic chondrocytes maintain normal Nkcc1 levels, GH causes an early Nkcc1 expression by cluster 4, even when compared to the control. In a recent study, we proposed that, in normal growing rats, Nkcc1 may have a major role in the onset of cell volume expansion [8]. Treatment with pharmacologic doses of GH has been shown to overcome the GH-resistance state and be effective in normalizing STAT5 phosphorylation [12,33]. Thus, it is tempting to propose that GH treatment could increase Nkcc1 levels

and so increase chondrocyte volume at an early stage. Further studies in this line of work would be of great importance.

## 4. Materials and Methods

### 4.1. Animals

The study was carried out in three-weeks-old female Sprague–Dawley rats (Charles River Laboratories, L'Arbrelese, France). The procedures involving animals and their care were conducted according to Spanish law on the use of experimental animals, which acknowledges the European Directive 86/609. The project proposal was approved by the Ethical Committee of the University of Oviedo, Spain (14 July 2015, PROAE 19/2015).

Rats were housed in light (12 light/dark cycles) and temperature-controlled rooms (21–23 °C). Diets were purchased from Ssniff Spezialdiäten GmbH (ref V1534. Soest, Germany). All animals had free access to tap water. Four groups of 10 animals were used: C (rats fed with normal diet), AD (rats fed with 0.5% adenine diet), ADGH (AD rats treated with GH), and PF (rats fed with normal diet, pair-fed with AD group). Recombinant human GH (rhGH) (Norditropin®), gently provided by Novo Nordisk Pharma, Madrid, Spain), was administered intraperitoneally to the ADGH group from day 14 to day 20 of the protocol, at a dosage of 3.3 mg/kg/day, given at 09.00 h and 17.00 h [34]. The other groups received the vehicle following an identical protocol of administration. Animals were sacrificed under a lethal dose of Dolethal® anesthesia after 21 days. Bromodeoxyuridine (BrdU) (100 mg/kg; Sigma Aldrich, Madrid, Spain) was injected intraperitoneally 1 and 8 h before sacrifice. Five days before sacrifice, 20 mg/kg of intraperitoneal calcein (Sigma, St Louis, MO, USA) was injected for the measurement of the OFA.

### 4.2. Blood Biochemistry

Serum concentrations of creatinine, urea nitrogen, calcium, and phosphate were measured by IDEXX laboratories (Barcelona, Spain).

### 4.3. Growth and Nutrition

Growth during the experimental protocol was assessed by measuring the total gained weight between days 0 and 21. Animals were weighed daily using a scale. Likewise, the length from the snout to the distal end of the tail was measured under anesthesia on day 21 of the protocol using a millimeter rule. Longitudinal growth rate (μm/day) was assessed by OFA in frontal sections from the right tibias. Sections were examined under an Olympus incident light fluorescent microscope (Olympus BX61, Olympus Optical, Barcelona, Spain) to detect calcein labels. Images were captured and measurements were made using Image J (National Institutes of Health, Bethesda, Maryland, MD, USA). The mean value measurement divided by 5 days was considered the osseous front advance per day, representing the daily longitudinal bone growth rate in each animal.

Food efficiency was calculated as the ratio between weight gained and food consumed (*g*/*g*) by each animal between days 0 and 24 of the protocol.

### 4.4. Sample Harvest and Processing

The rats' right tibias were fixated in glutaraldehyde 2%, ruthenium hexaammine trichloride 0.5%, and calcium chloride 5 mM in 0.025 M sodium cacodylate buffer (pH 7.4, osmolarity 300 mOsm). Then, they were in-block stained with a solution of 0.5% eosin in acetate buffered ethanol for 2 h at 4 °C, after which they were embedded in epoxy resin Durcupan (Sigma) and thinned by grinding to obtain 100-μm thick bone sections, as previously described by our group for the three-dimensional analysis of the GP [8].

The left tibias, fixed in 4% paraformaldehyde (PFA) and embedded in methyl methacrylate [35], were used for the histological and inmunofluorescence analyses.

### 4.5. Three-Dimensional Reconstruction of the Growth Plate

The bone thick sections were imaged with a confocal microscope Leica TCS SP8 (Leica Microsystems, Germany) equipped with a pulsed white light laser (470–670 nm), Acousto-Optical Beam Splitter (AOBS), and two internal hybrid single photon counting detectors, which was operated by Leica Application Suite X program (Leica Microsystems, Wetzlar, Germany). Z-stacks of 184.52 μm (x) × 184.52 μm (y) × 50 μm (z) with an X/Y resolution of 1024 × 1024 pixels were obtained by the sequential overlapping of 100 continuous images at an increment of Z-axis optical section of 0.5 μm. Two scans were performed along the XY plane, sequential in the Y axis, to obtain an image reconstruction of a complete column; see Supplementary Videos S1–6. The Leica LAS X 3D software was used for the 3D projection and the IMARIS v. 7.1.1. software (Bitplane, Switzerland) to obtain the cell structural parameters of the chondrocytes: cell volume, integrated optical density (IOD), and sphericity. The sequence of structural variation along a complete column was analyzed by measuring a total of 300 chondrocytes for each experimental group.

### 4.6. Immunohistochemistry and Immunofluorescence Analysis

The fluorescent immunodetection of Col2a1, Col10a1, Nkcc1, Aqp1, and Igf1was performed in 5 μm thick sections of methyl-methacrylate embedded left tibias. Antigen retrieval was performed with proteinase K 1 mg/mL 16 min at 37 °C for Igf1, hyaluronidase 2 mg/mL 30 min 37 °C for Nkcc1, and citrate buffer pH 8 30 min at 60 °C for Aqp1. A TNB blocking buffer made with 0.1 M TRIS-HCl, pH 7.5 0.15 M NaCl 0.5% TSA Blocking Reagent (FP1012, Perkin Elmer, Waltham, Massachusetts, MA, USA) was used. Antigen retrieval was performed with proteinase K 1 mg/mL 15 min at 37 °C for Col2a1, proteinase K 1 mg/mL 10 min at 37 °C for Col10a1, proteinase K 1 mg/mL 16 min at 37 °C for Igf-1, hyaluronidase 2 mg/mL 30 min 37 °C for Nkcc1, and citrate buffer pH 8 30 min at 60 °C for Aqp1. A TNB blocking buffer (75 min, RT) made from a TSA blocking reagent (Perkin Elmer, Waltham, MA, USA) was used. The primary antibodies used were as follows: anti-Col2a1 (#MA5-12789, Invitrogen, California, CA, USA) at 1:20 dilution, anti-Col10a1 (A6889, Abclonal, MA 01801, USA) at 1:20 dilution, anti-Igf1 (#PA5-27207, Invitrogen, California, CA, USA) at 1:200 dilution, anti-Aqp1 (ab15080, Abcam, Cambridge, UK) at 1:100 dilution, and anti-Nkcc1 (ab59791, Abcam, Cambridge, UK) at 1:100 dilution. Goat anti-mouse Alexa 594 (A-21155, Invitrogen, California, CA, USA), goat anti-rabbit Alexa 594 (#A-11012, Invitrogen, California, CA, USA), and goat anti-rabbit Alexa 488 (A11034, Invitrogen, California, CA, USA) were used as secondary antibodies, and sections were finally mounted with Vectashield Mounting Medium with DAPI (Vector Laboratories, Burlingame, California, CA, USA). Sections were examined and pictures taken with a confocal microscope, the Leica TCS SP8 (Leica Microsystems, Wetzlar, Germany), with the 20× magnification objective. Image J (National Institutes of Health, Bethesda, Maryland, MD, USA) was used to measure the fluorescence intensity on the whole chondrocyte columns.

Sections were examined and pictures taken with a confocal microscope, Leica TCS SP8 (Leica Microsystems, Germany), with the 20× magnification objective. Image J (National Institutes of Health, Bethesda, Maryland, MD, USA) was used to measure the fluorescence intensity on the whole chondrocyte columns and the position of chondrocytes in the GP.

### 4.7. Statistical Analysis

All statistical analyses utilized a 95% confidence level and were conducted using GraphPad Prism v. 7 (La Jolla, California, CA, USA).

To analyze the structural variation along the vertical column, chondrocytes were classified into the previously described differentiation clusters [8], based on their distance to the osseous invasion front. Means and standard deviations (SD) of the different structural parameters were determined for each cluster. Comparison among experimental groups was performed using a one-way ANOVA, followed by Tukey's multiple comparison test.

## 5. Conclusions

By applying for the first time a three-dimensional approach to study the abnormalities in the GP maturation of uremic chondrocytes, we have seen that uremic chondrocytes experience a delayed entrance into hypertrophy, preventing them from reaching a normal size by the end of the differentiation process. Growth hormone treatment appears to be able to compensate for this by triggering an early chondrocyte enlargement that may be somehow mediated by Nkcc1 action.

**Supplementary Materials:** Supplementary materials can be found at http://www.mdpi.com/1422-0067/21/12/4519/s1. Video S1. Representative video of a three-dimensional-reconstruction of Z-series confocal images of a thick bone section of an AD rat proliferative zone imaged with the confocal microscope. Travel through xz-projections of a confocal z-stack; Video S2. Representative video of a three-dimensional-reconstruction of Z-series confocal images of a thick bone section of an AD rat hypertrophic zone imaged with the confocal microscope. Travel through xz-projections of a confocal z-stack; Video S3. Representative video of a three-dimensional-reconstruction of Z-series confocal images of a thick bone section of an ADGH rat proliferative zone imaged with the confocal microscope. Travel through xz-projections of a confocal z-stack; Video S4. Representative video of a three-dimensional-reconstruction of Z-series confocal images of a thick bone section of an ADGH rat hypertrophic zone imaged with the confocal microscope. Travel through xz-projections of a confocal z-stack; Video S5. Representative video of a three-dimensional-reconstruction of Z-series confocal images of a thick bone section of an PF rat proliferative zone imaged with the confocal microscope. Travel through xz-projections of a confocal z-stack; Video S6. Representative video of a three-dimensional-reconstruction of Z-series confocal images of a thick bone section of an PF rat hypertrophic zone imaged with the confocal microscope. Travel through xz-projections of a confocal z-stack.

**Author Contributions:** Formal analysis, Á.F.-I., R.F., H.G.-P. and M.G.-B.; Funding acquisition, F.S.; Investigation, Á.F.-I., F.S. and J.M.L.; Methodology, Á.F.-I., R.F., L.A.-D., M.G.-B. and J.M.L.; Project administration, F.S.; Supervision, F.S. and J.M.L.; Writing–original draft, Á.F.-I.; Writing–review and editing, R.F., H.G.-P., L.A.-D., M.G.-B., F.S. and J.M.L. All authors have read and agreed to the published version of the manuscript.

**Funding:** This study was supported by Fundacion Nutrición y Crecimiento, by grants PI18/01757 (Plan Estatal I + D + I 2017–2020) from the Instituto de Salud Carlos III (Madrid, Spain) and GRUPIN14–20 from Fondos Europeos de Desarrollo Regional (FEDER), by Marie Skłodowska-Curie European Commission, by Fundación de la Universidad de Oviedo (FUO) and by Fundación para la Investigación Biomédica en Asturias (FINBA).

**Conflicts of Interest:** The authors declare no conflict of interest.

## Abbreviations

| | |
|---|---|
| BUN | Blood urea nitrogen |
| CKD | Chronic kidney disease |
| DAPI | 4′,6-diamidino-2-phenylindole |
| ECM | Extracellular matrix |
| GP | Growth plate |
| GH | Growth hormone |
| Igf1 | Insulin growth factor 1 |
| IOD | Integrated optical density |
| BrdU | Bromodeoxyuridine |
| Aqp1 | Aquaporin 1 |
| Nkcc1 | Sodium potassium calcium cotransporter 1 |
| Col2a1 | Collagen 2 alpha chain 1 |
| Col10a1 | Collagen 10 alpha chain 1 |

## References

1. Franke, D.; Winkel, S.; Gellermann, J.; Querfeld, U.; Pape, L.; Ehrich, J.H.; Haffner, D.; Pavicic, L.; Zivicnjak, M. Growth and maturation improvement in children on renal replacement therapy over the past 20 years. *Pediatr. Nephrol.* **2013**, *28*, 2043–2051. [CrossRef]
2. Harambat, J.; Cochat, P. Growth after renal transplantation. *Pediatr. Nephrol.* **2009**, *24*, 1297–1306. [CrossRef]
3. Fernández-Iglesias, Á.; López, J.M.; Santos, F. Growth plate alterations in chronic kidney disease. *Pediatr. Nephrol.* **2018**, *35*, 367–374. [CrossRef]

4. Hunziker, E.B. Mechanism of longitudinal bone growth and its regulation by growth plate chondrocytes. *Microsc. Res. Tech.* **1994**, *28*, 505–519. [CrossRef]
5. Aghajanian, P.; Mohan, S. The art of building bone: Emerging role of chondrocyte-to-osteoblast transdifferentiation in endochondral ossification. *Bone Res.* **2018**, *6*, 19. [CrossRef]
6. Breur, G.J.; VanEnkevort, B.A.; Farnum, C.E.; Wilsman, N.J. Linear relationship between the volume of hypertrophic chondrocytes and the rate of longitudinal bone growth in growth plates. *J. Orthop. Res.* **1991**, *9*, 348–359. [CrossRef]
7. Cooper, K.L.; Oh, S.; Sung, Y.; Dasari, R.R.; Kirschner, M.W.; Tabin, C.J. Multiple phases of chondrocyte enlargement underlie differences in skeletal proportions. *Nature* **2013**, *495*, 375–378. [CrossRef]
8. Fernández-Iglesias, Á.; Fuente, R.; Gil-Peña, H.; Alonso-Duran, L. A simple method based on confocal microscopy and thick sections recognizes seven subphases in growth plate chondrocytes. *Sci. Rep.* **2020**, *10*, 6935. [CrossRef] [PubMed]
9. Claramunt, D.; Gil-Peña, H.; Fuente, R.; García-López, E.; Loredo, V.; Hernández-Frías, O.; Ordoñez, F.A.; Rodríguez-Suárez, J.; Santos, F. Chronic kidney disease induced by adenine: A suitable model of growth retardation in uremia. *Am. J. Physiol. Ren. Physiol.* **2015**, *309*, 57–62. [CrossRef] [PubMed]
10. Claramunt, D.; Gil-Peña, H.; Fuente, R.; Hernández-Frías, O.; Santos, F. Animal models of pediatric chronic kidney disease. Is adenine intake an appropriate model? *Nefrologia* **2015**, *35*, 517–522. [CrossRef] [PubMed]
11. Santos, F.; Carbajo-Pérez, E.; Rodríguez, J.; Fernández-Fuente, M.; Molinos, I.; Amil, B.; García, E. Alterations of the growth plate in chronic renal failure. *Pediatr. Nephrol.* **2005**, *20*, 330–334. [CrossRef] [PubMed]
12. Claramunt, D.; Gil-Peña, H.; Fuente, R.; García-López, E.; Frías, O.H.; Ordoñez, F.A.; Rodríguez-Suárez, J.; Santos, F. Effects of growth hormone treatment on growth plate, bone and mineral metabolism of young rats with uremia induced by adenine. *Pediatr. Res.* **2017**, *82*, 888. [CrossRef] [PubMed]
13. Fernández-Fuente, M.; Santos, F.; Carbajo-Pérez, E.; Rodríguez, J.; Weruaga, A.; Amil, B.; Molinos, I.; García, E. Growth plate height of uremic rats is influenced by severity and duration of renal failure. *Pediatr. Nephrol.* **2004**, *19*, 187–192. [CrossRef] [PubMed]
14. Cobo, A.; López, J.M.; Carbajo, E.; Santos, F.; Alvarez, J.; Fernández, M.; Weruaga, A. Growth plate cartilage formation and resorption are differentially depressed in growth retarded uremic rats. *J. Am. Soc. Nephrol.* **1999**, *10*, 971–979.
15. Kronenberg, H. Developmental regulation of the growth plate. *Nature* **2003**, *423*, 332–336. [CrossRef]
16. Lupu, F.; Terwilliger, J.D.; Lee, K.; Segre, G.V.; Efstratiadis, A. Roles of Growth Hormone and Insulin-like Growth Factor 1 in Mouse Postnatal Growth. *Dev. Biol.* **2001**, *162*, 141–162. [CrossRef]
17. Sun, D.F.; Zheng, Z.; Tummala, P.; Oh, J.U.N.; Schaefer, F.; Rabkin, R. Chronic Uremia Attenuates Growth Hormone–Induced Signal Transduction in Skeletal Muscle. *J. Am. Soc. Nephrol.* **2004**, 2630–2636. [CrossRef]
18. Schaefer, F.; Chen, Y.; Tsao, T.; Nouri, P.; Rabkin, R. Impaired JAK-STAT signal transduction contributes to growth hormone resistance in chronic uremia. *J. Clin. Investig.* **2001**, *108*, 467–475. [CrossRef]
19. Tönshoff, B.; Kiepe, D.; Ciarmatori, S. Growth hormone/insulin-like growth factor system in children with chronic renal failure. *Pediatr. Nephrol.* **2005**, *20*, 279–289. [CrossRef]
20. Troib, A.; Guterman, M.; Rabkin, R.; Landau, D.; Segev, Y. Endurance exercise and growth hormone improve bone formation in young and growth-retarded chronic kidney disease rats. *Nephrol Dial. Transpl.* **2015**, *31*, 1–10. [CrossRef]
21. Troib, A.; Landau, D.; Kachko, L.; Rabkin, R.; Segev, Y. Epiphyseal growth plate growth hormone receptor signaling is decreased in chronic kidney disease-related growth retardation. *Kidney Int.* **2013**, *84*, 940–949. [CrossRef] [PubMed]
22. Wu, S.; Flint, J.K.; Rezvani, G.; De Luca, F. Nuclear factor-κB p65 facilitates longitudinal bone growth by inducing growth plate chondrocyte proliferation and differentiation and by preventing apoptosis. *J. Biol. Chem.* **2007**, *282*, 33698–33706. [CrossRef]
23. Gevers, E.F.; Hannah, M.J.; Waters, M.J.; Robinson, I.C.A.F. Regulation of rapid signal transducer and activator of transcription-5 phosphorylation in the resting cells of the growth plate and in the liver by growth hormone and feeding. *Endocrinology* **2009**, *150*, 3627–3636. [CrossRef]
24. Alvarez, J.; Balbín, M.; Fernández, M.; López, J.M. Collagen metabolism is markedly altered in the hypertrophic cartilage of growth plates from rats with growth impairment secondary to chronic renal failure. *J. Bone Miner. Res.* **2001**, *16*, 511–524. [CrossRef] [PubMed]

25. Nielsen, S.; Agre, P. The aquaporin family of water channels in kidney. *Kidney Int.* **1995**, *48*, 1057–1068. [CrossRef] [PubMed]
26. Bondy, C.; Chin, E.; Smitht, B.L.; Prestont, G.M.; Agrett, P. Developmental gene expression and tissue distribution of the CHIP28 water-channel protein. *Dev. Biol.* **1993**, *90*, 4500–4504. [CrossRef] [PubMed]
27. Bush, P.G.; Pritchard, M.; Loqman, M.Y.; Damron, T.A.; Hall, A.C. A key role for membrane transporter NKCC1 in mediating chondrocyte volume increase in the mammalian growth plate. *J. Bone Miner. Res.* **2010**, *25*, 1594–1603. [CrossRef] [PubMed]
28. Mehls, O.; Irzynjec, T.; Ritz, E.; Eden, S.; Kovàcs, G.; Klaus, G.; Floege, J.; Mall, G. Effects of rhGH and rhIGF-1 on renal growth and morphology. *Kidney Int.* **1993**, *44*, 1251–1258. [CrossRef] [PubMed]
29. Haffner, D.; Schaefer, F.; Nissel, R.; Wühl, E.; Tönshoff, B.; Mehls, O. Effect of Growth Hormone Treatment on the Adult Height of Children with Chronic Renal Failure. *N. Engl. J. Med.* **2000**, *343*, 923–930. [CrossRef]
30. Ohlsson, C.; Nilsson, A.; Isaksson, O.; Lindahl, A. Growth hormone induces multiplication of the slowly cycling germinal cells of the rat tibial growth plate. *Proc. Natl. Acad. Sci. USA* **1992**, *89*, 9826–9830. [CrossRef]
31. Isaksson, O.G.; Lindahl, A.; Nilsson, A.; Isgaard, J. Mechanism of the stimulatory effect of growth hormone on longitudinal bone growth. *Endocr. Rev.* **1987**, *8*, 426–438. [CrossRef] [PubMed]
32. Wu, S.; Morrison, A.; Sun, H.; De Luca, F. Nuclear factor-κB (NF-κB) p65 interacts with Stat5b in growth plate chondrocytes and mediates the effects of growth hormone on chondrogenesis and on the expression of insulin-like growth factor-1 and bone morphogenetic protein-2. *J. Biol. Chem.* **2011**, *286*, 24726–24734. [CrossRef] [PubMed]
33. Wiezel, D.; Assadi, M.H.; Landau, D.; Troib, A.; Kachko, L.; Rabkin, R.; Segev, Y. Impaired renal growth hormone JAK/STAT5 signaling in chronic kidney disease. *Nephrol. Dial. Transplant.* **2014**, *29*, 791–799. [CrossRef] [PubMed]
34. Kovács, G.T.; Oh, J.; Kovács, J.; Tönshoff, B.; Hunziker, E.B.; Zapf, J.; Mehls, O. Growth promoting effects of growth hormone and IGF-I are additive in experimental uremia. *Kidney Int.* **1996**, *49*, 1413–1421. [CrossRef]
35. Fuente, R.; Gil-Peña, H.; Claramunt-Taberner, D.; Hernández-Frías, O.; Fernández-Iglesias, Á.; Hermida-Prado, F.; Anes-González, G.; Rubio-Aliaga, I.; Lopez, J.M.; Santos, F. Marked alterations in the structure, dynamics and maturation of growth plate likely explain growth retardation and bone deformities of young Hyp mice. *Bone* **2018**, *116*, 187–195. [CrossRef] [PubMed]


# IV. Formation of the Epiphyseal Bone Plate

The formation of the epiphyseal bone plate, the flat bony structure that provides strength and firmness to the growth plate cartilage, was studied in the present study by using light, confocal and scanning electron microscopy. Results obtained evidenced that this bone tissue is generated by the replacement of the lower portion of the epiphyseal cartilage. However, this process differs considerably from the usual bone tissue formation through endochondral ossification. Osteoblasts deposit bone matrix on remnants of mineralized cartilage matrix that serve as a scaffold, but also on non-mineralized cartilage surfaces and as well as within the perivascular space. These processes occur simultaneously at sites located close to each other, so that, a core of the sheet of bone is established very quickly. Subsequently, thickening and reshaping occurs by appositional growth to generate a dense parallel-fibered bone structurally intermediate between woven and lamellar bone. All these processes occur in close relationship with a cartilage but most of the bone tissue is generated in a manner that may be considered as intramembranous-like. Overall, the findings here reported provide for the first time an accurate description of the tissues and events involved in the formation of the epiphyseal bone plate and gives insight into the complex cellular events underlying bone formation at different sites on the skeleton

**Article 4. Ángela Fernández-Iglesias,** Rocío Fuente, Helena Gil-Peña, Laura Alonso-Duran, Fernando Santos & José M. López. “The formation of the epiphyseal bone plate occurs via combined endochondral and intramembranous-like ossification”

Int J Mol Sci. 2021. 22(2):900, doi: 10.3390/ijms22020900

**Journal metrics (2019)**

2-year impact Factor 4.556

5-year impact Factor: 4.653

International Journal of
*Molecular Sciences*

MDPI

*Article*

# The Formation of the Epiphyseal Bone Plate Occurs via Combined Endochondral and Intramembranous-Like Ossification

**Ángela Fernández-Iglesias [1,2,†], Rocío Fuente [1,†], Helena Gil-Peña [1,2,3], Laura Alonso-Durán [1,2], Fernando Santos [1,2,3] and José Manuel López [1,4,*]**

[1] Division of Pediatrics, Department of Medicine, Faculty of Medicine, University of Oviedo, 33006 Oviedo, Asturias, Spain; angelafiglesias@gmail.com (Á.F.-I.); rociofuenteperez@gmail.com (R.F.); hgilpena@gmail.com (H.G.-P.); laurita.alonso86@gmail.com (L.A.-D.); fsantos@uniovi.es (F.S.)
[2] Instituto de Investigación Sanitaria del Principado de Asturias (ISPA), 33011 Oviedo, Asturias, Spain
[3] Department of Pediatrics, Hospital Universitario Central de Asturias (HUCA), 33011 Oviedo, Asturias, Spain
[4] Department of Morphology and Cellular Biology, Faculty of Medicine, University of Oviedo, 33006 Oviedo, Asturias, Spain
* Correspondence: jmlopez@uniovi.es
† Á.F.-I. and R.F. contributed equally to this work and should be considered as co-first authors.

**Abstract:** The formation of the epiphyseal bone plate, the flat bony structure that provides strength and firmness to the growth plate cartilage, was studied in the present study by using light, confocal, and scanning electron microscopy. Results obtained evidenced that this bone tissue is generated by the replacement of the lower portion of the epiphyseal cartilage. However, this process differs considerably from the usual bone tissue formation through endochondral ossification. Osteoblasts deposit bone matrix on remnants of mineralized cartilage matrix that serve as a scaffold, but also on non-mineralized cartilage surfaces and as well as within the perivascular space. These processes occur simultaneously at sites located close to each other, so that, a core of the sheet of bone is established very quickly. Subsequently, thickening and reshaping occurs by appositional growth to generate a dense parallel-fibered bone structurally intermediate between woven and lamellar bone. All these processes occur in close relationship with a cartilage but most of the bone tissue is generated in a manner that may be considered as intramembranous-like. Overall, the findings here reported provide for the first time an accurate description of the tissues and events involved in the formation of the epiphyseal bone plate and gives insight into the complex cellular events underlying bone formation at different sites on the skeleton.

**Keywords:** bone plate; endochondral ossification; intramembranous ossification; chondrocyte; osteoblast



**Citation:** Fernández-Iglesias, Á.; Fuente, R.; Gil-Peña, H.; Alonso-Durán, L.; Santos, F.; López, J.M. The Formation of the Epiphyseal Bone Plate Occurs via Combined Endochondral and Intramembranous-Like Ossification. *Int. J. Mol. Sci.* **2021**, *22*, 900. https://doi.org/10.3390/ijms22020900

Received: 14 December 2020
Accepted: 15 January 2021
Published: 18 January 2021



## 1. Introduction

The epiphyseal bone plate is a flat bony structure located between the epiphysis and the metaphysis of the long bones [1]. It holds the growth plate cartilage, providing the weakest area of the growing bone with strength and stability. In addition to structural support, the epiphyseal bone plate also has a nutritional role by allowing the passage of blood vessels from the epiphysis to form a capillary network that supplies the growth cartilage with oxygen, nutrients, and chemical signaling.

The epiphyseal bone plate is formed by ossification of the lower part of the epiphyseal cartilage after the development of the secondary ossification center. At the beginning, the secondary ossification center expands in all directions to form spongy bone trabeculae with a radial orientation. However, the mode of ossification substantially changes when the front nears the region facing the resting cartilage of the growth plate. At this location, cartilage is directly transformed into compact bone tissue to generate a flat plate with several layers of densely packed bony lamellae oriented transverse to the long axis of

the bone [2]. The formation of the epiphyseal bone plate has some peculiar characteristics that make it different from a standard endochondral ossification process. Firstly, it is considered as a specialized extension of the cortical bone [3], which is usually formed through direct-intramembranous ossification. Secondly, it is oriented perpendicular to the long axis of the bone, an unusual orientation since most bone structures are oriented such that they are stronger in the direction in which they support load [4]. Thirdly, it develops very quickly, so that transformation of cartilage into bone occurs faster than anywhere else in the bone [5]. Finally, it is formed in the region immediately adjacent to the resting cartilage of the growth plate and this close spatial proximity suggests that the latter could exert a great deal of influence on its development [6].

Despite the above considerations and the fact that the epiphyseal bone plate could be considered a structural component of the growth plate that influences its function, it has been largely unexplored and is one of the least understood parts of the long bones. Even little is known about how it is affected by diseases associated with growth failure and bone abnormalities. On this basis, it was the aim of the present work to obtain an overall overview of how the epiphyseal bone plate is formed in physiological conditions. To this end, we have performed a time course analysis of the epiphyseal development utilizing tibias of rats at different stages of growth. We have used light, confocal, and scanning electron microscopy to analyze the cellular aspects of the tissue development. The study provides a framework for future research on pathological conditions.

## 2. Results

The formation of the epiphyseal bone plate is a continuous process but in order to make the description easier to follow, we divided it into four stages characterized by changes in the amount of cartilage and bone formation.

Stage 1: The beginning of epiphyseal bone formation. The proximal epiphysis of the rat tibia was entirely cartilaginous at 3 days of age (Figure 1A). Despite its relatively homogeneous appearance, three zones without clearly defined borders could be recognized in the cartilage: (1) An outer cap of flatter chondrocytes located at the epiphyseal end; (2) an extensive intermediate zone with oval chondrocytes oriented randomly; and (3) a deep zone with chondrocytes aligned in columns. Zones 1 and 3 corresponded to the prospective articular and metaphyseal growth plate cartilages, respectively, whereas zone 2 corresponded to the epiphyseal cartilage that specifically guides bone tissue expansion to establish the secondary ossification center. The first cartilage canals in the epiphysis were observed at the age of 5 days, and by the day 8, chondrocytes in the middle of the epiphysis became hypertrophic, canals spread into the central region and the secondary ossification center was established (Figure 1B). The secondary ossification center was firstly spherical and smoothly bordered by hypertrophic cartilage (Figure 1C), but by 14 days of age, it became increasingly irregular and presented a heterogeneous inner surface with both smooth and irregular areas (Figure 1D).

Smooth and irregular areas in the secondary ossification center were not randomly distributed; smooth inner surfaces were found at the upper and lateral portions of the epiphysis, within a semicircular region below the articular cartilage, whereas a rugged inner surface was observed in the lower portion, that overlying the metaphyseal growth plate cartilage (Figure 1E). The upper-lateral region had the spatial arrangement of an inverted U-shape that underlay the surface of the bone head. It was relatively wide and uniform in thickness, although interruptions due to the primary channels derived from the perichondrium could be found (Figure 1D). The size and shape of chondrocytes varied along the radial direction and they were replaced by trabecular bole at the border with the bone marrow, so that the process of ossification in this cartilage was typically endochondral.

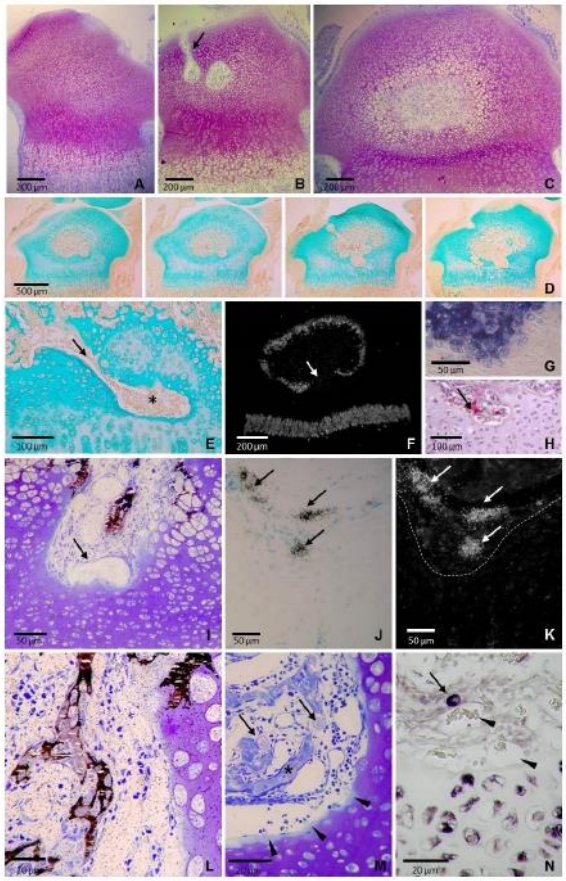

**Figure 1.** Sections of the tibial epiphysis at the beginning of epiphyseal bone formation. (**A**) Semithin section stained with toluidine of a 3-day-old tibia showing a completely cartilaginous epiphysis. (**B**) Semithin section stained with toluidine of an 8-day-old tibia showing a cartilage canal (arrow) and the early secondary ossification center. (**C**) Semithin section stained with toluidine of an 11-day-old tibia showing a central rounded marrow cavity smoothly bordered by hypertrophic cartilage. (**D**) Series of consecutive paraffin sections of a 14-day-old tibia stained with Alcian blue. The border of the epiphyseal marrow cavity is smooth at the upper and lateral portions and rugged in the lower portion. (**E**) A tongue or finger-like extension of marrow tissue (arrow) deeply penetrating into the epiphyseal cartilage of a 14-day-old tibia (asterisk). (**F**) Dark field microscopy of mRNA expression pattern of type X collagen of a 14-day-old tibia. Expression is found in chondrocytes of both the metaphyseal growth plate and the upper portion of the epiphyseal cartilage but no expression is found in the central region of the lower epiphyseal cartilage (arrow). (**G**) Alkaline phosphatase activity and (**H**) TRAP-positive cells (arrow) in a tongue of epiphyseal marrow tissue penetrating into the epiphyseal cartilage of a 14-day-old tibia. (**I**) A mineralized area adjacent to capillaries in a tongue of epiphyseal marrow tissue of a 14-day-old tibia stained with von Kossa and counterstained with toluidine blue (arrow). (**J**) Bright field and (**K**) dark field images of a section of a 14-day-old tibia hybridized with a $^{35}$S-labeled riboprobe for osteocalcin. Expressión is observed in some scattered cells (arrows) separated from the border of the cartilage (dotted white line). (**L**) Section of a of a 14-day-old tibia showing von Kossa positive cells located at the mid-depth zone of a finger-like extension of the marrow tissue. Cells are located in the intervascular region, distant from the border with the cartilage. (**M**) Semithin section of a 14-day-old tibia stained with toluidine showing the intimate juxtaposition of the capillaries to the cartilaginous matrix. A thin band of less stained cartilaginous matrix is observed in the border of the cartilage (arrowheads) and two rounded-shaped chondrocyte-like cells with a thin rim of metachromatic substance could be seen (arrows) close to the mineralized area that is stained in blue (asterisk). (**N**) Section of a 14-day-old tibia hybridized with a digoxygenin-labeled riboprobe for type II collagen showing a positive cell being well separated from the border of the cartilage (arrow), close to vascular vessels (arrowheads).

The lower region of the epiphyseal cartilage presented an irregular outline, with some tongues or finger-like extensions of marrow tissue that deeply penetrate into the epiphyseal cartilage to reach the border of the growth plate cartilage (Figure 1E). Local thinned areas of the cartilage resulting from marrow tissue extension appeared as holes or depressions that could be delineated by the very low or absent expression of type X collagen (Figure 1F) and high alkaline phosphatase (AP) staining (Figure 1G). Marrow tissue entering the cartilage contained blood vessels, numerous intervascular mesenchymal-type cells and some large multinucleated TRAP positive cells (Figure 1H). The cartilage-marrow interface did not have a uniform appearance since the stage of maturation of terminal chondrocytes varied in different areas depending on the thickness of the cartilage below. Unthinned areas presented terminal chondrocytes showing a hypertrophic-like shape whereas terminal chondrocytes at thinned areas were smaller, flatter, and stained slightly darker (Figure 1I). There was not a proper ossification front with invading capillary sprouts entering in open empty chondrocytic lacunae since most terminal lacunae remained closed with chondrocytes showing no signs of degeneration (Figure 1I). Mineral deposition occurred in the interterritorial matrix. Early scattered focal mineral deposits coalesced to form larger mineral aggregates in the matrix of terminal chondrocytes. Compact mineral aggregates were patchy and distributed towards the cartilage border, without a uniform mineralization front (Figure 1I). No mineralization of the cartilage matrix was detectable in areas of the cartilage thinned by the extension of the marrow tissue, where terminal chondrocytes were smaller, flatter and had not alkaline phosphatase activity (Figure 1I).Von Kossa positive staining was observed in small clusters of cells located in the intervascular spaces at the mid-depth zones of the finger-like extensions of marrow tissue (Figure 1I). These cells stained with alkaline phosphatase and were positive for osteocalcin expression (Figure 1J,K). They were small in size and appeared surrounded by a narrow mineralized matrix (Figure 1I,L). Formation of mineralized matrix was observed among cells both in the periphery and the center of clusters. These mineralized areas were located adjacent to capillaries and had no apparent connection with the cartilage surface; no remnants of mineralized cartilage matrix that could serve as a scaffold for bone deposition were found (Figure 1I,L). Capillaries occupied the deepest part of the tissue extensions and were mainly sinusoidal in shape with moderately dilated lumina. They were close to the cartilage, with intimate juxtaposition of the endothelial cells to the cartilaginous matrix (Figure 1I,L). The zones of contact presented a fairly smooth outline and were outlined by a thin band of less toluidine blue stained cartilaginous matrix, a fact indicating proteoglycan lost (Figure 1M). Analysis of 1 μm semithin sections revealed the presence of large, rounded-shaped cells with a centrally placed spherical nucleus and pale-staining cytoplasm surrounded by a thin rim of metachromatic substance (Figure 1M). These cells were interspersed among smaller cells in the intervascular space, close to mineralizing areas, and expressed type II collagen (Figure 1N). and could be considered as chondrocytes freed form the cartilage matrix that retained part of the proteoglycans of the pericellular matrix.

Stage 2: The earliest recognizable bone plate. The epiphyseal cartilage was progressively replaced by bone between postnatal day 11 and 14 so that by day 19 the epiphysis exhibited greatly reduced cartilage and a well-formed marrow space with a large amount of newly formed bone tissue (Figure 2A).

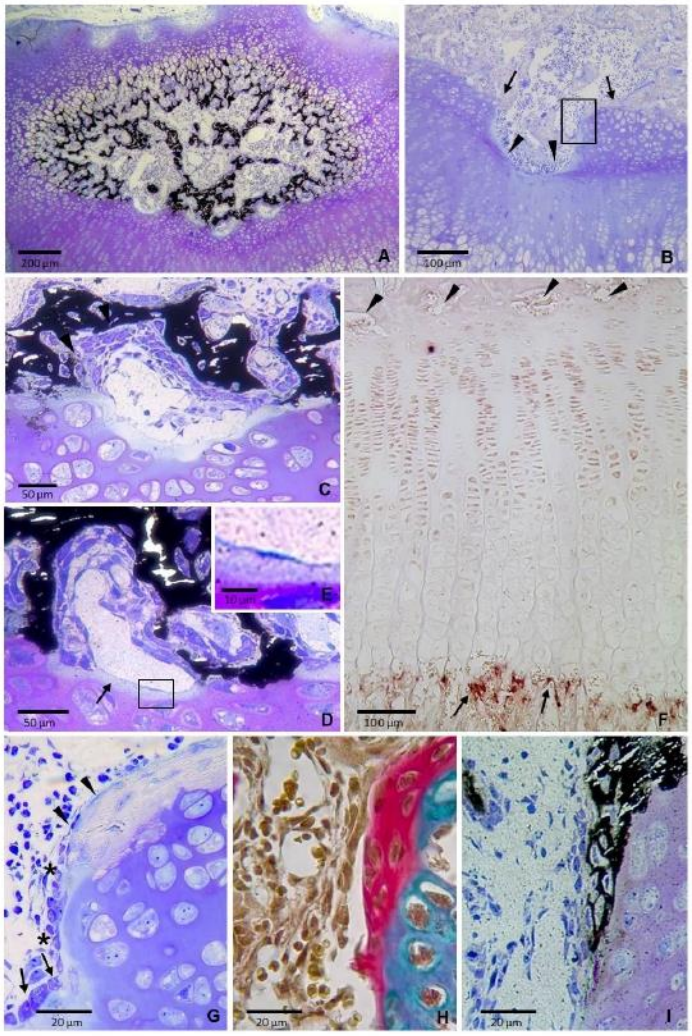


**Figure 2.** Sections of the tibial epiphysis of 19 day-old rats. (**A**) Section stained with von Kossa and counterstained with toluidine blue showing that the epiphyseal bony tissue displays a "bicycle wheel" pattern at the upper portion and a bridge-like disposition at the lower portion. (**B**) Semithin section stained with toluidine blue showing rounded hollows (arrowheads) and ridges (arrows) in the epiphyseal cartilage. Boxed area is shown at a higher magnification in figure G. (**C**) Section stained with von Kossa and counterstained with toluidine blue showing that the cell composition differs between the upper and lower surfaces of the mineralized plate-like elements. (**D**) Section stained with von Kossa and counterstained with toluidine blue showing a moderately dilated capillary interposed between the cartilage and the bone forming cells. It is close to the surface of the cartilage, where a thin band of less stained cartilaginous matrix is present (arrows). Boxed area is shown at a higher magnification in figure E. (**E**) Magnification of the boxed area in D showing the close contact between the capillary and the cartilage. (**F**) Immunohistochemistry for CD31 showing positive capillaries at the metaphyseal chondro–osseous junction (arrows) whereas virtually no signal is visible in capillaries located at the epiphyseal end (arrowheads). (**G**) Magnification of the boxed area in B showing that the cartilage is directly covered by a layer of mineralized tissue that is weakly stained. Note that chondrocytes are not hypertrophic and have a well-preserved structure. Cells at the surface are flattened (arrowheads) and change to cuboidal at mid-depth of the hollow (arrow) with a transition zone in between (asterisks). (**H**) Section of a region equivalent to that shown in figure G stained with Alcian blue/acid fuchsin. The two tissues are stained differentially, with a sharp boundary visible between them. (**I**) Equivalent region to those shown in figures G and H stained von Kossa and counterstained with toluidine blue showing mineralized matrix being directly deposited on the cartilage.

Marked differences in bone microarchitecture were observed between the upper and the lower borders of the epiphyseal bone marrow cavity at this age. Bone tissue at the upper portion consisted of narrow trabeculae that were continuous with the radially oriented calcified longitudinal septa of the hypertrophic cartilage. The overall radial organization of the trabeculae at this region gave the bone marrow a "bicycle wheel" pattern (Figure 2A). On the other hand, bone at the lower portion had a bridge-like structure with a series of "piers", which corresponded to the areas of direct contact between the cartilage and the bone, spaced from each other by plate-like bony segments of moderate thickness separated from the underlying epiphyseal cartilage by a tissue composed of capillaries and intervascular cells (Figure 2A). The upper and lower surfaces of the mineralized plate-like elements differed in the shape and arrangement of the adjoining cells; the lower surface was covered by several layers of spindle-shaped cells arranged in diffuse sheets whereas the upper surface was lined by a layer of cells with a more regular shape (Figure 2C,D). Some of the cells closest to the lower bone surface became partially or completely embedded in the mineralized matrix whereas the farthest ones were close to capillaries (Figure 2C,D). Cells at the upper side were more cuboidal and displayed a pseudoepithelial arrangement (Figure 2C,D), characteristic features of active osteoblasts lining a bone forming surface. Capillaries were moderately dilated and lied in close contact with the cartilage surface (Figure 2D,E).There was little to no positive immunohistochemical staining for CD31 in epiphyseal capillaries unlike those at the border with the hypertrophic chondrocytes in the metaphysis that were positively immunostained (Figure 2F).

The "piers" of the bridge corresponded to areas of contact between cartilage and the mineralized tissue, where the two tissues laid side-by-side without any interposing transition region (Figure 2G,H). The two tissues were stained differentially with Toluidine blue in semithin sections (Figure 2G) and also with Alcian blue/alizarin red in paraffin sections (Figure 2H) and a sharp boundary was visible between them. Likewise, von Kossa staining also revealed a clear border between mineralized and non-mineralized tissues (Figure 2I). The cartilage appeared to be covered by several layers of flat spindle-shaped cells embedded in mineralized matrix. These cells were arranged in rows with their long axis oriented parallel to each other and the surface of the tissue and the shape of the cells on the surface varied from cuboidal to flat (Figure 2G). Morphological features were compatible with laminar bone deposited directly on the cartilage, with cuboidal osteoblasts in active bone forming areas and quiescent bone lining cells in not active zones. Chondrocytes directly covered by the calcified tissue had not the appearance of hypertrophic chondrocytes, they were not substantially enlarged and had a well-preserved structure, with moderate abundant cytoplasm and clearly visible nuclei containing nucleoli (Figure 2G).

Stage 3: Thickening by appositional growth. An almost continuous bony structure is found along the border of the growth plate cartilage by the age of 24-days. Analysis of calcein labeling under the confocal microscopy evidenced that fluorescence was located mainly around the blood vessels, indicating that bone tissue formation was associated with the pattern of vascularization (Figure 3A). Osteoblasts and osteoclasts were located on the opposite sides of the bone plate in a manner consistent with a bone-forming surface in the side oriented toward the bone marrow and a bone resorption surface in the side oriented toward the cartilage of the growth plate (Figure 3B–J).

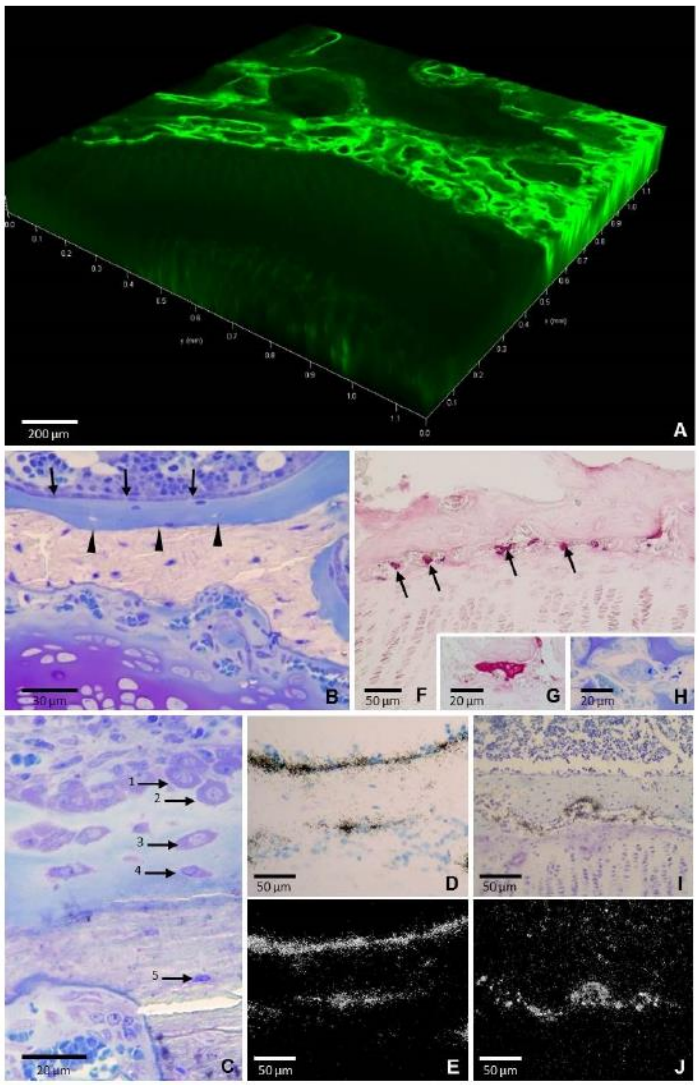


**Figure 3.** Sections of the tibial epiphysis of a 24-day-old rat. (**A**) Confocal microscopy showing a 3D projection reconstructed from z-stack images of bone tissue labeled with calcein. Fluorescence (green) is located around the blood vessels and this gives rise to an arrangement of circles whereas the underlying growth plate cartilage is completely devoid of fluorescence. (**B**) Semithin section stained with toluidine blue showing a continuous monolayer of cuboidal osteoblasts (arrows) on the surface of the bone plate. Below the osteoblasts is a thick layer of blue-stained osteoid and beneath it, there is the unstained mineralized bone. A sharp boundary between osteoid and mineralized bone is observed (arrowheads). (**C**) Semithin section stained with toluidine blue showing the gradual transformation of the phenotype of the osteoblasts that became trapped in the osteoid (1–2) to osteoid-osteocytes (3–4) and osteocytes (5). (**D**) Bright field and (**E**) dark field images of a section hybridized with a $^{35}$S-labeled riboprobe for osteocalcin showing a continuous band of positive signal on the surface of the upper side whereas only some scattered cells are positive at the lower side. (**F**) TRAP-positive osteoclasts at the narrow space between the bone plate and the growth plate cartilage (red stained, arrows). (**G**) Higher magnification of a TRAP positive cell. (**H**) Image of the same cell in a semithin section stained with toluidine blue. (**I**) Bright field and (**J**) dark field images of a section hybridized with a 35S-labeled riboprobe for gelatinaseB showing that expression is restricted to the lower side.

Osteoblasts formed a continuous epithelium-like monolayer of cuboidal cells on the surface of the upper side. Directly underneath the layer of osteoblasts was a thick layer of osteoid and beneath the latter was the mineralized bone. Osteoid and mineralized

bone could be distinguished in semithin sections by the positive toluidine blue staining of the former and the almost complete lack of staining of the latter, so that a sharp boundary between the unmineralized and mineralized zones was observed (Figure 3B,C). Microscopic analysis in semithin sections provided a clear picture of a gradual addition of new osteoid and osteoid-osteocytes from the surface to the deeper layers. The osteoid-osteocytes nearest the bone-forming surface stained intensely with toluidine blue while those further away were smaller, flattened and stained moderately (Figure 3C). Osteocalcin expression was visualized as a smoothly continuous band on the surface of the upper side whereas it was only found in a few scattered cells at the lower side (Figure 3D,E). On the other hand, large multinucleated TRAP-positive osteoclasts (Figure 3F–H) and high gelatinase B expression were observed at the lower side (Figure 3I,J), both indicating active osteoclastic bone resorption at this area.

Stage 4: Mature bone plate. The cartilage of the lower region of the epiphysis was completely removed and the epiphyseal bone plate acquired most of its adult structural characteristics By the age of 35 days. It appeared as a flat layer of bone tissue separated from the underlying growth plate cartilage by a gap about 50 μm wide, although the two structures remained bridged by a discrete number of thin bony extensions where a direct contact between cartilage and mineralized bone persisted (Figure 4A,B). Several relatively thick trabeculae arose from the upper side of the bone plate and joined it to the trabecular meshwork of the epiphysis (Figure 4A,C). The plate was perforated by tiny foramina (Figure 4D) through which blood vessels passed from the epiphyseal marrow to ramify and form a rich network close to the resting cartilage. The bone tissue had a layered arrangement, but a preferential fiber orientation was not systematically present. Collagen fibers were wavy and appeared highly interlaced (Figure 4E). Likewise, the osteocytes were not aligned in clear layers (Figure 4B,E). The bone tissue in the bone plate appeared to be structurally intermediate between woven-fibered and parallel-fibered bone and, then it could be categorized as parallel-fibered bone.

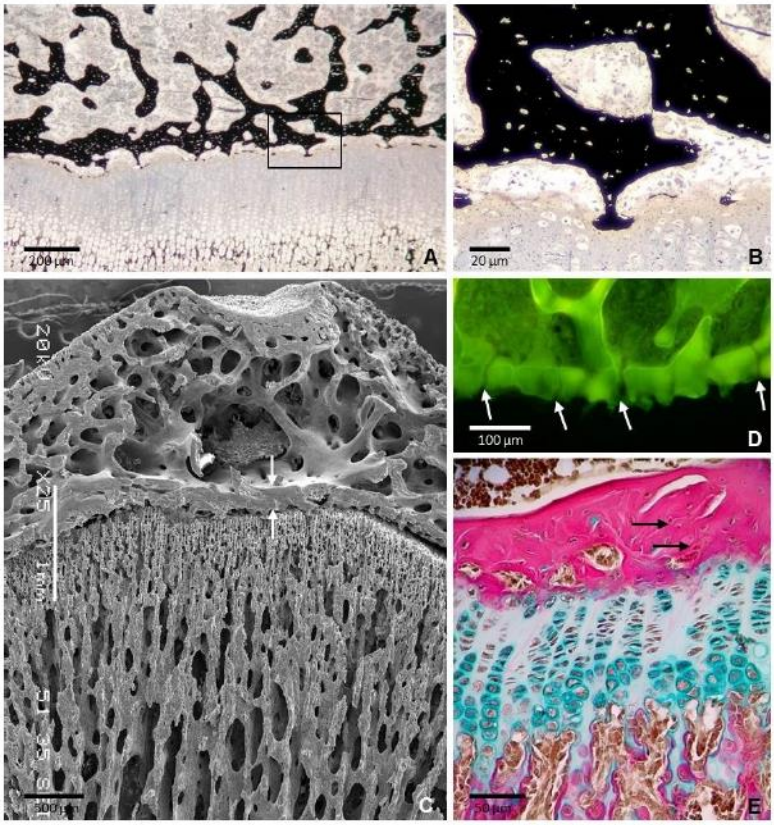


**Figure 4.** Sections of the tibial epiphysis of a 35 day-old rat. (**A**) Section stained with von Kossa showing that the epiphyseal bone plate and the underlying growth plate are bridged by a number of thin bony extensions. Boxed area is shown at a higher magnification in figure B. (**B**) Magnification of the boxed area in A showing a bone-cartilage contact. Note that osteocytes in the mineralized matrix are not aligned do not show a clear orientation. (**C**) SEM image showing that the epiphyseal plate is thicker than the cortical bone of the epiphysis (arrows). Note the continuity of the bone plate with the trabecular meshwork of the epiphysis. (**D**) Confocal microscopy image of a 3D projection reconstructed from z-stack images showing the foramina of the plate through which blood vessels passed (arrows). (**E**) Paraffin section stained with Alcian blue/acid fuchsin showing that collagen fibers are densely packed but are not arranged in a regular parallel pattern (arrows).

## 3. Discussion

The results in the present paper give, for the first time, the microscopic details of the formation of the epiphyseal bone plate. This process involves a mode of ossification that is temporally, spatially, and histologically distinct from other bony structures. During the formation of the epiphyseal bone plate, bone is deposited by osteoblasts on remnants of mineralized cartilage matrix that serve as a scaffold but also on non-mineralized cartilage surfaces and as well as within the perivascular space. The process occurs simultaneously at various sites of the epiphyseal cartilage located close to each other within a short period of time, so that a core of the sheet of bone is established very quickly. Once this early bone plate is formed, thickening and reshaping takes place through appositional growth, bone is laid down by osteoblasts in one side whereas osteoclastic resorption takes part on the opposite side. The final result is the fast formation of dense parallel-fibered bone, structurally intermediate between woven bone and lamellar bone. Time is critical in this process because the structure must be formed to reinforce the growth plate cartilage before the increase in the mechanical load associated with the onset of walking. Together, our results show that the lower portion of the epiphyseal cartilage quickly completes its transformation into dense bone in a manner that is different to any other site in the bone

and may be interpreted as mainly intramembranous-like in type, although it takes place in close relationship with a cartilage.

Intramembranous and endochondral ossification have been usually regarded as separate and different modes of ossification. Nevertheless, osteoblasts are the cells responsible for bone formation in both types and the main difference between them rests on whether osteoblasts deposit bone matrix with or without a preformed cartilage model. Osteoblasts are not able to deposit bone matrix by themselves in one specific direction since they have not different domains of the plasma membrane. Osteoblasts require a spatial framework serving as a scaffold to migrate and deposit properly structured bone tissue, so that each type of scaffolds greatly influences the osteoblast behavior [7]. Bone formation occurs on either one of three types of scaffolds: Unmineralized tissue, mineralized cartilage, and preexisting bone. The first corresponds to de novo intramembranous bone formation, the second to endochondral bone formation and the third to periosteal bone formation. The findings of our study support that the formation of the epiphyseal bone plate concurrently involves these three types of scaffolds for osteoblast activity and this result is in accordance with previous studies assessing that both intramembranous and endochondral ossification occur simultaneously during the development of some types of bones. In this way, although it is generally assumed that a long bone is formed by endochondral ossification, much of its postnatal ossification occurs subperiosteally and so is essentially intramembranous [8]. Additionally, a combination of both intramembranous and endochondral ossification has been reported to occur simultaneously during craniofacial bone development [9], clavicle formation [10], fracture healing of mandible [11], and bone lengthening through callus distraction [12,13].

The development of long bones is a complex process that results in the formation of a mature form with a specificarchitectural organization that is of major importance because the strength of a bone is partially dependent of the occurrence of accurate amounts of compact and cancellous osseous tissues arranged in a precise spatial pattern [14,15]. Although bone formation has been deeply studied at the metaphyseal side of the growth plate [16–19], the amount of research on epiphyseal ossification is so scarce that there is not even consensus on the terminology of the tissue that forms the epiphyses at early stages of the development, when they are entirely cartilaginous. The name "epiphyseal cartilage" has been used by several authors [20–22] but it has never been accepted into general use since it may lead to a certain ambiguity because other authors have used it as a synonym of growth plate. Since there is no available alternative name, in the present work we use the term "epiphyseal cartilage" to refer the cartilage from which epiphysis are entirely built at perinatal stages. This cartilage later will give rise to the articular cartilage at the end of the bone, trabecular bone in the middle and a plate of dense bone at the base of the epiphysis. The present work shows that the formation of the secondary ossification center separates a previous continuous tissue bulk into upper and lower parts that will evolve in different ways. The upper cartilage gives rise to the articular cartilage and to the secondary growth plate and whereas the lower one generates the bone plate.

The secondary growth plate is a hemispherical structure that determines the size and three-dimensional shape of the epiphysis in each particular bone [4,23]. Ossification at the secondary growth plate presents many comparable aspects to that at the metaphyseal growth plate. Chondrocytes first proliferate at the upper portion and subsequently undergo an increase in cell size. Mineralization occurs in the radial septa between the terminal hypertrophic chondrocytes and osteoblasts form bone tissue on persisting calcified radial septa that serve as scaffolding according to a typical endochondral ossification. By contrasts, the ossification of the lower epiphyseal cartilage varies substantially from a typical endochondral ossification. Chondrocytes do not undergo hypertrophy and do not produce a mineralized matrix that guides bone deposition by osteoblasts. Furthermore, the vascular invading front is not smooth but there are sites with increased cartilage resorption that give rise to finger-like extensions of the bone marrow tissue that penetrate the cartilage deep enough to reach the resting zone of the growth plate. These structures have not been

explicitly reported in previous studies but can be observed in the iconographic content of some of these preceding works [4,24–29]. Their formation involves cartilage resorption that is uncoupled to bone formation, a feature also found in the development of the cartilage canals that precede the formation of secondary ossification center. Cartilage canals are channels containing blood vessels and perivascular cells that originate at the perichondrial surface and invade the epiphyseal cartilage in a radial direction [24,30]. They serve to nourish the cartilage and also as a path to supply the epiphysis with mesenchymal stem cells coming from the perichondrium [31,32], two functions that could be also performed by the channels through lower epiphyseal cartilage. The mature bone plate is perforated and this is of major importance because these perforations allow the passage of blood vessels from the epiphysis to form a capillary network close to the resting cartilage of the growth plate. Blood vessels penetrate the epiphyseal cartilage before its ossification and the perforations are formed by subsequent layering of bone tissue around them. The extensions of the bone marrow tissue into the lower part of the epiphyseal cartilage could be a path by which osteogenic cells could quickly reach the zone where the bone plate is going to be formed. It is interesting to note that the osteogenic cells could reach different depths into the partially degrading cartilage. Since the microenvironmental conditions at different depths vary because of the different stage of maturation of terminal chondrocytes and also of the greater or less proximity to the resting cartilage of the growth plate, osteogenic cells can respond differently depending on their location. This could explain the findings in our study that osteoblasts may use different types of scaffolds for bone deposition during the formation of the epiphyseal bone plate. In this way, it is well known that osteoblasts can respond differently to stimuli depending on the bone compartment where they are located [33]. It has been reported that osteoblasts at the metaphyseal side of the growth plate radically change the mode of bone deposition to form a proper horizontal bone plate after surgical excision of the growth plate and subsequent reimplantation in the inverted orientation [34,35].

The results in our study indicate that capillaries are located just ahead of the finger-like extensions of bone marrow tissue that penetrate into the epiphyseal cartilage before the formation of the bone plate. Furthermore, direct bone formation occurs in the interstitial space close to them, a fact that suggests that capillaries may be part of the scaffold that guides the deposition of bone matrix by osteoblasts. This result is coherent with the general finding in any type of ossification that bone formation is tightly associated with the development of new blood vessels. Endothelial cells produce paracrine factors that affect osteoblast function or differentiation [36,37]. A specific subtype of capillary termed type H has been recently reported to be specifically associated with osteogenesis [38,39]. These capillaries are densely surrounded by osteoprogenitor cells and characterized by high expression of CD31 and endomucin. Type H vessels have been studied in trabecular bone adjacent to the growth plate, where they are organized as straight columns interconnected at their distal end and can direct bone formation by releasing factors that stimulate proliferation and differentiation of osteoprogenitor cells into osteoblasts. In the present study, we have found a close relationship between capillaries and bone deposition in the interstitial space during the formation of the bone plate, but their structural characteristics and the lack of immunoreactivity for CD31do not match with those of the metaphyseal type H vessels.

One remarkable finding of the present study is the existence of chondrocytes freed from the cartilage matrix in the zone where the bone plate is formed. Released viable chondrocytes have also been reported during the formation of cartilage canals, at the beginning of the formation of the secondary ossification centers [32,40] but, to our knowledge, they have not been reported before in later stages. Freed chondrocytes have been suggested to re-enter the cell cycle and further differentiate to other cell types, including osteoblasts, and take part in the ossification of the epiphysis [41]. Consistent with this possibility is the fact that chondrocytes display a remarkable capacity to differentiate into other cell types depending on the characteristics of the local microenvironment [42]. Furthermore, it has been reported that the initiation of endochondral ossification at the secondary os-

sification center occurs via the direct transdifferentiation of chondrocytes to osteoblasts and not by canonical endochondral ossification processes [43]. Likewise, chondrocytes located at singular sites like the border of the cartilage rudiments and the bony collar [44], the closing growth plate of aged rats [29], or the mixed spicules during fracture healing [45] differentiate according to uncommon ways and gives rise to exceptional phenotypes [46]. Even the long time accepted idea that hypertrophic chondrocytes are programmed to die during the process of endochondral ossification has been revised by recent studies using lineage tracing techniques that have identified different models for chondrocyte-to-osteoblast transdifferentiation [33,47–49]. In this way, results in the present study support the possibility that chondrocytes may be contribute to the formation of the epiphyseal bone plate.

In summary, our present study provides an accurate description of the tissues and events involved in the formation of the epiphyseal bone plate. We have identified some features that have not been previously reported and may be significant for understanding this bone structure. Overall, our work gives insight into the complex cellular events underlying bone formation at different sites on the skeleton and provides a basis for future studies on this relatively little investigated region of the bone.

## 4. Materials and Methods

Male Sprague-Dawley rats were obtained from the animal facility building of the University of Oviedo. Rats were sacrificed on days 3, 5, 8, 11, 14, 19, 24, and 35 after birth. We used five animals per age group except in the age-group of 35 days in which an additional rat was included ($n = 6$). Rats were injected intraperitoneally with calcein 20 mg/kg (Sigma, St Louis, MO, USA) three days before sacrifice. The procedures involving animals and their care were conducted according to Spanish law on the use of experimental animals, which acknowledges the European Directive 86/609. The project proposal was approved by the Ethical Committee of the University of Oviedo, Spain (14 July 2015, PROAE 19/2015).

Tibiae were isolated and cut through the sagittal plane of the proximal epiphysis into two equal sized parts, obtaining four tibial halves from each animal. One tibial half was embedded in paraffin to obtain sections which were used for both histochemical and in situ hybridization studies. The second tibial half was processed for mineralization studies. The third tibial half was processed to obtain semithin sections and the last tibial half was processed for confocal microscopy. Tibiae of the additional rat of the 35 days old group were processed for scanning electron microscopy.

For histochemical, immunohistochemistry and in situ hybridization studies, tissues were fixed by immersion in 4% paraformaldehyde at 4 °C for 12 h, rinsed in PBS, decalcified in 10% EDTA (pH 7.0) for 48 h at 4 °C, dehydrated through a graded ethanol series, cleared in xylene and embedded in paraffin. Sections were serially cut at a thickness of 5 µm and mounted on Superfrost Plus slides (Menzel-Glaser, Thermo Fisher Scientific, Germany). Trichromic staining was carried out by using Weigert's hematoxylin/Alcian blue/picrofuchsin, which distinguished cartilage matrix (blue) from bone matrix (red). For analysis of alkaline phosphatase (AP) staining, sections were pretreated with 10 mM $MgCl_2$ solution to reactivate the enzyme and subsequently incubated with a substrate solution containing 0.16 mg/mL 5 bromo 4 chloro 3 indolylphosphate and 0.33 mg/mL nitroblue tetrazolium in 100 mM Tris, 100 mM NaCl, 50 mM $MgCl_2$, pH 9.5, for 30 min at room temperature. Tartrate resistant acid phosphatase (TRAP) activity, a marker of osteoclast precursor cells and mature osteoclasts, was also determined histochemically by incubation of sections with 50 mM sodium acetate (pH 5.2) containing 0.15% Napthol AS TR phosphate, 50 mM sodium tartrate, and 0.1% Fast Red T.R. (Sigma).

Immunohistochemistry for CD31 was applied by using a rabbit polyclonal antibody (Abcam, Cambridge, MA, USA). Sections were deparaffinized, hydrated and treated with a solution of 0.05% pepsin (Sigma) in 0.01 M HCl (pH 2) at 37 °C for 15 min for antigen retrieval. After $H_2O_2$ inactivation and unspecific antibodies blocking, slices were incubated overnight with the primary antibody (1:100). Immunostaining was then performed by using

an ExtrAvidin Peroxidase Staining Kit for rabbit antibodies (Sigma-Aldrich, Saint Louis, MO, USA).

In situ hybridization studies were performed as reported previously [50]. Sections were hybridized to $^{35}$S-labeled antisense riboprobes and subsequently exposed to photographic emulsion at 4 °C for several days, developed, fixed, cleared and counterstained with 0.02% toluidine blue. Sections hybridized with a labeled-sense riboprobe were used as negative controls. Either, sense or antisense $^{35}$S-uridine triphosphate-labeled RNA probes were synthesized from the corresponding linearized DNA using the appropiate RNA polymerases. Probes for in situ hybridization were as follows: The probe for type II collagen was a 550 bp Pst I fragment from the amino-terminal portion of rat pro-α1(II) chain cloned in PGEM 3Zf-vector. Type X collagen probe was a 650-bp HindIII fragment containing 360 bp of non-collagenous (NC1) domain and 290 bp of 3′-untranslated sequence of the mouse type X collagen gene, subcloned into the HindIII site of pBluescript. The rat and mouse genes (RGD ID: 2371 vs. RGD ID: 735282) share 96.0–97.0 sequence similarity (ncbi.nlm.nih.gov/genome). The gelatinase B probe was generated by subcloning into pBluescript a 1353 BamHI fragment obtained by RT-PCR from embryo RNA with the following oligonucleotides: 5′ TGGCACCATCATAACATCACCT and 5′ AGAAGAAAATCTTCTTGGGCTG (GenBank acces. nb. NM_031055). The probe for murine osteocalcin consisted of a 212-bp fragment amplified from embryo RNA with the oligonucleotides 5′-TCTCTCTGCTCACTCTGCTGG and 5′AGCAGGGTTAAGCTCACACTand subcloned into pBluescript vector. Digoxigenin-11-UTP-labeled single-stranded RNA probes were also used for type-II collagen to get a better spatial resolution of chondrocytes freed form the cartilage matrix. Probes were prepared with the DIG RNA labeling mix (Boehringer Mannheim, IN, USA), and the hybridized probe was detected with the alkaline-phosphatase-coupled anti-DIG antibody (Boehringer Mannheim).

For studies of matrix mineralization, tissues were fixed in 4% paraformaldehyde in PBS for 5 h at 4 °C, dehydrated in acetone, embedded in Durkupan-ACM (Sigma) and sectioned at 2 µm on a Reicher Ultracut E ultramicrotome. The von Kossa staining was used to detect mineralization by setting sections in 1% $AgNO_3$ for 60 min at room temperature and fixed with 5% sodium hyposulfite.

Semithin sections were obtained from tissues fixed in 2% glutaraldehyde and 0.7% ruthenium hexamine trichloride (RHT) (Strem Chemicals, MA, USA) in 0.05 M cacodylate buffer, pH 7.4, for 3 h at 4 °C. They were then postfixed in 1% osmium tetroxide and 0.7% RHT in cacodylate buffer for 2 h. After washing, they were dehydrated with acetone, embedded in Durkupan-ACM (Sigma), sectioned at 0.5 µm on a Reicher Ultracut E ultramicrotome and stained with toluidine blue.

Bone samples for confocal microscopy were processed as previously reported [51]. Briefly, tibial samples were fixated in glutaraldehyde 2%, RHT 0.5%, and calcium chloride 5 mM in 0.025 M sodium cacodylate buffer (pH 7.4, osmolarity 300 mOsm). Then, they were embedded in epoxy resin Durcupan (Sigma), thinned by grinding to obtain 100-µm thick bone sections and imaged with a confocal microscope Leica TCS SP8 (Leica Microsystems, Wetzlar, Germany) equipped with a pulsed white light laser (470–670 nm), Acousto-Optical Beam Splitter (AOBS), and two internal hybrid single photon counting detectors, which was operated by Leica Application Suite X program (Leica Microsystems).

Bone samples for scanning electron microscopy were dehydrated in a graded series of acetone and critical-point dried in a Bomar SPC-900 EX critical-point dryer. Samples were glued to standard SEM stubs, coated with gold in a Sputtering Balzers SCD 004 and viewed with a JEOL JSM-5600 scanning electron microscope operated at 20 kV.

**Author Contributions:** Conceptualization, J.M.L., H.G.-P. and F.S.; methodology, Á.F.-I., R.F. and L.A.-D.; investigation, J.M.L., H.G.-P., F.S., Á.F.-I., R.F. and L.A.-D.; project administration, H.G.-P. and F.S.; writing—original draft preparation, J.M.L.; writing—review and editing, F.S., H.G.-P., Á.F.-I., R.F. and L.A.-D.; funding acquisition, J.M.L., H.G.-P. and F.S. All authors have read and agreed to the published version of the manuscript.

**Funding:** This research was funded by the Ministerio de Ciencia, Innovación y Universidades, Proyectos de Investigación en Salud Convocatoria 2018, Instituto de Salud Carlos III (PI18/01757), the European Commission for Marie Sklodowska-Curie Fellowships 2019, European Regional Development Funds 2013–2016 (ERDF, Grupin 14-020), the Foundation of the University of Oviedo (FUO) and by the Fundación para la Investigación y la Innovación Biosanitaria del Principado de Asturias (FINBA) and Instituto de Investigación Sanitaria del Principado de Asturias (ISPA).

**Institutional Review Board Statement:** The procedures involving animals and their care were conducted according to Spanish law on the use of experimental animals, which acknowledges the European Directive 86/609. The project proposal was approved by the Ethical Committee of the University of Oviedo, Spain (14 July 2015, PROAE 19/2015).

**Informed Consent Statement:** Not applicable.

**Data Availability Statement:** The data that support the findings of this study are available from the corresponding author upon reasonable request.

**Acknowledgments:** We acknowledge to Marta Alonso Guervós and Víctor Vega for their excellent technical assistant in the CSLM and SEM analyses, respectively.

**Conflicts of Interest:** The authors declare no conflict of interest.

## References

1. Shapiro, F. Developmental Bone Biology. In *Pediatric Orthopedic Deformities*; Springer International Publishing: Cham, Switzerland, 2016; Volume 1, pp. 1–158.
2. Xie, M.; Chagin, A.S. The epiphyseal secondary ossification center: Evolution, development and function. *Bone* **2021**, *142*, 115701. [CrossRef] [PubMed]
3. Love, S.M.; Ganey, T.; Ogden, J.A. Postnatal Epiphyseal Development: The Distal Tibia and Fibula. *J. Pediatr. Orthop.* **1990**, *10*, 298–305. [CrossRef] [PubMed]
4. Stokes, I.A. Mechanical effects on skeletal growth. *J. Musculoskelet. Neuronal Interact.* **2002**, *2*, 277–280. [PubMed]
5. Rivas, R.; Shapiro, F. Structural stages in the development of the long bones and epiphyses: A study in the New Zealand white rabbit. *J. Bone Jt. Surg. Am.* **2002**, *84*, 85–100. [CrossRef]
6. Delgado-Martos, M.J.; Fernández, A.T.; Canillas, F.; Quintana-Villamandos, B.; Santos-Del-Riego, S.; Delgado-Martos, E.; Martos-Rodríguez, A.; Delgado-Baeza, E. Does the epiphyseal cartilage of the long bones have one or two ossification fronts? *Med. Hypotheses* **2013**, *81*, 695–700. [CrossRef]
7. Kerschnitzki, M.; Wagermaier, W.; Roschger, P.; Seto, J.; Shahar, R.; Duda, G.N.; Mundlos, S.; Fratzl, P. The organization of the osteocyte network mirrors the extracellular matrix orientation in bone. *J. Struct. Biol.* **2011**, *173*, 303–311. [CrossRef]
8. Hall, B.K. Bone. In *Bones and Cartilage*, 2nd ed.; Hall, B.K., Ed.; Elsevier Science Publishing Co. Inc.: Amsterdam, The Netherlands; Academic Press Inc.: San Diego, CA, USA, 2015; pp. 17–42.
9. Li, X.; Yang, S.; Jing, D.; Qin, L.; Zhao, H.; Yang, S. Type II collagen-positive progenitors are major stem cells to control skeleton development and vascular formation. *bioRxiv* **2020**. [CrossRef]
10. Nagashima, H.; Sugahara, F.; Watanabe, K.; Shibata, M.; Chiba, A.; Sato, N. Developmental origin of the clavicle, and its implications for the evolution of the neck and the paired appendages in vertebrates. *J. Anat.* **2016**, *229*, 536–548. [CrossRef]
11. Yu, Y.Y.; Lieu, S.; Hu, D.; Miclau, T.; Colnot, C. Site Specific Effects of Zoledronic Acid during Tibial and Mandibular Fracture Repair. *PLoS ONE* **2012**, *7*, e31771. [CrossRef]
12. Forriol, F.; Denaro, L.; Longo, U.G.; Taira, H.; Maffulli, N.; Denaro, V. Bone lengthening osteogenesis, a combination of intramembranous and endochondral ossification: An experimental study in sheep. *Strateg. Trauma Limb Reconstr.* **2010**, *5*, 71–78. [CrossRef]
13. Runyan, C.M.; Gabrick, K.S. Biology of Bone Formation, Fracture Healing, and Distraction Osteogenesis. *J. Craniofacial Surg.* **2017**, *28*, 1380–1389. [CrossRef] [PubMed]
14. Mackie, E.J.; Tatarczuch, L.; Mirams, M. The skeleton: A multi-functional complex organ. The growth plate chondrocyte and endochondral ossification. *J. Endocrinol.* **2011**, *211*, 109–121. [CrossRef] [PubMed]
15. Olsen, B.R.; Reginato, A.M.; Wang, W. Bone Development. *Annu. Rev. Cell Dev. Biol.* **2000**, *16*, 191–220. [CrossRef] [PubMed]
16. Hallett, S.A.; Ono, W.; Ono, N. Growth Plate Chondrocytes: Skeletal Development, Growth and Beyond. *Int. J. Mol. Sci.* **2019**, *20*, 6009. [CrossRef] [PubMed]
17. Hunziker, E.B. Mechanism of longitudinal bone growth and its regulation by growth plate chondrocytes. *Microsc. Res. Technol.* **1994**, *28*, 505–519. [CrossRef] [PubMed]
18. Kronenberg, H.M. Developmental regulation of the growth plate. *Nat. Cell Biol.* **2003**, *423*, 332–336. [CrossRef] [PubMed]
19. Ballock, R.T.; O'Keefe, R.J. The biology of the growth plate. *J. Bone Jt. Surg. Am.* **2003**, *85*, 715–726. [CrossRef]
20. Shapiro, F. Epiphyseal and Physeal Cartilage Vascularization: A Light Microscopic and Tritiaded Thymidine Autoradio-graphic Study of Cartilage Canals in Newborn and Young Postnatal Rabbit Bone. *Anat. Rec.* **1998**, *252*, 140–148. [CrossRef]

21. Kavanagh, E.; Ashhurst, D.E. Development and Aging of the Articular Cartilage of the Rabbit Knee Joint: Distribution of Biglycan, Decorin, and Matrilin-1. *J. Histochem. Cytochem.* **1999**, *47*, 1603–1615. [CrossRef]
22. Petersen, W.; Tsokos, M.; Pufe, T. Expression of VEGF121 and VEGF165 in hypertrophic chondrocytes of the human growth plate and epiphyseal cartilage. *J. Anat.* **2002**, *201*, 153–157. [CrossRef]
23. Shailam, R.; Jaramillo, D.; Kan, J.H. Growth arrest and leg-length discrepancy. *Pediatr. Radiol.* **2013**, *43*, 155–165. [CrossRef] [PubMed]
24. Blumer, M.J.; Longato, S.; Richter, E.; Pérez, M.T.; Konakci, K.Z.; Fritsch, H. The role of cartilage canals in endochondral and perichondral bone formation: Are there similarities between these two processes? *J. Anat.* **2005**, *206*, 359–372. [CrossRef] [PubMed]
25. Lee, E.R.; Lamplugh, L.; Davoli, M.A.; Beauchemin, A.; Chan, K.; Mort, J.S.; Leblond, C.P. Enzymes active in the areas un-dergoing cartilage resorption during the development of the secondary ossification center in the tibiae of rats ages 0–21 days: I. Two groups of proteinases cleave the core protein of aggrecan. *Dev. Dyn.* **2001**, *222*, 52–70. [CrossRef] [PubMed]
26. Davoli, M.A.; Lamplugh, L.; Beauchemin, A.; Chan, K.; Mordier, S.; Mort, J.S.; Murphy, G.; Docherty, A.J.; Leblond, C.P.; Lee, E.R. Enzymes active in the areas undergoing cartilage resorption during the development of the secondary ossification center in the tibiae of rats aged 0–21 days. II. Two proteinases, gelatinase B and collagenase-3, are implicated in the lysis of collagen fibrils. *Dev. Dyn.* **2001**, *222*, 71–88. [CrossRef] [PubMed]
27. Stempel, J.; Fritsch, H.; Pfaller, K.; Blumer, M. Development of articular cartilage and the metaphyseal growth plate: The localization of TRAP cells, VEGF, and endostatin. *J. Anat.* **2011**, *218*, 608–618. [CrossRef]
28. Morini, S.; Continenza, M.A.; Ricciardi, G.; Gaudio, E.; Pannarale, L. Development of the microcirculation of the secondary ossification center in rat humeral head. *Anat. Rec. Adv. Integr. Anat. Evol. Biol.* **2004**, *278*, 419–427. [CrossRef]
29. Roach, H.I.; Mehta, G.; Oreffo, R.O.; Clarke, N.M.; Cooper, C. Temporal Analysis of Rat Growth Plates: Cessation of Growth with Age Despite Presence of a Physis. *J. Histochem. Cytochem.* **2003**, *51*, 373–383. [CrossRef]
30. Blumer, M.; Longato, S.; Fritsch, H. Localization of tartrate-resistant acid phosphatase (TRAP), membrane type-1 matrix metalloproteinases (MT1-MMP) and macrophages during early endochondral bone formation. *J. Anat.* **2008**, *213*, 431–441. [CrossRef]
31. Blumer, M.; Longato, S.; Fritsch, H. Structure, formation and role of cartilage canals in the developing bone. *Ann. Anat. Anat. Anz.* **2008**, *190*, 305–315. [CrossRef]
32. Álvarez, J.; Costales, L.; López-Muñiz, A.; López, J.M. Chondrocytes are released as viable cells during cartilage resorption associated with the formation of intrachondral canals in the rat tibial epiphysis. *Cell Tissue Res.* **2005**, *320*, 501–507. [CrossRef]
33. Serowoky, M.A.; Arata, C.E.; Crump, J.G.; Mariani, F.V. Skeletal stem cells: Insights into maintaining and regenerating the skeleton. *Development* **2020**, *147*, dev179325. [CrossRef] [PubMed]
34. Abad, V.; Uyeda, J.A.; Temple, H.T.; de Luca, F.; Baron, J. Determinants of Spatial Polarity in the Growth Plate. *Endocrinology* **1999**, *140*, 958–962. [CrossRef] [PubMed]
35. Abad, V.; Meyers, J.L.; Weise, M.; Gafni, R.I.; Barnes, K.M.; Nilsson, O.; Bacher, J.D.; Baron, J. The Role of the Resting Zone in Growth Plate Chondrogenesis. *Endocrinology* **2002**, *143*, 1851–1857. [CrossRef]
36. Maes, C. Role and Regulation of Vascularization Processes in Endochondral Bones. *Calcif. Tissue Int.* **2013**, *92*, 307–323. [CrossRef] [PubMed]
37. Grosso, A.; Burger, M.G.; Lunger, A.; Schaefer, D.J.; Banfi, A.; Di Maggio, N. It Takes Two to Tango: Coupling of Angiogene-sis and Osteogenesis for Bone Regeneration. *Front. Bioeng. Biotechnol.* **2017**, *5*, 68. [CrossRef] [PubMed]
38. Sivaraj, K.K.; Adams, R.H. Blood vessel formation and function in bone. *Development* **2016**, *143*, 2706–2715. [CrossRef]
39. Peng, Y.; Wu, S.; Li, Y.; Crane, J.L. Type H blood vessels in bone modeling and remodeling. *Theranostics* **2020**, *10*, 426–436. [CrossRef]
40. Blumer, M.; Longato, S.; Schwarzer, C.; Fritsch, H. Bone development in the femoral epiphysis of mice: The role of cartilage canals and the fate of resting chondrocytes. *Dev. Dyn.* **2007**, *236*, 2077–2088. [CrossRef]
41. Cole, A.A.; Cole, A.M., Jr. Are perivascular cells in cartilage canals chondrocytes? *J. Anat.* **1989**, *165*, 1–8.
42. Shapiro, I.M.; Adams, C.S.; Freeman, T.; Srinivas, V. Fate of the hypertrophic chondrocyte: Microenvironmental perspec-tives on apoptosis and survival in the epiphyseal growth plate. *Birth. Defects. Res. C Embryo Today* **2005**, *75*, 330–339. [CrossRef]
43. Aghajanian, P.; Xing, W.; Cheng, S.; Mohan, S. Epiphyseal bone formation occurs via thyroid hormone regulation of chon-drocyte to osteoblast transdifferentiation. *Sci. Rep.* **2017**, *7*, 10432. [CrossRef] [PubMed]
44. Riminucci, M.; Bradbeer, J.N.; Corsi, A.; Gentili, C.; Descalzi, F.; Cancedda, R.; Bianco, P. Vis-à-Vis Cells and the Priming of Bone Formation. *J. Bone Miner. Res.* **1998**, *13*, 1852–1861. [CrossRef] [PubMed]
45. Scammell, B.E.; Roach, H.I. A new role for the chondrocyte in fracture repair: Endochondral ossification includes direct bone formation by former chondrocytes. *J. Bone Miner. Res.* **2009**, *11*, 737–745. [CrossRef] [PubMed]
46. Mizuhashi, K.; Nagata, M.; Matsushita, Y.; Ono, W.; Ono, N. Growth Plate Borderline Chondrocytes Behave as Transient Mesenchymal Precursor Cells. *J. Bone Miner. Res.* **2019**, *34*, 1387–1392. [CrossRef]
47. Aghajanian, P.; Mohan, S. The art of building bone: Emerging role of chondrocyte-to-osteoblast transdifferentiation in endochondral ossification. *Bone Res.* **2018**, *6*, 19. [CrossRef]
48. Wong, S.A.; Hu, D.P.; Slocum, J.; Lam, C.; Nguyen, M.; Miclau, T., 3rd; Marcucio, R.S.; Bahney, C.S. Chondrocyte-to-Osteoblast Transformation in Mandibular Fracture Repair. *J. Orthop. Res.* **2020**. [CrossRef]

49. Newton, P.T.; Li, L.; Zhou, B.; Schweingruber, C.; Hovorakova, M.; Xie, M.; Sun, X.; Sandhow, L.; Artemov, A.V.; Ivashkin, E.; et al. A radical switch in clon-ality reveals a stem cell niche in the epiphyseal growth plate. *Nature* **2019**, *567*, 234–238. [CrossRef]
50. Alvarez, J.; Costales, L.; Serra, R.; Balbín, M.; López, J.M. Expression patterns of matrix metalloproteinases and vascular en-dothelial growth factor during epiphyseal ossification. *J. Bone Miner. Res.* **2005**, *20*, 1011–1021. [CrossRef]
51. Fernández-Iglesias, Á.; Fuente, R.; Gil-Peña, H.; Alonso-Duran, L.; García-Bengoa, M.; Santos, F.; López, J.M. A simple method based on confocal microscopy and thick sections recognizes seven subphases in growth plate chondrocytes. *Sci. Rep.* **2020**, *10*, 1–10. [CrossRef]

# VI.ADDITIONAL RESULTS

# | ANALYSIS OF UREMIC GROWTH PLATE CHONDROCYTES

## Growth Plate Key Markers

The pattern of expression of Sox9 was phenotypically similar between experimental groups, but a general diminished intensity of expression, more significant at Cluster 1 and at the hypertrophy clusters (Clusters 5 to 7), was observed in all groups when compared with the C group (Figure 10).

The expression of PTHrP was also analyzed by immunofluorescence. No apparent changes in the pattern of PTHrP expression were found and its levels of expression were reduced in all groups compared with the C group for all cluster except for cluster 5. In cluster 2 and 5 when AD levels parallel with those of C (Figure 10).

Also, it was performed immunofluorescence of IHH expression. The AD group showed similar levels from Cluster 1 to 6 its levels parallel when compared with the C group but end up with a significantly reduced expression in Cluster 7. Conversely, the PF group start with reduced levels when compared with the C and AD groups. Although its levels parallel from Cluster 2 to 4, it showed significantly increased levels at the hypertrophic clusters compared with the AD group. The ADGH group showed no apparent changes with the AD group until Cluster 7, when its levels increase to parallel with those of the C group (Figure 10).

## Alterations of the GH-IGF1 Axis during CKD

The pattern of the distribution of Stat5b was phenotypically similar between experimental groups, but its levels of expression were significantly reduced in all groups (AD and PF) compared with the C group in cluster 7. GH treatment did not produce changes in the Stat5b levels during the prehypertrophic clusters, but showed significantly reduced levels during cluster 6 compared to AD. In cluster 7, its levels parallel with those of AD again (Figure 11).

The expression of SOCS2 was also analyzed by immunofluorescence. No apparent changes in the pattern of SOCS2 were found and its levels of expression were reduced in all groups compared with the C group for all cluster except for cluster 2. In cluster 2, AD and ADGH levels parallel with those of C (Figure 11).

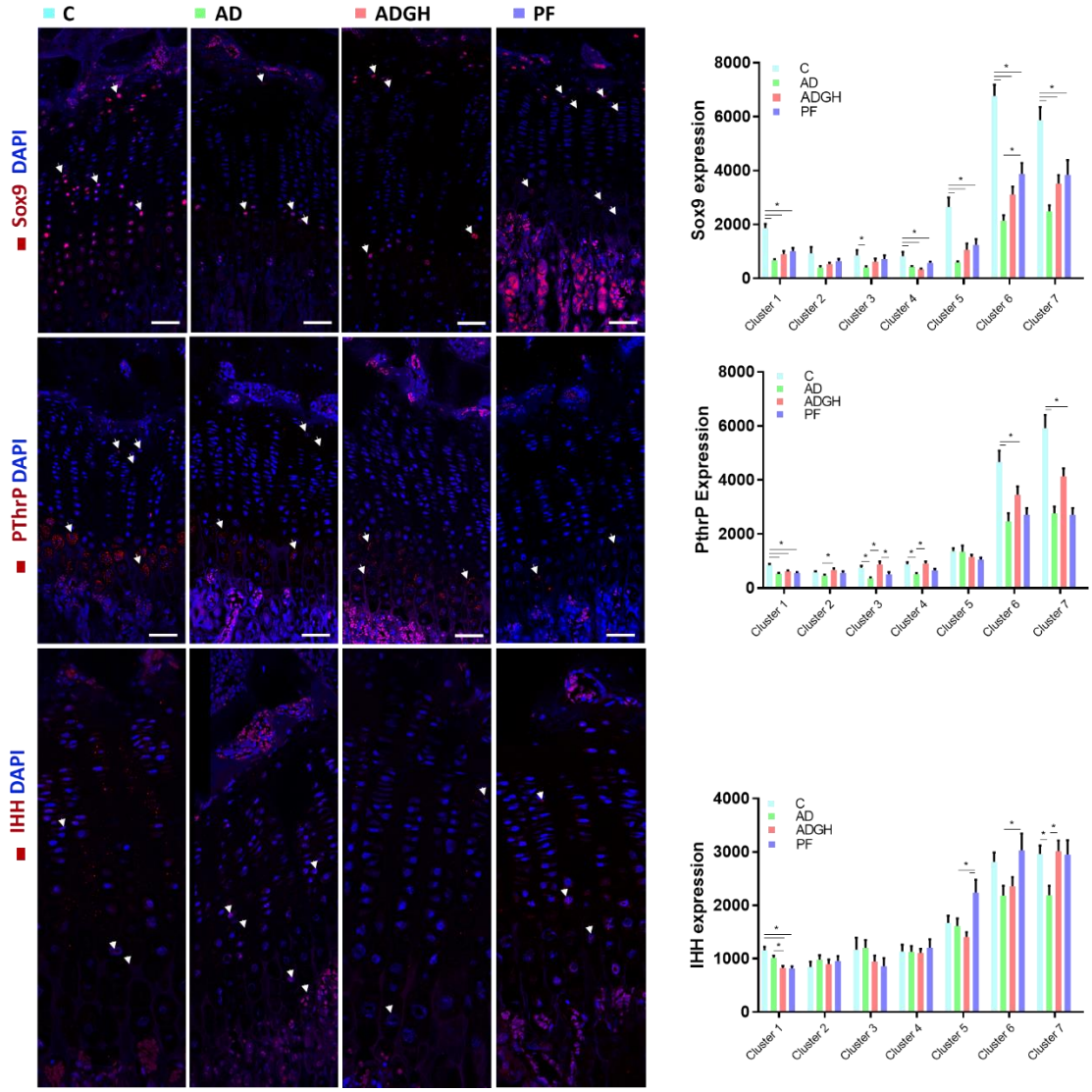


**Figure 10. Immunohistochemical analysis of the expression of key regulators of the GP.** Representative images are shown for Sox9 (red), PTHrP (red) and IHH (red) and their corresponding quantifications in the seven described clusters. Arrowheads mark some of the labeled cells. Blue nuclei are stained by DAPI. DAPI, 4,6-diamidino-2-phenylindole; C, control rats; AD, adenine 0.5% rats; ADGH, adenine 0.5% rats treated with GH; PF, pair-fed rats; Sox9, SRY-Box Transcription Factor 9, PTHrP, Parathyroid hormone related protein; IHH, Indian hedgehog. Values are mean ± SEM. * p value < 0.05.

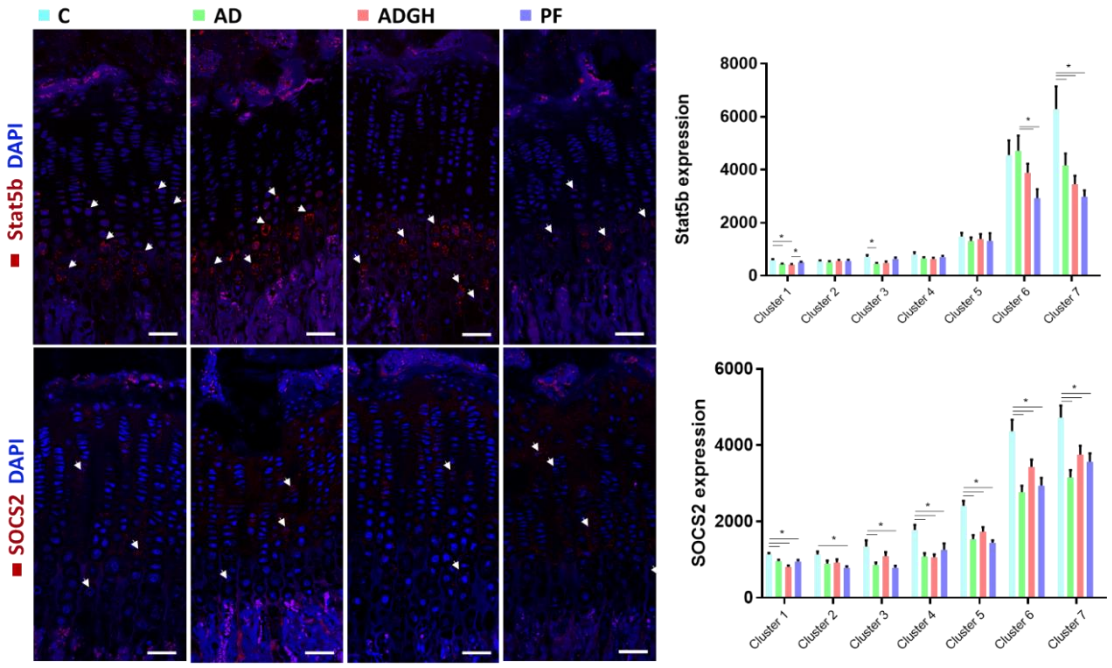


**Figure 11. Immunohistochemical analysis of the expression of the JAK2/STAT5b pathway members.** Representative images are shown for Stat5b (red), and SOCS2 (red) and their corresponding quantifications in the seven described clusters. Arrowheads mark some of the labeled cells. Blue nuclei are stained by DAPI. DAPI, 4,6-diamidino-2-phenylindole; C, control rats; AD, adenine 0.5% rats; ADGH, adenine 0.5% rats treated with GH; PF, pair-fed rats; Stat5b, Signal transducer and activator of transcription 5B; SOCS2, Suppressor of cytokine signaling 2. Values are mean ± SEM. * p value < 0.05.

# VII.DISCUSSION

# | THREE-DIMENSIONAL ANALYSIS OF CHONDROCYES

## Processing Procedure

The spectral confocal microscope analysis of bone samples showed that both the quality of the preservation and the IOD of hypertrophic chondrocytes varied noticeably depending on fixation and staining conditions (**Table 1, II**). Two procedures reached the highest value (9.9): (1) fixation in glutaraldehyde 2%, ruthenium hexaammine trichloride 0.5% and calcium chloride 5 mM in 0.025 M sodium cacodylate buffer (pH 7.4, osmolarity 300 mOsm) (F3) followed by staining with a solution of eosin 0.5% in acetate buffered ethanol 60% pH 4.8 during 2 hours at 4 °C (2) the same fixation (F3) followed by staining with a solution of eosin of higher concentration (1%) at the same pH (4.8) for a longer time (4 hours). When values for the three simple parameters in the two procedures were compared it was found that both SI and CP were higher in the first procedure (3.40 vs 3.25 and 3.60 vs 3.45, respectively) whereas the second procedure showed a higher value for IOD (3.2 vs 2.9). The quality of cell preservation was prioritized over fluorescence intensity and the procedure using lower eosin concentration during less time was selected. Although the penetrating properties of formaldehyde are stronger than those of glutaraldehyde, this distributed homogeneously into the slices of about 2 mm in thickness of the GP and effectively preserved the structure of hypertrophic chondrocytes giving good overall cytoplasmic and nuclear detail. Formaldehyde, limited to low concentrations because of its high osmolarity, did not improve structural preservation, slightly increased cell shrinkage and considerably decreased signal-to-background fluorescence ratios. Ruthenium hexamine trichloride was effective to prevent the loss of matrix proteoglycans and shrinkage of chondrocytes at the two concentrations tested (0.5 and 0.7%) and thus, the 0.5% concentration was chosen. Addition of calcium chloride to the fixative improved structural preservation of chondrocytes while not decreasing signal-to-background autofluorescence ratio. These results confirm that minor changes during tissue processing induce noticeable changes in the preservation of hypertrophic chondrocytes [76]. Chondrocytes showed a strong and clean fluorescence signal dispersed throughout the cytoplasm (**Figure 1A, II**). The fluorescence signal appeared diffused in the intercellular matrix and almost absent in the nuclear region. Fluorescence signal was more intense in the perinuclear region and appeared constituted by a network of granulo-filamentous structures. Comparative analysis of confocal and electron micrographs (**Figure 1A–C, II**) revealed that fluorescent signal corresponds to the area where organelles were concentrated. Perinuclear cytoplasm contained abundant rough endoplasmic reticulum, scattered mitochondria, and some lipid droplets. The excitation-emission map of the samples treated with the selected procedure (**Figure 1D–F**) showed a broad range of effective excitation wavelengths and peaks in intensity at excitation/emission wavelengths of 531/556 nm.

Matched control samples fixed in the same way but without eosin staining showed a clear different map in which the peak at 531/556 nm disappeared and a smaller one was found

at 649/674, a result that demonstrates that a substantial fraction of the fluorescence signal in the first sample came from eosin labelling.

Fluorescent labelling was observed in chondrocytes throughout the GP, with highest levels in proliferative chondrocytes and a progressively decreasing levels towards the hypertrophic zone (**Figure 2, II**). Analysis of thick sections with the confocal microscopy avoids damage to the integrity of the chondrocytes caused by mechanical sectioning and this allows to visualize entire chondrocytes inside their native lacunae preserving cell-matrix interactions. Eosin has quite good penetration into thick tissue sections of GP cartilage and stains the cytoplasm of the chondrocytes providing a strong fluorescent signal that resisted solvent dehydration, epoxy resin embedding and heat polymerization. Eosin is usually not regarded as a fluorochrome but results in the present work shows its utility for fluorescence labelling of chondrocytes, and this agrees with some previous studies in which eosin staining and confocal microscopy were used to analyze the three-dimensional distribution of cytoplasmic constituents of protein nature [77–79] and also for tissue pathology diagnosis [80,81]. Although eosin possesses only 20% the fluorescence quantum yield of more conventional fluorophores, such as fluorescein and rhodamine, eosin conjugated to either an immunoglobulin G (IgG) or steptavidin has been also proposed as an alternative to fluorescein in immunofluorescence [82,83]. Furthermore, eosin forms protein–dye complexes whose absorbance is proportional to the concentration of protein [84–86] and it has been used as a fluorescent probe for estimating a wide range of proteins by spectroscopy [84,87,88].

It is also of note that embedding of the GP in epoxy resin reduced refractive disparity between the different tissue constituents and this decreased random light scattering and increased penetration of light for imaging. Analysis of the maximum depth at which images can be obtained in the samples revealed that there was effective photon penetration along the Z-axis up to 70 microns depth for both the excitation laser and the emission fluorescence, being the detector gain was adjusted from 36% (surface) to 57% (Z: 70 µm). As a result, the three-dimensional reconstruction of focal image stacks of hypertrophic chondrocytes allowed to obtain images of intact entire chondrocytes inside their lacunae with a relatively smooth surface and minimal irregular shrinkage or cell collapse even for those adjacent to the vascular invasion front. The complete serial optical sections, from the surface to depth = 70 µm, are shown in **Supplementary video 1 (II).**

The findings of this study support the usefulness of an easy and inexpensive approach, based on in block eosin staining followed by embedding in epoxy resin and grinding, to analyze growth plate chondrocytes by confocal microscopy.

## Analysis of Cell Changes During Chondrocyte Proliferation and Hypertrophy

The size, shape and cytoplasm density of the chondrocytes disposed in vertical columns exhibit a range of continuous variation from the top to the bottom. The GP shows a multilayered horizontal stratification but precise transition lines between contiguous zones cannot be established because variation is continuous. Quantitative values of cell volume, shape and cytoplasmic density obtained from each chondrocyte were used to perform a hierarchical cluster analysis and to objectively grade the chondrocytes of the GP. Comparison in a multidimensional array of quantitative values allowed to define distances between chondrocytes and to establish seven categories or clusters. Chondrocytes in a particular cluster share common characteristics and are more similar to each other than to those in the other clusters. A hierarchical dendrogram showing the order of successive agglomerations and a cluster plot are shown in **Figure 3 (II).** Four layers corresponding to different stages of differentiation are classically considered in the GP: resting, proliferating, prehypertrophic, and hypertrophic. Results obtained in the present analysis show some of these layers defined by subjective cell morphological criteria can be subdivided into several subphases. According to our results, chondrocyte cell volume remains unchanged in the clusters 1 to 4 and then a statistically significant increase takes place in the transition from cluster 4 to cluster 5 (**Figure 4, II**).

Since cell enlargement triggers the switch to hypertrophy, it could be considered that transition from cluster 4 to cluster 5 corresponds to the transition from the proliferating to the hypertrophic stage. Thus, cluster analysis allows to differentiate four subphases in the pre-hypertrophic stage (clusters 1 to 4) and three subphases in the hypertrophic stage (clusters 5 to 7). When clusters of the hypertrophic stage were analyzed it was found that transition from cluster 4 to cluster 5 was associated with a significant increase in cell volume without significant change in cytoplasm density. However, an increase of cell volume and decrease of the cytoplasmic density, both statistically significant, took place in the transition from cluster 5 to cluster 6. Finally, cell volume increase without cytoplasmic density variation occurred in the transition from cluster 6 to cluster 7.

## Growth Plate Markers

The seven clusters of chondrocytes were evaluated by immunohistochemistry of chondrocyte markers of maturity and activity, including Col2a1, a structural component of the cartilage matrix that may act as an extracellular signaling molecule suppressing chondrocyte hypertrophy; Col10a1, a short-chain collagen associated with hypertrophy of chondrocytes and involved in the ossification of cartilage; Sox9, a transcription factor essential for chondrocyte differentiation; Igf1, a growth factor that stimulates both proliferation and hypertrophy of chondrocytes by paracrine/autocrine mechanisms; Aqp1, a water channel protein that is responsible for high water permeability of chondrocyte membrane during hypertrophy; and

NKCC1, a secondary active transport system that is responsible for cell volume regulation. Immunohistochemical analysis of GP cartilage (**Figure 5, II**) showed that Col2a1 is expressed throughout the GP but it decreases as chondrocytes become hypertrophic and ceases in the chondrocytes near the zone of mineralization.

Analysis of immunohistochemical staining demonstrated intense signal in clusters 1 to 5 but it significantly decreased in the transition from cluster 5 to cluster 6 whereas no signal was observed in the cluster 7. By contrast, Col10a1 had the inverse distribution of Col2a1, signal was absent in clusters 1 to 3, raised in cluster 4, increased in cluster 5 and reached high levels in clusters 6 and 7. The restricted expression of Col10a1 within the hypertrophic zone of the GP supports that it enables the removal of type II collagen fibrils and participates in the mineralization process. Sox9 was observed throughout the GP in all chondrocyte layers, with low values in clusters 1 to 4 and significant increases in the transitions from cluster 4 to cluster 5 and from cluster 5 to cluster 6 where it peaks. Finally, it significantly decreased in the transitions from cluster 6 to cluster 7. These results are coincident with previous reporting that Sox9 has essential roles in successive steps of the chondrocyte differentiation pathway [89,90]. Aqp1 and Nkcc1 proteins showed equally low signal levels in clusters 1 to 4 but Nkcc1 exhibited a significant increase in the transition from cluster 4 to cluster 5 whereas Aqp1 expression remained low in the cluster 5. Both transport proteins showed high signal levels in cluster 6, where Nkcc1 reached the peak level to slightly decrease in cluster 7, although without significant difference. However, Aqp1 signal continuously increased during hypertrophy and reached the highest level in cluster 7. Such differences in the expression profiles during chondrocyte hypertrophy suggest that Nkcc1 may have a major role in the onset of cell volume expansion (cluster 5) whereas Aqp1 may have its main function in the later stages of the process (cluster 7). One major factor that determines ion mobility and the net movement of water into the chondrocyte is the interaction with an ionic microenvironment with high cationic content due to the concentration of fixed negative charges on proteoglycans of the cartilage extracellular matrix. Interactions between transported molecules with the microenvironment and both active and passive membrane transport proteins have been documented in cell volume regulation of chondrocytes [17,91]. Igf1 expression was in the clusters 1 to 4 and a significant increase occurred in the transition from cluster 4 to cluster 5. Likewise, significant increases were also found in the transition from cluster 5 to cluster 6 and in the transition from cluster 6 to cluster 7, where reached the highest expression level. This data supports the view that Igf1 promotes the anabolic actions associated with the increased biosynthetic activity of chondrocyte hypertrophy [92].

The occurrence of four clusters in the pre-hypertrophic stage is remarkable because only two categories of chondrocytes, resting and proliferating, have so far been defined. This result implies that proliferating zone has a less uniform structure than usually considered. Previous works have reported that chondrocytes possess nearly the same structure from the beginning to the end of the proliferating zone [93]. However functional differences among the various

segments of the columns have also been reported. The establishment of clonal columns of chondrocytes is a major process that precisely occurs at the transition from the resting to the proliferating zone. Likewise, the rate of cell proliferation varies through the proliferating zone of the GP and changes in gene expression associated with regional differences in proliferative activity have been reported [94,95]. Since cells approximately double in size prior to mitosis and this involves both protein synthesis and energy production, it is expected that different proliferation activity may result in structural differences. Immunohistochemical analysis revealed that no differences among clusters 1 to 3 are found for Col2a1, Col10a1 or Sox9. Type II collagen and Sox9 remained unchanged at cluster 4 but Col10a1expression was first found at some chondrocytes of this cluster.

Since chondrocyte cell volume remained unchanged in the clusters 1 to 4 and significantly increased in the transition from cluster 4 to cluster 5, it could be concluded that Col10a1expression is turned on before the beginning of cell volume increment. Results obtained in the present work suggest that quantitative analysis of volume, shape and cytoplasm of chondrocytes could be a specific and sensitive method to detect differences in the activity of proliferative chondrocytes.

# | ANALYSIS GROWTH PLATE IN UREMIA

## Experimental Model and Growth Retardation

Many animal models have been developed that simulate the different etiopathogenic mechanisms of chronic kidney failure. In 1974, Chantler and Holliday first described the use of an experimental model of uremia induced by two-stage 5/6th nephrectomy in prepubertal rats to investigate growth failure in CKD [96]. From then on, this rat model has been extensively used to this end despite some important limitations and technical difficulties such as high animal mortality, variability in the degree of renal function reduction, need of surgery, non-reversibility of renal lesion, and postsurgical period of acute renal failure.

For this work, an experimental model of CKD caused by 0.5% adenine diet in young rats was used. This procedure was formerly described by our group as a non-invasive, and reproducible method to investigate CKD-induced growth retardation and to analyze growth plate and bone abnormalities in rats [40]. Our experimental protocol resulted in moderate renal failure, as reflected by BUN and serum creatinine concentrations that were about five times higher in the AD group than in the control and PF groups, and growth retardation, as previously described by our group [40].

As corresponds to the uremic state, the AD rats ate less than the ad libitum-fed rats with normal renal function (control group). It is of note that a similar degree of growth retardation was found in the AD and PF groups. In this model of uremia, a greater degree of growth impairment in the AD rats could have been achieved by a higher dose of adenine in their diets, as adenine is not well tolerated by rats and causes more severe bone diseases than in rats with subtotal nephrectomy [41].

## The Growth Plate in Uremia

The impairment of growth was associated with several modifications in the morphology and dynamics of the GP, as previously reported [20,50]. The height of the GP was significantly reduced in uremic and PF rats. It has been indistinctly described to be increased, reduced, or unchanged compared to the controls, a fact suggesting that it could be dependent to a great extent on the severity of the uremia [45]. AD rats presented smaller GPs, and this reduction was accompanied by a significantly reduced hypertrophic stratum (**Table 3, III**). Previous studies are coincident with these findings and also show that the GP height reduction is caused by alterations in the hypertrophic zone rather than by modifications in the proliferative activity, although this is also reduced in CKD [40,44].

## Three-Dimensional Analysis of Uremic Chondrocytes

The hypertrophy of GP chondrocytes is known to be the main contributor to bone lengthening [14]. The hypertrophic chondrocytes of uremic rats have been reported to achieve a lower final size than those of control animals [20]. This process is characterized by a widespread increase in cell volume and has been studied previously, especially with respect to its regulation [8]. However, information regarding how the cell volume increase occurs is limited. The increase in chondrocyte volume has been reported to result from three sequential phases, as mentioned in the I.INTRODUCTION section [18].

We demonstrated here that the chondrocytes of uremic animals started with a reduced chondrocyte volume and cell density, as seen in cluster 1. The GP chondrocytes of normal growing rats started enlarging in the transition from cluster 3 to 4, when the beginning of hypertrophy occurs. Conversely, by cluster 4, uremic chondrocytes seemed unable to start increasing and volume enlargement appeared to be delayed until the transition from cluster 4 to 5. Our results suggest that uremic chondrocytes, by cluster 4, had the same amount of proteins as normal chondrocytes (**Figure 2B, III**), but, somehow, they were unable to use this to start enlarging, causing hypertrophy to be delayed. Interestingly, the start of the hypertrophy was quite abrupt, as seen in the transition from cluster 4 to 5 and 5 to 6, when they underwent two phases of marked volume increase, causing the cell cytoplasm density to decay, compared to the control (**Figure 2A,C, III**). At a later stage of hypertrophy, the behavior of normal and uremic chondrocytes became parallel, both experiencing a phase characteristic of true hypertrophy. These results suggest that, in CKD, chondrocytes are not able to reach a normal terminal chondrocyte volume because they experience a delayed start to hypertrophy and seem unable to catch up, reaching the end of the maturation process with a reduced size. The chondrocytes of PF animals mostly show the same behavior as uremic chondrocytes, as suggested by the cell volume pattern across all the GP clusters. This could suggest that some of the GP alterations during CKD are not caused by uremia itself but are partially triggered by associated nutritional disorders. More marked differences between the chondrocytes of PF and AD rats had likely been found by inducing a more severe degree of renal failure [45]. However, in this model of uremia, this would have required a higher concentration of adenine in the diet, which is not well tolerated by rats and induces life-threatening inflammation [40].

## Alterations of the GH-IGF1 Axis

Studies in mice lacking the GH receptor and/or Igf1 suggested that only 17% of postnatal growth occurs independent of the GH/IGF-1 axis [97]. Growth impairment in CKD children has been explained mainly by a reduced IGF-I bioavailability, in part owing to a GH-resistance state caused by a postreceptorial defect in the JAK2-STAT5b signaling pathway downstream of the GH, as shown in the liver, skeletal muscle, and GP [62,65,98–100]. Our findings revealed low Igf1

expression levels in the prehypertrophic clusters and a significant increase in the transition from cluster 4 to cluster 5, coincident with the onset of chondrocyte hypertrophy in the transition from cluster 5 to cluster 6 and in the transition from cluster 6 to cluster 7, to reach the highest expression level at the later stage of the hypertrophy process (**Figure 2, III**) [101]. In uremic chondrocytes, this pattern of expression was preserved, but there were significantly reduced levels of expression across the GP, more importantly in the hypertrophic clusters. These results are in line with those previously seen by Troib et al. [63], which showed reduced protein expression, suggesting that a decrease in the action of GH during CKD, in turn, leads to a decreased local Igf1 level. GP Igf1 expression was reduced in the food-restricted, pair-fed, normal control rats compared with the ad libitum-fed, normal rats (**Figure 2, III).** This again indicated that the suppressed GP Igf1 expression in CKD is in part secondary to anorexia and reduced nutrient intake.

Reduced levels of Igf1 mRNA and protein were associated with chronic anorexic states or prolonged fasting or food restriction [63,100,102]. Gevers et al. [103] demonstrated that fasting attenuates the Stat5 phosphorylation response to GH therapy in the liver and the GP cartilage of GH-deficient mice, which could partly explain the similar behavior of uremic and pair-fed animal chondrocytes. Also, Troib et al, 2013 [63], by analyzing the JAK2/STAT5 pathway in CKD, reported unchanged levels of total STAT5 protein in CKD, but reduced levels of relative STAT5 phosphorylation (p-STAT5/STAT5). GH signals through the Jak/Stat signaling pathway via Jak2 tyrosine kinase phosphorylation of the two very homologous transcription factors, Stat5a and Stat5b. Gene disruption studies have shown that these proteins have both non-redundant and shared roles in signaling [104]. Anyhow, it has been reported that the transcription factor Stat5b mediates the GH promoting effect on IGF-1 expression and on chondrogenesis [105]. Interestingly, when quantifying Stat5b protein levels independently of Stat5a in our CKD group, it was observed that the pattern of expression of Stat5b protein was similar to that of control chondrocytes, but significantly reduced in cluster 7 (**Figure 11).** It could be hypothesized that STAT5a is increasing its levels at this stage as a compensation mechanism in response to the decrease in STAT5b levels. That could partly explain the normal STAT5b levels observed by Troib et al (2013) and would also reflect in low Igf1 levels, given that Stat5b is the solely mediator of Igf1 expression in chondrocytes [63].

In CKD, a major cause of attenuated JAK/STAT signaling seems to be the increase in tissue SOCS2 expression, which is the chief negative feedback inhibitor of GHR action. SOCS2 is known to have a role in linear growth: SOCS2(-/-) mice show increased longitudinal skeletal growth associated with deregulated GH/IGF-1 signaling. Interestingly, even though increased levels of SOCS2 mRNA have been described in growth plates of immature rats with growth retardation and CKD [63], in our experimental model we did not observe changes in the levels of SOCS2 protein expression by immunofluorescence (**Figure 11**). This difference in results could be due to the experimental approach and should be addressed in the future by performing additional experiments.

## Regulators of Proliferation and Hypertrophy

Other factors besides GH and IGF-I contribute to the rate of bone growth through endochondral ossification, including the control of chondrocyte cell volume and proliferation rates. Type II and type X collagens are the most abundant proteins found in the GP. Type II is the predominant structural collagen present in all zones of the GP and is the main protein that is responsible for providing the tissue with a fibrillar framework to arrange chondrocytes as well as other extracellular matrix components (ECM). Type X collagen is an ECM component expressed exclusively by hypertrophic chondrocytes. No changes were observed in the pattern of expression of Col2a1 in uremic GPs, but we did note an early Col10a1 expression, by cluster 3. Interestingly, previous studies also revealed a generalized decrease in collagen expression and changes in its architecture, which were especially marked in the hypertrophic cartilage of 5/6 nephrectomized rats (**Figure 3**, **III**) [46].

The distribution of the transporters and channels that regulate water and electrolyte traffic through the cell membrane was also analyzed, given its importance in the cell enlargement characteristic of normal growing rats started enlarging in the transition from cluster 3 to 4, when the beginning of hypertrophy occurs. Conversely, by cluster 4, uremic chondrocytes seemed unable to start increasing and volume enlargement appeared to be delayed until the transition from cluster 4 to 5. Our results suggest that uremic chondrocytes, by cluster 4, had the same amount of proteins as normal chondrocytes (**Figure 2B**, **III**), but, somehow, they were unable to use this to start enlarging, causing hypertrophy to be delayed. Interestingly, the start of the hypertrophy was quite abrupt, as seen in the transition from cluster 4 to 5 and 5 to 6, when they underwent two phases of marked volume increase, causing the cell cytoplasm density to decay, compared to the control (**Figure 2AC**, **III**).

The immunohistochemistry of some well-defined molecular landmarks at distinct stages of chondrocyte differentiation was performed with the aim of defining non reported altered pathways related to the GP alterations in CKD. PTHrP is been described to be expressed mainly by chondrocytes at the periarticular and the reserve zone, but its receptor is found particularly in the prehypertrophic cells and lower proliferative. The mechanism of PTHrP activity is achieved by delaying the hypertrophic differentiation in the lower proliferative zone by maintaining cells in the prehypertrophic phenotype. When proliferation is completed, chondrocytes at the prehypertrophic zone release IHH, which stimulates PTHrP synthesis via a feedback loop [8,106]. In the uremic GP, the protein expression PTHrP was found to be diminished, but IHH was unchanged. Similarly, Sox9 expression, a transcription factor essential for the adequate dynamic of the GP, was found to be diminished in uremia (**Figure 10**). Further investigation of the downstream member of this signaling pathways could be relevant to understand the effect of its alterations in the growth impairment phenotype secondary to uremia.

## Growth Hormone Treatment

High pharmacological doses of GH accelerate growth velocity [51] and improve the final height of patients with CKD [107]. The effects of GH therapy in the GP chondrocytes of uremic rats have not been extensively studied. The present study found that GH administration normalized the growth rate, measured by OFA, and the height of both the GP and the hypertrophic stratum (**Table 2,3, III**). Remarkably, the three-dimensional study of the uremic chondrocytes treated with GH revealed that, whereas chondrocytes, like untreated chondrocytes, start with a reduced chondrocyte volume, the pattern of chondrocyte volume increase was partly normalized at the prehypertrophic clusters compared to the control. GH appeared to be able to successfully enable uremic chondrocytes to enter hypertrophy, and in cluster 4, they present normal volumes. In the remaining phases, GH chondrocytes underwent the same volume enlargement as the untreated uremic chondrocytes, but, coming from a higher volume, they reached cluster 7 with a significantly increased volume. Even if GH was not able to normalize the pattern of hypertrophy in uremic chondrocytes from clusters 5 to 7, it was able to stimulate a chondrocyte cell volume enlargement from clusters 3 to 5 (**Figure 2AC, III**). These data are consistent with the previous findings stating that GH acts locally at the GP to recruit resting chondrocytes into a proliferative state [108], as well as to stimulate local Igf1 production, which then stimulates the proliferation of chondrocytes [11,108,109]. In turn, our data suggest that GH treatment stimulates protein synthesis at the prehypertrophic stages of chondrocytes, causing an early increase in the volume of chondrocytes and allows them to complete the maturation process with normal parameters of volume and cytoplasm cell density. Moreover, GH increases Igf1 levels (**Figure 3, III**)**.** Thus, Igf1 may play a role in the GH's compensatory mechanism of chondrocyte volume increase. Findings in experimental animals and in humans have shown that the absence or mutations of the STAT5b gene, the major mediator of the GH-regulated IGF-1 gene expression, are associated with diminished postnatal growth, GH resistance, and reduced IGF-I synthesis [102]. We did not find changes in the pattern or levels of expression of nor Stat5b or SOCS2 due to GH treatment (**Figure 11**). Anyhow, in this study, GH was able to raise Aqp1 levels at the prehypertrophic stages and allow chondrocytes to enter hypertrophy with significantly increased levels compared to uremic chondrocytes (cluster 4 to 5), a result that differs from previously published studies [101]. The level of Aqp1 expression in GH-treated chondrocytes, even if significantly lower than the control in most of the GP, has the same pattern of variation across the GP than untreated chondrocytes, indicating that, even though Aqp1 is still functioning, it could not be a part of the mechanism by which GH normalizes the chondrocyte volume in uremic conditions (**Figure 3, III**). However, it is interesting to note that, whereas uremic chondrocytes maintain normal Nkcc1 levels, GH causes an early Nkcc1 expression by cluster 4, even when compared to the control (**Figure 3, III**). In a recent study, we proposed that, in normal growing rats, Nkcc1 may have a major role in the onset of cell volume expansion [8]. Treatment with pharmacologic doses of GH has been shown to overcome the GH-resistance state and be effective in normalizing STAT5 phosphorylation [20,68]. Thus, it is

tempting to propose that GH treatment could increase Nkcc1 levels and so increase chondrocyte volume at an early stage. Further studies in this line of work would be of great importance.

# | FORMATION OF THE EPIPHYSEAL BONE PLATE

The results in presented here give, for the first time, the microscopic details of the formation of the epiphyseal bone plate. This process involves a mode of ossification that is temporally, spatially, and histologically distinct from other bony structures. During the formation of the epiphyseal bone plate, bone is deposited by osteoblasts on remnants of mineralized cartilage matrix that serve as a scaffold but also on non-mineralized cartilage surfaces and as well as within the perivascular space. The process occurs simultaneously at various sites of the epiphyseal cartilage located close to each other within a short period of time, so that a core of the sheet of bone is established very quickly. Once this early bone plate is formed, thickening and reshaping takes place through appositional growth, bone is laid down by osteoblasts in one side whereas osteoclastic resorption takes part on the opposite side. The final result is the fast formation of dense parallel-fibered bone, structurally intermediate between woven bone and lamellar bone. Time is critical in this process because the structure must be formed to reinforce the growth plate cartilage before the increase in the mechanical load associated with the onset of walking. Together, our results show that the lower portion of the epiphyseal cartilage quickly completes its transformation into dense bone in a manner that is different to any other site in the bone and may be interpreted as mainly intramembranous in type, although it takes place in close relationship with a cartilage.

Intramembranous and endochondral ossification have been usually regarded as separate and different modes of ossification. Nevertheless, osteoblasts are the cells responsible for bone formation in both types and the main difference between them rests on whether osteoblasts deposit bone matrix with or without a preformed cartilage model. Osteoblasts are not able to deposit bone matrix by themselves in one specific direction since they have not different domains of the plasma membrane. Osteoblasts require a spatial framework serving as a scaffold to migrate and deposit properly structured bone tissue, so that each type of scaffolds greatly influences the osteoblast behavior [110]. Bone formation occurs on either one of three types of scaffolds: unmineralized tissue, mineralized cartilage and preexisting bone. The first corresponds to de novo intramembranous bone formation, the second to endochondral bone formation and the third to periosteal bone formation. The findings of our study support that the formation of the epiphyseal bone plate concurrently involves these three types of scaffolds for osteoblast activity and this result is in accordance with previous studies assessing that both intramembranous and endochondral ossification occur simultaneously during the development of some types of bones. In this way, although it is generally assumed that a long bone is formed by endochondral ossification, much of its postnatal ossification occurs subperiosteally and so is essentially intramembranous [111]. Additionally, a combination of both intramembranous and endochondral ossification has been reported to occur simultaneously during craniofacial bone development [112], clavicle formation [113], fracture healing of mandible [114] and bone lengthening through callus distraction [115,116].

The development of long bones is a complex process that results in the formation of a mature form with a specific architectural organization that is of major importance because the strength of a bone is partially dependent of the occurrence of accurate amounts of compact and cancellous osseous tissues arranged in a precise spatial pattern [117,118]. Although bone formation has been deeply studied at the metaphyseal side of the growth plate, the amount of research on epiphyseal ossification is so scarce that there is not even consensus on the terminology of the tissue that forms the epiphyses at early stages of the development when they are entirely cartilaginous. The name “epiphyseal cartilage” has been used by several authors [119–121] but it has never been accepted into general use since it may lead to a certain ambiguity because other authors have used it as a synonym of growth plate. Since there is no available alternative name, in the present work we use the term “epiphyseal cartilage” to refer the cartilage from which epiphysis are entirely built at perinatal stages. This cartilage later will give rise to the articular cartilage at the end of the bone, trabecular bone in the middle and a plate of dense bone at the base of the epiphysis. The present work shows that the formation of the secondary ossification center separates a previous continuous tissue bulk into upper and lower parts that will evolve in different ways. The upper cartilage gives rise to the articular cartilage and to the secondary growth plate and whereas the lower one generates the bone plate.

The secondary growth plate is a hemispherical structure that determines the size and three-dimensional shape of the epiphysis in each particular bone [28,122]. Ossification at the secondary growth plate presents many comparable aspects to that at the metaphyseal growth plate. Chondrocytes first proliferate at the upper portion and subsequently undergo an increase in cell size. Mineralization occurs in the radial septa between the terminal hypertrophic chondrocytes and osteoblasts form bone tissue on persisting calcified radial septa that serve as scaffolding according to a typical endochondral ossification. By contrasts, the ossification of the lower epiphyseal cartilage varies substantially from a typical endochondral ossification. Chondrocytes do not undergo hypertrophy and do not produce a mineralized matrix that guides bone deposition by osteoblasts. Furthermore, the vascular invading front is not smooth but there are sites with increased cartilage resorption that give rise to finger-like extensions of the bone marrow tissue that penetrate the cartilage deep enough to reach the resting zone of the growth plate. These structures have not been explicitly reported in previous studies but can be observed in the iconographic content of some of these preceding works [28,123–128]. Their formation involves cartilage resorption that is uncoupled to bone formation, a feature also found in the development of the cartilage canals that precede the formation of secondary ossification center. Cartilage canals are channels containing blood vessels and perivascular cells that originate at the perichondrial surface and invade the epiphyseal cartilage in a radial direction [129]. They serve to nourish the cartilage and also as a path to supply the epiphysis with mesenchymal stem cells coming from the perichondrium [129,130], two functions that could be also performed by the channels through lower epiphyseal cartilage. The mature bone

plate is perforated, and this is of major importance because these perforations allow the passage of blood vessels from the epiphysis to form a capillary network close to the resting cartilage of the growth plate. Blood vessels penetrate the epiphyseal cartilage before its ossification and the perforations are formed by subsequent layering of bone tissue around them. The extensions of the bone marrow tissue into the lower part of the epiphyseal cartilage could be a path by which osteogenic cells could quickly reach the zone where the bone plate is going to be formed. It is interesting to note that the osteogenic cells could reach different depths into the partially degrading cartilage. Since the microenvironmental conditions at different depths vary because of the different stage of maturation of terminal chondrocytes and also of the greater or less proximity to the resting cartilage of the growth plate, osteogenic cells can respond differently depending on their location. This could explain the findings in our study that osteoblasts may use different types of scaffolds for bone deposition during the formation of the epiphyseal bone plate. In this way, it is well known that osteoblasts can respond differently to stimuli depending on the bone compartment where they are located [131]. It has been reported that osteoblasts at the metaphyseal side of the growth plate radically change the mode of bone deposition to form a proper horizontal bone plate after surgical excision of the growth plate and subsequent reimplantation in the inverted orientation [9,132].

The results in our study indicate that capillaries are located just ahead of the finger-like extensions of bone marrow tissue that penetrate the epiphyseal cartilage before the formation of the bone plate. Furthermore, direct bone formation occurs in the interstitial space close to them, a fact that suggests that capillaries may be part of the scaffold that guides the deposition of bone matrix by osteoblasts. This result is coherent with the general finding in any type of ossification that bone formation is tightly associated with the development of new blood vessels. Endothelial cells produce paracrine factors that affect osteoblast function or differentiation [133,134]. A specific subtype of capillary termed type H has been recently reported to be specifically associated with osteogenesis [135,136]. These capillaries are densely surrounded by osteoprogenitor cells and can direct bone formation by releasing factors that stimulate proliferation and differentiation of osteoprogenitor cells into osteoblasts. These capillaries are densely surrounded by osteoprogenitor cells and characterized by high expression of CD31 and endomucin. Type H vessels have been studied in trabecular bone adjacent to the growth plate, where they are organized as straight columns interconnected at their distal end and can direct bone formation by releasing factors that stimulate proliferation and differentiation of osteoprogenitor cells into osteoblasts. In the present study, we have found a close relationship between capillaries and bone deposition in the interstitial space during the formation of the bone plate, but their structural characteristics and the lack of immunoreactivity for CD31 do not match with those of the metaphyseal type H vessels.

One remarkable finding of the present study is the existence of chondrocytes freed from the cartilage matrix in the zone where the bone plate is formed. Released viable chondrocytes have also been reported during the formation of cartilage canals, at the beginning of the

formation of the secondary ossification centers [130,137] but, to our knowledge, they have not been reported before in later stages. Freed chondrocytes have been suggested to re-enter the cell cycle and further differentiate to other cell types, including osteoblasts, and take part in the ossification of the epiphysis [138]. Consistent with this possibility is the fact that chondrocytes display a remarkable capacity to differentiate into other cell types depending on the characteristics of the local microenvironment [139]. Furthermore, it has been reported that the initiation of endochondral ossification at the secondary ossification center occurs via the direct transdifferentiation of chondrocytes to osteoblasts and not by canonical endochondral ossification processes [140]. Likewise, chondrocytes located at singular sites like the border of the cartilage rudiments and the bony collar [141], the closing growth plate of aged rats [128], or the mixed spicules during fracture healing [142] differentiate according to uncommon ways and gives rise to exceptional phenotypes [143]. Even the long-time accepted idea that hypertrophic chondrocytes are programmed to die during the process of endochondral ossification has been revised by recent studies using lineage tracing techniques that have identified different models for chondrocyte-to-osteoblast transdifferentiation [131,144–146]. In this way, results in the present study support the possibility that chondrocytes may be contribute to the formation of the epiphyseal bone plate.

In summary, our present study provides an accurate description of the tissues and events involved in the formation of the epiphyseal bone plate. We have identified some features that have not been previously reported and may be significant for understanding this bone structure. Overall, our work gives insight into the complex cellular events underlying bone formation at different sites on the skeleton and provides a basis for future studies on this relatively little investigated region of the bone.

# VIII.CONCLUSIONS/ CONCLUSIONES

# | CONCLUSIONS

1. Confocal microscopy technique described in this study is useful to image and obtain quantitative data on growth plate chondrocytes.
2. Growth plate chondrocytes can be graded in seven different clusters, with four subphases in the pre-hypertrophic stage (clusters 1 to 4) and three subphases in the hypertrophic stage (clusters 5 to 7).
3. Major modifications induced by uremia in the morphology and dynamics of the GP are:
    a. Reduction of the final chondrocyte volume.
    b. Delay of the beginning of the chondrocyte hypertrophy process.
4. Growth hormone treatment improves growth impairment and reverts the effects of uremia on the final chondrocyte volume.
5. In the animal model of uremia here described, growth hormone treatment likely compensates for the disturbance of chondrocyte maturation in CKD by triggering an early chondrocyte enlargement that could be mediated by Nkcc1.
6. The mechanism of formation of the epiphyseal bone plate is specific and distinctive of this structure, following a process that may be interpreted intramembranous-like ossification.

# | CONCLUSIONES

1. La técnica de microscopía confocal descrita en esta tesis doctoral es útil para obtener imágenes y datos cuantitativos de los condrocitos de la placa de crecimiento.

2. Los condrocitos de la placa de crecimiento se pueden clasificar en siete grupos diferentes, con cuatro subfases en la etapa prehipertrófica (grupos 1 a 4) y tres subfases en la etapa hipertrófica (grupos 5 a 7).

3. Las principales modificaciones inducidas por la uremia en la morfología y dinámica de la placa de crecimiento son:
    a. Reducción del volumen final de condrocitos.
    b. Retraso del inicio del proceso de hipertrofia de condrocitos.

4. El tratamiento con hormona del crecimiento mejora el deterioro del crecimiento y revierte los efectos de la uremia sobre el volumen final de condrocitos.

5. En el modelo animal de uremia aquí descrito, el tratamiento con hormona del crecimiento probablemente compensa la alteración de la maduración de los condrocitos en la ERC desencadenando un agrandamiento temprano de los condrocitos que podría estar mediado por Nkcc1.

6. El mecanismo de formación de la placa ósea epifisaria es específico y distintivo de esta estructura, siguiendo un proceso que guarda similitud con la osificación intramembranosa.

# IX.REFERENCES

1. Benyi, E.; Sävendahl, L. The physiology of childhood growth: Hormonal regulation. *Horm. Res. Paediatr.* **2017**, *88*, 6–14.

2. Karlberg, J. A biologically-oriented mathematical model (ICP) for human growth. *Acta Paediatr. Scand. Suppl.* **1989**, *350*, 70–94.

3. Mehta, A.; Hindmarsh, P.C.; Stanhope, R.G.; Turton, J.P.G.; Cole, T.J.; Preece, M.A.; Dattani, M.T. The role of growth hormone in determining birth size and early postnatal growth, using congenital growth hormone deficiency (GHD) as a model. *Clin. Endocrinol. (Oxf).* **2005**, *63*, 223–231.

4. Hindmarsh, P.C.; Smith, P.J.; Brook, C.G.D.; Matthews, D.R. The relationship between height velovity and growth hormone secretion in short prepubertal children. *Clin. Endocrinol. (Oxf).* **1987**, *27*, 581–591.

5. Granados, A.; Gebremariam, A.; Lee, J.M. Relationship between timing of peak height velocity and Pubertal Staging in Boys and Girls. *J. Clin. Res. Pediatr. Endocrinol.* **2015**, *7*, 235–237.

6. Abbassi, V. Growth and normal puberty. *Pediatrics* **1998**, *102*, 507–11.

7. Roselló-Díez, A.; Joyner, A.L. Regulation of long bone growth in vertebrates; it is time to catch-up. *Endocr. Rev.* **2015**, er.2015-1048.

8. Kronenberg, H. Developmental regulation of the growth plate. *Nature* **2003**, *423*, 332–336.

9. Abad, V.; Meyers, J.L.; Weise, M.; Gafni, R.I.; Barnes, K.M.; Nilsson, O.; Bacher, J.D.; Baron, J. The role of the resting zone in growth plate chondrogenesis. *Endocrinology* **2002**, *143*, 1851–1857.

10. Buckwalter, J.A.; Mower, D.; Ungar, R.; Schaeffer, J.; Ginsberg, B. Morphometric analysis of chondrocyte hypertrophy. *J. Bone Joint Surg. Am.* **1986**, *68*, 243–255.

11. Hunziker, E.B. Mechanism of longitudinal bone growth and its regulation by growth plate chondrocytes. *Microsc. Res. Tech.* **1994**, *28*, 505–519.

12. Hunziker, E.B.; Schenk, R.K. Physiological mechanisms adopted by chondrocytes in regulating longitudinal bone growth in rats. *J. Physiol.* **1989**, *414*, 55–71.

13. Wilsman, N.J.; Farnum, C.E.; Leiferman, E.M.; Fry, M.; Barreto, C. Differential growth by growth plates as a function of multiple parameters of chondrocytic kinetics. *J. Orthop. Res.* **1996**, *14*, 927–936.

14. Breur, G.J.; VanEnkevort, B.A.; Farnum, C.E.; Wilsman, N.J. Linear relationship between the volume of hypertrophic chondrocytes and the rate of longitudinal bone growth in growth plates. *J. Orthop. Res.* **1991**, *9*, 348–359.

15. Kember, N. Cell kinetics and the control of bone growth. *Acta Paediatr.* **1993**, *391*, 61–5.

16. Hunziker, E.B.; Schenk, R.K.; Cruz-Orive, L.M. Quantitation of chondrocyte performance in growth-plate cartilage during longitudinal bone growth. *J. Bone Joint Surg. Am.* **1987**, *69*, 162–173.

17. Bush, P.G.; Parisinos, C.A.; Hall, A.C. The osmotic sensitivity of rat growth plate chondrocytes in situ; clarifying the mechanisms of hypertrophy. *J. Cell. Physiol.* **2008**, *214*, 621–629.

18. Cooper, K.L.; Oh, S.; Sung, Y.; Dasari, R.R.; Kirschner, M.W.; Tabin, C.J. Multiple phases of

chondrocyte enlargement underlie differences in skeletal proportions. *Nature* **2013**, *495*, 375–378.

19. Bush, P.G.; Pritchard, M.; Loqman, M.Y.; Damron, T.A.; Hall, A.C. A key role for membrane transporter NKCC1 in mediating chondrocyte volume increase in the mammalian growth plate. *J. Bone Miner. Res.* **2010**, *25*, 1594–1603.

20. Claramunt, D.; Gil-Peña, H.; Fuente, R.; García-López, E.; Frías, O.H.; Ordoñez, F.A.; Rodríguez-Suárez, J.; Santos, F. Effects of growth hormone treatment on growth plate, bone and mineral metabolism of young rats with uremia induced by adenine. *Pediatr. Res.* **2017**, *82*, 888.

21. Van Der Eerden, B.C.J.; Karperien, M.; Wit, J.M. Systemic and Local Regulation of the Growth Plate. *Endocr. Rev.* **2003**, *24*, 782–801.

22. Wajnrajch, M.P.; Gertner, J.M.; Harbison, M.D.; Chua Jr., S.C.; Leibel, R.L. Nonsense mutation in the human growth hormone-releasing hormone receptor causes growth failure analogous to the little (lit) mouse. *Nat. Genet.* **1996**, *12*, 88–90.

23. Wagner, J.K.; Eble, A.; Hindmarsh, P.C.; Mullis, P.E. Prevalence of human GH-1 gene alterations in patients with isolated growth hormone deficiency. *Pediatr. Res.* **1998**, *43*, 105–110.

24. Shapiro, F. *Developmental Bone Biology. In Pediatric Orthopedic Deformities*; 2016;

25. Xie, M.; Chagin, A.S. The epiphyseal secondary ossification center: Evolution, development and function. *Bone* **2021**, *142*, 115701.

26. Love, S.M.; Ganey, T.; Ogden, J.A. Postnatal epiphyseal development: the distal tibia and fibula. *J. Pediatr. Orthop.* **1990**, *10*, 298–305.

27. Stokes, I.A.F. Mechanical effects on skeletal growth. *J. Musculoskelet. Neuronal Interact.* **2002**, *2*, 277–280.

28. Rivas, R.; Shapiro, F. Structural stages in the development of the long bones and epiphyses: a study in the New Zealand white rabbit. *J. Bone Joint Surg. Am.* **2002**, *84*, 85–100.

29. Delgado-Martos, M..; Touza Fernández, A.; Canillas, F.; Quintana-Villamandos, B.; Santos del Riego, S.; Delgado-Martos, E.; Martos-Rodriguez, A.; Delgado-Baeza, E. Does the epiphyseal cartilage of the long bones have one or two ossification fronts? *Med. Hypotheses* **2013**, *81*, 695–700.

30. Webster, A.C.; Nagler, E. V; Morton, R.L.; Masson, P. Chronic Kidney Disease. *Lancet* **2016**, *6736*, 1–15.

31. Stevens, P.E.; Levin, A. Evaluation and management of chronic kidney disease: synopsis of the kidney disease: improving global outcomes 2012 clinical practice guideline. *Ann. Intern. Med.* **2013**, *158*, 825–830.

32. Franke, D.; Winkel, S.; Gellermann, J.; Querfeld, U.; Pape, L.; Ehrich, J.H.; Haffner, D.; Pavicic, L.; Zivicnjak, M. Growth and maturation improvement in children on renal replacement therapy over the past 20 years. *Pediatr Nephrol* **2013**, *28*, 2043–2051.

33. Harambat, J.; Bonthuis, M.; van Stralen, K.J.; Ariceta, G.; Battelino, N.; Bjerre, A.; Jahnukainen, T.; Leroy, V.; Reusz, G.; Sandes, A.R.; et al. Adult height in patients with advanced CKD requiring renal replacement therapy during childhood. *Clin. J. Am. Soc. Nephrol.* **2014**, *9*, 92–99.

34. Furth, S.L.; Stablein, D.; Fine, R.N.; Powe, N.R.; Fivush, B. a. Adverse clinical outcomes associated with short stature at dialysis initiation: a report of the North American Pediatric Renal Transplant Cooperative Study. *Pediatrics* **2002**, *109*, 909–913.

35. Schaefer, F.; Seidel, C.; Binding, a; Gasser, T.; Largo, R.H.; Prader, a; Schärer, K. Pubertal growth in chronic renal failure. *Pediatr. Res.* **1990**, *28*, 5–10.

36. Harambat, J.; Cochat, P. Growth after renal transplantation. *Pediatr. Nephrol.* **2009**, *24*, 1297–1306.

37. Rees, L.; Jones, H. Nutrition and growth in children with chronic kidney disease. *Pediatr. Nephrol.* **2013**, *28*, 527–536.

38. Fine, R.N. Etiology and treatment of growth retardation in children with chronic kidney disease and end-stage renal disease: a historical perspective. *Pediatr. Nephrol.* **2010**, *25*, 725–32.

39. Mehls, O.; Ritz, E.; Krempien, B.; Gilli, G.; Link, K.; Willich, E.; Schärer, K. Slipped epiphyses in renal osteodystrophy. *Arch. Dis. Child.* **1975**, *50*, 545–554.

40. Claramunt, D.; Gil-Peña, H.; Fuente, R.; García-López, E.; Loredo, V.; Hernández-Frías, O.; Ordoñez, F.A.; Rodríguez-Suárez, J.; Santos, F. Chronic kidney disease induced by adenine: a suitable model of growth retardation in uremia. *Am. J. Physiol. Renal Physiol.* **2015**, *309*, F57-62.

41. Claramunt, D.; Gil-Peña, H.; Fuente, R.; Hernández-Frías, O.; Santos, F. Animal models of pediatric chronic kidney disease. Is adenine intake an appropriate model? *Nefrologia* **2015**, *35*, 517–522.

42. Mehls, O.; Ritz, E.; Gilli, G.; Schmidt-Gayk, H.; Krempien, B.; Kourist, B.; Wesch, H.; Prager, P. Skeletal changes and growth in experimental uremia. *Nephron* **1977**, *18*, 288–300.

43. Cobo, A.; Carbajo, E.; Santos, F.; Garcia, E.; Lopez, J.M. Morphometry of uremic rat growth plate. *Miner. Electrolyte Metab.* **1996**, *22*, 192–195.

44. Cobo, A.; López, J.M.; Carbajo, E.; Santos, F.; Alvarez, J.; Fernández, M.; Weruaga, A. Growth plate cartilage formation and resorption are differentially depressed in growth retarded uremic rats. *J. Am. Soc. Nephrol.* **1999**, *10*, 971–9.

45. Fernández-Fuente, M.; Santos, F.; Carbajo-Pérez, E.; Rodríguez, J.; Weruaga, A.; Amil, B.; Molinos, I.; García, E. Growth plate height of uremic rats is influenced by severity and duration of renal failure. *Pediatr. Nephrol.* **2004**, *19*, 187–192.

46. Alvarez, J.; Balbín, M.; Fernández, M.; López, J.M. Collagen metabolism is markedly altered in the hypertrophic cartilage of growth plates from rats with growth impairment secondary to chronic renal failure. *J. Bone Miner. Res.* **2001**, *16*, 511–524.

47. Sanchez, C.P.; Salusky, I.B.; Kuizon, B.D.; Abdella, P.; Jüppner, H.; Goodman, W.G. Growth of long bones in renal failure: Roles of hyperparathyroidism, growth hormone and calcitriol. *Kidney Int.* **1998**, *54*, 1879–1887.

48. Sanchez, C.P.; He, Y.Z. Growth hormone therapy in calcium-loaded rats with renal failure. *Endocrinology* **2004**, *145*, 3375–3385.

49. Sanchez, C.P.; He, Y. zhu Effects of thyroparathyroidectomy, exogenous calcium, and short-term calcitriol therapy on the growth plate in renal failure. *J. Am. Soc. Nephrol.* **2003**, *14*, 148–158.

50. Santos, F.; Carbajo-Pérez, E.; Rodríguez, J.; Fernández-Fuente, M.; Molinos, I.; Amil, B.; García, E. Alterations of the growth plate in chronic renal failure. *Pediatr. Nephrol.* **2005**, *20*, 330–4.

51. Mehls, O.; Irzynjec, T.; Ritz, E.; Eden, S.; Kovàcs, G.; Klaus, G.; Floege, J.; Mall, G. Effects of rhGH and rhIGF-1 on renal growth and morphology. *Kidney Int.* **1993**, *44*, 1251–1258.

52. Haffner, D.; Schaefer, F.; Nissel, R.; Wühl, E.; Tönshoff, B.; Mehls, O.; Subjects, S. Effect of Growth Hormone Treatment on the Adult Height of Children with Chronic Renal Failure. *N. Engl. J. Med.* **2000**, *343*, 923–930.

53. Amil, B.; Santos, F.; Rodríguez, J.; Carbajo, E.; García, E. Efecto de la hormona de crecimiento y del calcitriol sobre la placa de crecimiento de ratas urémicas. *Nefrología* **2003**, *XXIII*, 23–26.

54. Hunziker, E.B.; Wagner, J.; Zapf, J. Differential effects of insulin-like growth factor I and growth hormone on developmental stages of rat growth plate chondrocytes in vivo. *J. Clin. Invest.* **1994**, *93*, 1078–86.

55. Darnell, J.E. STATs and gene regulation. *Science (80-. ).* **1997**, *277*, 1630–1635.

56. Woelfle, J.; Chia, D.J.; Rotwein, P. Mechanisms of growth hormone (GH) action: Identification of conserved Stat5 binding sites that mediate GH-induced insulin-like growth factor-I gene activation. *J. Biol. Chem.* **2003**, *278*, 51261–51266.

57. Woelfle, J.; Billiard, J.; Rotwein, P. Acute control of insulin-like growth factor-I gene transcription by growth hormone through Stat5b. *J. Biol. Chem.* **2003**, *278*, 22696–22702.

58. Kofoed, E.M.; Hwa, V.; Little, B.; Woods, K.A.; Buckway, C.K.; Tsubaki, J.; Pratt, K.L.; Bezrodnik, L.; Jasper, H.; Tepper, A.; et al. Growth Hormone Insensitivity Associated with a *STAT5b* Mutation. *N. Engl. J. Med.* **2003**, *349*, 1139–1147.

59. Yasukawa, H.; Sasaki, A.; Yoshimura, A. Negative regulation of cytokine singaling pathways. *Annu. Rev. Immunol.* **2000**, *2*, 143–164.

60. Edmondson, S.R.; Baker, N.L.; Oh, J.; Kovacs, G.; Werther, G.A.; Mehls, O. Growth hormone receptor abundance in tibial growth plates of uremic rats: GH/IGF-I treatment. *Kidney Int.* **2000**, *58*, 62–70.

61. Hanna, J.D.; Santos, F.; Foreman, J.W.; Chan, J.C.; Han, V.K. Insulin-like growth factor-I gene expression in the tibial epiphyseal growth plate of growth hormone-treated uremic rats. *Kidney Int.* **1995**, *47*, 1374–1382.

62. Schaefer, F.; Chen, Y.; Tsao, T.; Nouri, P.; Rabkin, R. Impaired JAK-STAT signal transduction contributes to growth hormone resistance in chronic uremia. *J. Clin. Invest.* **2001**, *108*, 467–475.

63. Troib, A.; Landau, D.; Kachko, L.; Rabkin, R.; Segev, Y. Epiphyseal growth plate growth hormone receptor signaling is decreased in chronic kidney disease-related growth retardation. *Kidney Int* **2013**, *84*, 940–949.

64. Woelfle, J.; Rotwein, P. In vivo regulation of growth hormone-stimulated gene transcription by STAT5b. *Am. J. Physiol. Endocrinol. Metab.* **2004**, *286*, E393-401.

65. Sun, D.F.; Zheng, Z.; Tummala, P.; Oh, J.U.N.; Schaefer, F.; Rabkin, R. Chronic Uremia Attenuates Growth Hormone – Induced Signal Transduction in Skeletal Muscle. *J. Am. Soc. Nephrol.* **2004**, 2630–2636.

66. Rabkin, R.; Sun, D.F.; Chen, Y.; Tan, J.; Schaefer, F. Growth hormone resistance in uremia, a role for impaired JAK/STAT signaling. *Pediatr. Nephrol.* **2005**, *20*, 313–318.

67. Yoshimura, A.; Nishinakamura, H.; Matsumura, Y.; Hanada, T. Negative regulation of cytokine signaling and immune responses by SOCS proteins. *Arthritis Res. Ther.* **2005**, *7*, 100–110.

68. Wiezel, D.; Assadi, M.H.; Landau, D.; Troib, A.; Kachko, L.; Rabkin, R.; Segev, Y. Impaired renal growth hormone JAK/STAT5 signaling in chronic kidney disease. *Nephrol. Dial. Transplant.* **2014**, *29*, 791–799.

69. Hunziker, E.B.; Lippuner, K.; Shintani, N. How best to preserve and reveal the structural intricacies of cartilaginous tissue. *Matrix Biol.* **2014**, *39*, 33–43.

70. Hunziker, E.B.; Herrmann, W.; Schenk, R.K. Ruthenium hexammine trichloride (RHT)-mediated interaction between plasmalemmal components and pericellular matrix proteoglycans is responsible for the preservation of chondrocytic plasma membranes in situ during cartilage fixation. *J. Histochem. Cytochem.* **1983**, *31*, 717–727.

71. Hayat, M.A. *Fixation for Electron Microscopy*; Academic P.; Elsevier Inc., 1981; ISBN 978-0-12-333920-1.

72. Baker, J.R. The Structure and Chemical Composition of the. *Quart. J. Micr. Sci* **1944**, *85*, 1–71.

73. Fleming, G.R.; Knight, A.W.E.; Morris, J.M.; Morrison, R.J.S.; Robinson, G.W. Picosecond fluorescence studies of xanthene dyes. *J. Am. Chem. Soc.* **1977**, *99*, 4306–4311.

74. Fuente, R.; Gil-Peña, H.; Claramunt-Taberner, D.; Hernández-Frías, O.; Fernández-Iglesias, Á.; Hermida-Prado, F.; Anes-González, G.; Rubio-Aliaga, I.; Lopez, J.M.; Santos, F. Marked alterations in the structure, dynamics and maturation of growth plate likely explain growth retardation and bone deformities of young Hyp mice. *Bone* **2018**, *116*, 187–195.

75. Kovács, G.T.; Oh, J.; Kovács, J.; Tönshoff, B.; Hunziker, E.B.; Zapf, J.; Mehls, O. Growth promoting effects of growth hormone and IGF-I are additive in experimental uremia. *Kidney Int.* **1996**, *49*, 1413–1421.

76. Loqman, M.Y.; Bush, P.G.; Farquharson, C.; Hall, A.C. A cell shrinkage artefact in growth plate chondrocytes with common fixative solutions: importance of fixative osmolarity for maintaining morphology. *Eur. Cell. Mater.* **2010**, *19*, 214–227.

77. de Carvalho, H.F.; Taboga, S.R. Fluorescence and confocal laser scanning microscopy imaging of elastic fibers in hematoxylin-eosin stained sections. *Histochem. Cell Biol.* **1996**, *106*, 587–592.

78. Wu, Y.; Li, B.; Gao, X.M. Selective fluorescence of zymogen granules of pancreatic acinar cells stained with hematoxylin and eosin. *Biotech. Histochem.* **2002**, *77*, 291–293.

79. Capani, F.; Deerinck, T.J.; Ellisman, M.H.; Bushong, E.; Bobik, M.; Martone, M.E. Phalloidin-eosin followed by photo-oxidation: a novel method for localizing F-actin at the light and electron microscopic levels. *J. Histochem. Cytochem.* **2001**, *49*, 1351–1361.

80. Luo, T.; Lu, Y.; Liu, S.; Lin, D.; Qu, J. Enhanced Visualization of Hematoxylin and Eosin Stained Pathological Characteristics by Phasor Approach. **2017**.

81. Castellanos, M.R.; Nehru, V.M.; Pirog, E.C.; Optiz, L. Fluorescence microscopy of H&E stained cervical biopsies to assist the diagnosis and grading of CIN. *Pathol. Res. Pract.*

**2018**, *214*, 605–611.

82. Hulspas, R.; Bioconsulting, C.T.; Keij, J.F. Avidin-EITC: an alternative to avidin-FITC in confocal scanning laser microscopy. *J. Histochem. Cytochem.* **1993**.

83. Deerinck, T.J.; Martone, M.E.; Lev-Ram, V.; Green, D.P.; Tsien, R.Y.; Spector, D.L.; Huang, S.; Ellisman, M.H. Fluorescence photooxidation with eosin: a method for high resolution immunolocalization and in situ hybridization detection for light and electron microscopy. *J. Cell Biol.* **1994**, *126*, 901–910.

84. Waheed, A.A.; Gupta, P.D. Estimation of submicrogram quantities of protein using the dye eosin Y. *J. Biochem. Biophys. Methods* **2000**, *42*, 125–132.

85. Waheed, A.A.; Gupta, P.D. Application of an eosin B dye method for estimating a wide range of proteins. *J. Biochem. Biophys. Methods* **1996**, *33*, 187–196.

86. Jordanides, X.J.; Lang, M.J.; Song, X.; Fleming, G.R. Solvation Dynamics in Protein Environments Studied by Photon Echo Spectroscopy. *J. Phys. Chem. B* **1999**, *103*, 7995–8005.

87. Ni, Y.; Liu, Q.; Kokot, S. Spectrophotometric study of the interaction between chlorotetracycline and bovine serum albumin using Eosin y as site marker with the aid of chemometrics. *Spectrochim. Acta - Part A Mol. Biomol. Spectrosc.* **2011**, *78*, 443–448.

88. Birla, L.; Cristian, A.M.; Hillebrand, M. Absorption and steady state fluorescence study of interaction between eosin and bovine serum albumin. *Spectrochim. Acta - Part A Mol. Biomol. Spectrosc.* **2004**, *60*, 551–556.

89. Akiyama, H.; Chaboissier, M.C.; Martin, J.F.; Schedl, A.; De Crombrugghe, B. The transcription factor Sox9 has essential roles in successive steps of the chondrocyte differentiation pathway and is required for expression of Sox5 and Sox6. *Genes Dev.* **2002**, *16*, 2813–2828.

90. Hallett, S.A.; Ono, W.; Ono, N. Growth plate chondrocytes: Skeletal development, growth and beyond. *Int. J. Mol. Sci.* **2019**, *20*, 1–17.

91. Loqman, M.Y.; Bush, P.G.; Farquharson, C.; Hall, A.C. Suppression of mammalian bone growth by membrane transport inhibitors. *J. Cell. Biochem.* **2013**, *114*, 658–668.

92. Yakar, S.; Werner, H.; Rosen, C.J. Insulin-like growth factors: Actions on the skeleton. *J. Mol. Endocrinol.* **2018**, *61*, T115–T137.

93. Farquharson, C.; Loveridge, N. Cell proliferation within the growth plate of long bones assessed by bromodeoxyuridine uptake and its relationship to glucose 6-phosphate dehydrogenase activity. *Bone Miner.* **1990**, *10*, 121–130.

94. Aizawa, T.; Kokubun, S.; Tanaka, Y. Apoptosis and proliferation of growth plate chondrocytes in rabbits. *J. Bone Joint Surg. Br.* **1997**, *79*, 483–486.

95. Tchetina, E. V; Mwale, F.; Poole, A.R. Changes in Gene Expression Associated with Matrix Turnover , Chondrocyte Proliferation and Hypertrophy in the Bovine Growth Plate. **2014**, *6*, 89–97.

96. Chantler, C.; Lieberman, E.; Holliday, M.A. A rat model for the study of growth failure in uremia. *Pediatr. Res.* **1974**, *8*, 109–113.

97. Lupu, F.; Terwilliger, J.D.; Lee, K.; Segre, G. V; Efstratiadis, A. Roles of Growth Hormone and Insulin-like Growth Factor 1 in Mouse Postnatal Growth. **2001**, *162*, 141–162.

98. Fernández-Iglesias, Á.; López, J.M.; Santos, F. Growth plate alterations in chronic kidney disease. *Pediatr. Nephrol.* **2018**, *35*, 367–374.

99. Tönshoff, B.; Kiepe, D.; Ciarmatori, S. Growth hormone/insulin-like growth factor system in children with chronic renal failure. *Pediatr. Nephrol.* **2005**, *20*, 279–289.

100. Troib, A.; Guterman, M.; Rabkin, R.; Landau, D.; Segev, Y. Endurance exercise and growth hormone improve bone formation in young and growth-retarded chronic kidney disease rats. *Nephrol Dial Transpl.* **2015**, 1–10.

101. Fernández-Iglesias, Á.; Fuente, R.; Gil-peña, H.; Alonso-duran, L. A simple method based on confocal microscopy and thick sections recognizes seven subphases in growth plate chondrocytes. *Sci. Rep.* **2020**, *10*, 6935.

102. Wu, S.; Morrison, A.; Sun, H.; De Luca, F. Nuclear factor-κB (NF-κB) p65 interacts with Stat5b in growth plate chondrocytes and mediates the effects of growth hormone on chondrogenesis and on the expression of insulin-like growth factor-1 and bone morphogenetic protein-2. *J. Biol. Chem.* **2011**, *286*, 24726–24734.

103. Gevers, E.F.; Hannah, M.J.; Waters, M.J.; Robinson, I.C.A.F. Regulation of rapid signal transducer and activator of transcription-5 phosphorylation in the resting cells of the growth plate and in the liver by growth hormone and feeding. *Endocrinology* **2009**, *150*, 3627–3636.

104. Davey, H.W.; McLachlan, M.J.; Wilkins, R.J.; Hilton, D.J.; Adams, T.E. STAT5b mediates the GH-induced expression of SOCS-2 and SOCS-3 mRNA in the liver. *Mol. Cell. Endocrinol.* **1999**, *158*, 111–116.

105. Wu, S.; Flint, J.K.; Rezvani, G.; De Luca, F. Nuclear factor-κB p65 facilitates longitudinal bone growth by inducing growth plate chondrocyte proliferation and differentiation and by preventing apoptosis. *J. Biol. Chem.* **2007**, *282*, 33698–33706.

106. Späth, S.-S.; Andrade, A.C.; Chau, M.; Nilsson, O. Local regulation of growth plate cartilage. *Endocr. Dev.* **2011**, *21*, 12–22.

107. Haffner, D.; Schaefer, F.; Nissel, R.; Wühl, E.; Tönshoff, B.; Mehls, O. Effect of Growth Hormone Treatment on the Adult Height of Children with Chronic Renal Failure. *N. Engl. J. Med.* **2000**, *343*, 923–930.

108. Ohlsson, C.; Nilsson, A.; Isaksson, O.; Lindahl, A. Growth hormone induces multiplication of the slowly cycling germinal cells of the rat tibial growth plate. *Proc. Natl. Acad. Sci. U. S. A.* **1992**, *89*, 9826–9830.

109. Isaksson, O.G.; Lindahl, A.; Nilsson, A.; Isgaard, J. Mechanism of the stimulatory effect of growth hormone on longitudinal bone growth. *Endocr. Rev.* **1987**, *8*, 426–438.

110. Kerschnitzki, M.; Wagermaier, W.; Roschger, P.; Seto, J.; Shahar, R.; Duda, G.N.; Mundlos, S.; Fratzl, P. The organization of the osteocyte network mirrors the extracellular matrix orientation in bone. *J. Struct. Biol.* **2011**, *173*, 303–311.

111. Hall, B.K. *Bone. In Bones and Cartilage*; Hall, B.K., Ed.; 2nd editio.; Elsevier Science Publishing Co Inc, 2015;

112. Li, X.; Yang, S.; Jing, D.; Qin, L.; Zhao, H.; Yang, S. Type II collagen-positive progenitors are major stem cells to control skeleton development and vascular formation. *bioRxiv* **2020**, 2020.09.06.284588.

113. Nagashima, H.; Sugahara, F.; Watanabe, K.; Shibata, M.; Chiba, A.; Sato, N.

Developmental origin of the clavicle, and its implications for the evolution of the neck and the paired appendages in vertebrates. *J. Anat.* **2016**, *229*, 536–548.

114. Yu, Y.Y.; Lieu, S.; Hu, D.; Miclau, T.; Colnot, C. Site specific effects of zoledronic acid during tibial and mandibular fracture repair. *PLoS One* **2012**, *7*, e31771.

115. Forriol, F.; Denaro, L.; Longo, U.G.; Taira, H.; Maffulli, N.; Denaro, V. Bone lengthening osteogenesis, a combination of intramembranous and endochondral ossification: an experimental study in sheep. *Strateg. trauma limb Reconstr.* **2010**, *5*, 71–78.

116. Runyan, C.M.; Gabrick, K.S. Biology of Bone Formation, Fracture Healing, and Distraction Osteogenesis. *J. Craniofac. Surg.* **2017**, *28*, 1380–1389.

117. Mackie, E.J.; Tatarczuch, L.; Mirams, M. The skeleton: A multi-functional complex organ. The growth plate chondrocyte and endochondral ossification. *J. Endocrinol.* **2011**, *211*, 109–121.

118. Olsen, B.R.; Reginato, A.M.; Wang, W. Bone development. *Annu. Rev. Cell Dev. Biol.* **2000**, *16*, 191–220.

119. Shapiro, F. Epiphyseal and physeal cartilage vascularization: a light microscopic and tritiated thymidine autoradiographic study of cartilage canals in newborn and young postnatal rabbit bone. *Anat. Rec.* **1998**, *252*, 140–148.

120. Kavanagh, E.; Ashhurst, D.E. Development and aging of the articular cartilage of the rabbit knee joint: Distribution of biglycan, decorin, and matrilin-1. *J. Histochem. Cytochem. Off. J. Histochem. Soc.* **1999**, *47*, 1603–1616.

121. Petersen, W.; Tsokos, M.; Pufe, T. Expression of VEGF121 and VEGF165 in hypertrophic chondrocytes of the human growth plate and epiphyseal cartilage. *J. Anat.* **2002**, *201*, 153–157.

122. Shailam, R.; Jaramillo, D.; Kan, J.H. Growth arrest and leg-length discrepancy. *Pediatr. Radiol.* **2013**, *43 Suppl 1*, S155-65.

123. Blumer, M.J.F.; Longato, S.; Richter, E.; Pérez, M.T.; Konakci, K.Z.; Fritsch, H. The role of cartilage canals in endochondral and perichondral bone formation: are there similarities between these two processes? *J. Anat.* **2005**, *206*, 359–372.

124. Lee, E.R.; Lamplugh, L.; Davoli, M.A.; Beauchemin, A.; Chan, K.; Mort, J.S.; Leblond, C.P. Enzymes active in the areas undergoing cartilage resorption during the development of the secondary ossification center in the tibiae of rats ages 0-21 days: I. Two groups of proteinases cleave the core protein of aggrecan. *Dev. Dyn. an Off. Publ. Am. Assoc. Anat.* **2001**, *222*, 52–70.

125. Davoli, M.A.; Lamplugh, L.; Beauchemin, A.; Chan, K.; Mordier, S.; Mort, J.S.; Murphy, G.; Docherty, A.J.; Leblond, C.P.; Lee, E.R. Enzymes active in the areas undergoing cartilage resorption during the development of the secondary ossification center in the tibiae of rats aged 0-21 days: II. Two proteinases, gelatinase B and collagenase-3, are implicated in the lysis of collagen fibrils. *Dev. Dyn. an Off. Publ. Am. Assoc. Anat.* **2001**, *222*, 71–88.

126. Stempel, J.; Fritsch, H.; Pfaller, K.; Blumer, M.J.F. Development of articular cartilage and the metaphyseal growth plate: the localization of TRAP cells, VEGF, and endostatin. *J. Anat.* **2011**, *218*, 608–618.

127. Morini, S.; Pannarale, L.; Franchitto, A.; Donati, S.; Gaudio, E. Microvascular features and ossification process in the femoral head of growing rats. *J. Anat.* **1999**, *195*, 225–233.

128. Roach, H.I.; Mehta, G.; Oreffo, R.O.C.; Clarke, N.M.P.; Cooper, C. Temporal analysis of rat growth plates: cessation of growth with age despite presence of a physis. *J. Histochem. Cytochem. Off. J. Histochem. Soc.* **2003**, *51*, 373–383.

129. Blumer, M.J.F.; Longato, S.; Fritsch, H. Structure, formation and role of cartilage canals in the developing bone. *Ann. Anat. = Anat. Anzeiger Off. organ Anat. Gesellschaft* **2008**, *190*, 305–315.

130. Alvarez, J.; Costales, L.; López-Muñiz, A.; López, J.M. Chondrocytes are released as viable cells during cartilage resorption associated with the formation of intrachondral canals in the rat tibial epiphysis. *Cell Tissue Res.* **2005**, *320*, 501–507.

131. Serowoky, M.A.; Arata, C.E.; Crump, J.G.; Mariani, F. V. Skeletal stem cells: Insights into maintaining and regenerating the skeleton. *Dev.* **2020**, *147*.

132. Abad, V.; Uyeda, J.A.; Temple, H.T.; De Luca, F.; Baron, J. Determinants of Spatial Polarity in the Growth Plate. *Endocrinology* **1999**, *140*, 958–962.

133. Maes, C. Role and regulation of vascularization processes in endochondral bones. *Calcif. Tissue Int.* **2013**, *92*, 307–323.

134. Grosso, A.; Burger, M.G.; Lunger, A.; Schaefer, D.J.; Banfi, A.; Di Maggio, N. It Takes Two to Tango: Coupling of Angiogenesis and Osteogenesis for Bone Regeneration. *Front. Bioeng. Biotechnol.* **2017**, *5*, 68.

135. Sivaraj, K.K.; Adams, R.H. Blood vessel formation and function in bone. *Development* **2016**, *143*, 2706–2715.

136. Peng, Y.; Wu, S.; Li, Y.; Crane, J.L. Type H blood vessels in bone modeling and remodeling. *Theranostics* **2020**, *10*, 426–436.

137. Blumer, M.J.F.; Longato, S.; Schwarzer, C.; Fritsch, H. Bone development in the femoral epiphysis of mice: the role of cartilage canals and the fate of resting chondrocytes. *Dev. Dyn. an Off. Publ. Am. Assoc. Anat.* **2007**, *236*, 2077–2088.

138. Cole, A.A.; Cole, M.B. Are perivascular cells in cartilage canals chondrocytes? *J. Anat.* **1989**, *165*, 1–8.

139. Shapiro, I.M.; Adams, C.S.; Freeman, T.; Srinivas, V. Fate of the hypertrophic chondrocyte: microenvironmental perspectives on apoptosis and survival in the epiphyseal growth plate. *Birth Defects Res. C. Embryo Today* **2005**, *75*, 330–339.

140. Aghajanian, P.; Xing, W.; Cheng, S.; Mohan, S. Epiphyseal bone formation occurs via thyroid hormone regulation of chondrocyte to osteoblast transdifferentiation. *Sci. Rep.* **2017**, *7*, 1–12.

141. Riminucci, M.; Bradbeer, J.N.; Corsi, A.; Gentili, C.; Descalzi, F.; Cancedda, R.; Bianco, P. Vis-à-vis cells and the priming of bone formation. *J. bone Miner. Res. Off. J. Am. Soc. Bone Miner. Res.* **1998**, *13*, 1852–1861.

142. Scammell, B.E.; Roach, H.I. A new role for the chondrocyte in fracture repair: endochondral ossification includes direct bone formation by former chondrocytes. *J. bone Miner. Res. Off. J. Am. Soc. Bone Miner. Res.* **1996**, *11*, 737–745.

143. Mizuhashi, K.; Nagata, M.; Matsushita, Y.; Ono, W.; Ono, N. Growth Plate Borderline Chondrocytes Behave as Transient Mesenchymal Precursor Cells. *J. bone Miner. Res. Off. J. Am. Soc. Bone Miner. Res.* **2019**, *34*, 1387–1392.

144. Aghajanian, P.; Mohan, S. The art of building bone: Emerging role of chondrocyte-to-osteoblast transdifferentiation in endochondral ossification. *Bone Res.* **2018**, *6*.

145. Wong, S.A.; Hu, D.P.; Slocum, J.; Lam, C.; Nguyen, M.; Miclau, T.; Marcucio, R.S.; Bahney, C.S. Chondrocyte-to-osteoblast transformation in mandibular fracture repair. *J. Orthop. Res. Off. Publ. Orthop. Res. Soc.* **2020**.

146. Newton, P.T.; Li, L.; Zhou, B.; Schweingruber, C.; Hovorakova, M.; Xie, M.; Sun, X.; Sandhow, L.; Artemov, A. V; Ivashkin, E.; et al. A radical switch in clonality reveals a stem cell niche in the epiphyseal growth plate. *Nature* **2019**, *567*, 234–238.

# X. SUPPLEMENTARY VIDEOS

# | SUPPLEMENTARY VIDEOS

**Supplementary Videos 1.** Representative video of a three-dimensional-reconstruction of Z-series confocal images of a thick bone section imaged with the confocal microscope. Video was made via the “Movie Maker” function with the increase in display time in association with the depth of the optical section. Travel through xy-projections of a confocal z-stack.

**Supplementary Video 2.** Representative video of a three-dimensional-reconstruction of Z-series confocal images of a thick bone section imaged with the confocal microscope. Video was made via the “Movie Maker” function with the increase in display time in association with the depth of the optical section. Travel through xz-projections of a confocal z-stack.

**Supplementary Video 3.** Representative video of a 3D reconstruction of chondrocytes at proliferative and early hypertrophic zones tracked in successive confocal planes obtained with IMARIS software image software.

**Supplementary Video 4.** Representative video of a 3D reconstruction of chondrocytes at the hypertrophy zone tracked in successive confocal planes obtained with IMARIS software image software.

**Supplementary Video 5.** Representative video of a three-dimensional-reconstruction of Z-series confocal images of a thick bone section of an AD rat proliferative zone imaged with the confocal microscope. Video was made via the “Movie Maker” function with the increase in display time in association with the depth of the optical section. Travel through xz-projections of a confocal z-stack.

**Supplementary Video 6.** Representative video of a three-dimensional-reconstruction of Z-series confocal images of a thick bone section of an AD rat hypertrophic zone imaged with the confocal microscope. Video was made via the “Movie Maker” function with the increase in display time in association with the depth of the optical section. Travel through xz-projections of a confocal z-stack.

**Supplementary Video 7.** Representative video of a three-dimensional-reconstruction of Z-series confocal images of a thick bone section of an ADGH rat proliferative zone imaged with the confocal microscope. Video was made via the “Movie Maker” function with the increase in display time in association with the depth of the optical section. Travel through xz-projections of a confocal z-stack.

**Supplementary Video 8.** Representative video of a three-dimensional-reconstruction of Z-series confocal images of a thick bone section of an ADGH rat hypertrophic zone imaged with the confocal microscope. Video was made via the “Movie Maker” function with the increase in display time in association with the depth of the optical section. Travel through xz-projections of a confocal z-stack.

**Supplementary Video 9.** Representative video of a three-dimensional-reconstruction of Z-series confocal images of a thick bone section of an PF rat proliferative zone imaged with the confocal microscope. Video was made via the “Movie Maker” function with the increase in display time in association with the depth of the optical section. Travel through xz-projections of a confocal z-stack.

**Supplementary Video 10.** Representative video of a three-dimensional-reconstruction of Z-series confocal images of a thick bone section of an PF rat hypertrophic zone imaged with the confocal microscope. Video was made via the “Movie Maker” function with the increase in display time in association with the depth of the optical section. Travel through xz-projections of a confocal z-stack.

# XI. FUNDING AND DIFFUSION

# | FUNDING


- Contratos predoctorales. Instituto de Investigación Sanitaria del Principado de Asturias. 2017.
- EMBO Short-Term Fellowship. 2018. Endocrine Unit. Massachusetts General Hospital.


# | DIFUSSION

- ***Fernández-Iglesias, A****., Fuente R, Gil-Peña H, O, Alonso-Duran, L., López, JM., Santos, F.* 3D microscopy analysis of bone development. Uremic growth plate discloses alterations, reversed by GH treatment, in the process of hypertrophy. SEBD 17th Meeting. Online. November 18-20, 2020. Poster.

- ***Fernández-Iglesias, A****., Fuente R, Gil-Peña H, Hernández-Frías O, Alonso-Duran, L., López, JM., Santos, F.* A 3D approach for quantification of alterations in uremic growth plates chondrocytes. ORS 2020 Annual Meeting. Phoenix (Arizona, EEUU), February 8-11, 2020. Poster.

- ***Fernández-Iglesias, A****., Fuente R, Gil-Peña H, Hernández-Frías O, Alonso-Duran, L., López, JM., Santos, F.* Three-dimensional microscopy analysis of growth plate disturbances in chronic kidney disease. IPNA. Venice (Italy), October 17-21, 2019. Oral communication.

- ***Fernández-Iglesias****, A., Fuente R., Gil-Peña, H., Santos, F., López J.* (2017). Confocal microscopy for *in toto* imaging of the bone growth plate. Joint Congress. Gijon (Asturias, Spain). October, 24-27, 2017. Oral communication.